3. RESULTS AND DISCUSSION

I. ENZYME AND BIODEGRADATION STUDY

3.1 Isolation and purification of fungi

Isolation and purification of sterilized wood samples and fungal fruiting bodies was carried out to check their adaptation potential on different growth media as listed in (Table 3). Among different media used, Malt Extract Agar (MEA) media was found to be more suitable for the growth of the most of the fungal isolates. Pure cultures were established by serial culture technique and pure cultures of all these strains were maintained at 4 ^{o}C in refrigerator to study further parameters.

3.1.1 Screening of white rot fungi

All the purified strains were subjected to Bavendamm's test to distinguish between the white rot and brown rot fungi by using the technique proposed by Bavendam (1928). Among them, *Trametes hirsuta* and *Trametes versicolor* were selected for further study due to higher production of ligninolytic enzymes during primary screening. Moreover, *Trametes hirsuta* and *Trametes versicolor* grew much adaptively as compared to other strains on MEA media. Growth of mycelia of *T. hirsuta* was thick and white fluffy, and cotton like covering the entire media while *T. versicolor* grew, forming thin white mat of mycelia. In Bavendamm's test, both the

strains started browning of media after 3rd day of inoculation and the plates turned completely brown on 6th days of incubation. Further incubation resulted into bleaching of media with complete removal of the brown colour from the plate. When compared with our isolates, pure cultures of *Trametes hirsuta* (Acc No NTCC 729/C) and *Trametes versicolor* (Acc No NTCC 165/S) obtained from Forest Research Institute (FRI), Dehra Dun were found to be more potent in the production of ligninolytic enzymes. Therefore, subsequent study was carried out on these strains procured from FRI.

3.2 Determination of enzyme activity

3.2.1 Solid State Fermentation (SSF)

Solid Substrate Fermentation (SSF) is an important mode of fermentation occurring in the absence of free water, employing an inert or a natural substrate used as solid support (Pandey *et al.* 2000; Couto and Sanroman 2005; Koyani and Rajput 2015) which also mimics the natural condition for the organism. This technique has impelled several researches offering the possibility of using food processing wastes, agricultural residues and by-products of agro-based industries making the process much more efficient from both economical and environmental points of view (Chayya and Gupte 2013).

SSF process resolves the problem of solid waste disposal, requires cheaper raw materials and low energy, also gives concentrated metabolites and lower risks of contamination (Pandey 1991, 2003; Gessesse and Mamo 1999; Kalogeris *et al*. 2003; Suryanarayan 2003; Osma *et al*. 2007). Nevertheless, solid state fermentation is acquiring a special relevancy in the field of the biotechnological processes. In recent years, the process of production of ligninolytic enzymes by filamentous fungi (especially white rot) which colonize the substrates in SSF have reignited interest of many researchers to convert cheap substrates into valuable products (Koyani 2011; Koyani and Rajput 2015). Fermentation by white rot fungi have been applied to the decomposition of numerous xenobiotics for decolourization and detoxification of dyes released by the textile industries, delignification, biopulping and various applications in the wood fibre industry (Couto *et al*. 2004, 2006a, b; Bohmer *et al*. 2006, 2010; Kues *et al*. 2007; Robinson and Nigam 2008; Cajthaml *et al*. 2009; Mazumder *et al*. 2009, Singh *et al*. 2011b). White rot fungi naturally prefer to grow on surfaces and

requires less moisture; therefore compared to submerged fermentation (SmF), it seems reasonable to attempt SSF (Bohmer *et al*. 2011). Successful fermentation by filamentous organisms in SmF can be very challenging, as SmF utilizes free flowing liquid substrates which are best suited for microorganisms like bacteria that require high moisture (Subramaniyam and Vimala 2012).

Several studies emphasized SSF as the most economical method for enhancing the process for ligninolytic enzyme production by fungi (Gupte *et al.* 2007; Pant and Adholeya 2007; Patel *et al.* 2009; Sanghvi *et al.* 2010, 2011; Koyani 2011; Koyani and Rajput 2015). Looking to the advantages of SSF, in the present study, the process of SSF was opted for production of ligninolytic enzymes using two white rot fungi *Trametes hirsuta* and *Trametes versicolor* by means of agro-industrial wastes as substrate. Different agro-industrial wastes like wheat straw, rice straw, sugarcane bagasse, sawdust, etc. were employed to scale up the production of ligninolytic enzymes like manganese peroxidase (MnP), manganese independent peroxidise (MnIP), laccase (Lac) and lignin peroxidise (LiP). Agro-industrial wastes are generated in vast quantity every year. Considering environmental and economical aspects, countries around the world have found it as alternatives for the reuse of these wastes (Mussatto *et al*. 2012). Moreover, it is inexpensive, readily available (Rodriguez-Jasso *et al*. 2013) and provide an environment similar to the natural habitat of fungi (Koyani and Rajput 2015).

Solid-state fermentation has enormous potential for production of laccase at low cost if agricultural wastes are used as support-substrates for *T. versicolor*. Enhanced production of laccase and MnP by *Pluerotus ostreatus* and that of LiP and MnP by *Phanerochaete chrysosporium* was observed when cultivated on a 1:1 mixture of wheat bran and neem hull waste under SSF (Verma and Datta 2002). However, Moldes *et al*. (2003a) obtained high laccase yields with *Trametes hirsuta* by using grape seed as a substrate under SSF. Similarly, Revankar *et al.* (2007) also reported wheat bran as the best substrate for laccase production under SSF condition using *Ganoderma* sp. The use of corncob showed enhanced production of lignin peroxidase by *Phaerochaete chrysosporium* on SSF media (Asgher *et al*. 2006) whereas, Marnyye *et al*. (2002) established that the growth of white rot fungi *Pleurotus ostreatus*, and *Pleurotus pulmonarius* on coffee pulp results in the higher production laccase. In year 2005 and 2007, Rosales *et al*. aimed to investigate the

feasibility of kiwi fruit wastes as a substrate for laccase production and reported increased production of laccase by *Trametes hirsuta* when grown on crushed orange peelings. Therefore, utilization of such wastes on one hand resulted in considerable reduction in production costs while on the other hand promoted high enzymatic levels. Thus, not only fungi, but also the selection of suitable substrate are one of the key factors determining the success of the fermentation process.

3.2.2 Optimization assays under SSF

i) Optimization of agro-industrial waste used as substrates

Variation in the enzyme productions by fungi mainly results due to adaptation to different substrates and natural conditions (Conesa *et al.* 2002). Hence, initial efforts have been made for the production of ligninolytic enzymes using different agro-industrial waste, i.e wheat straw, rice straw, saw dust, pigeon pea (*Cajanus cajan*) pod shells and sugarcane bagasse as a sole source of substrate without any mineral supplementation using *Trametes hirsuta* and *Trametes versicolor*. All the five agro-industrial residues tested in the present study supported good growth and enzyme production by both strains *viz*. *T. hirsuta and T. versicolor* (Fig.12 and 13).

Trametes hirsuta showed maximum enzyme productivity (168.69 IU/ml) of manganese peroxidase and (177.64 IU/ml) manganese independent peroxidase with sawdust, while laccase (221.27 IU/ml) and lignin peroxidase (58.44 IU/ml) with wheat straw (Fig. 12). Though *T. hirsuta* showed sufficient growth on sugarcane bagasse, it was found less efficient for enzyme production. In case of *T. versicolor* all the substrates exhibited efficient enzyme activity, but comparatively pod shells of pigeon pea gave a maximum production of manganese peroxidase, manganese independent peroxidase, laccase (i.e. 171.91, 168.69 and 203.61 IU/ml, respectively) except the production of lignin peroxidase (56.39 IU/ml) which was recorded highest in sugarcane bagasse (Fig. 13). Our results indicate that differences in lignocellulolytic enzyme yield depend upon variation of the growth substrates, which is in agreement of earlier researches (Lorenzo *et al.* 2002; Silva *et al.* 2005; Songulashvili *et al.* 2007; Elisashvili *et al*. 2008; Elisashvili *et al.* 2009). Reddy *et al.* (2003b) used banana waste (leaf biomass and pseudostems) for the production of lignolytic and cellulolytic enzymes by using *Pleurotus ostreatus* and *Pleurotus sajor-caju*. However, Kurt and Buyukalaca (2010) studied enzyme activities of

Pleurotus spp. (*P. ostreatus* and *P. sajor-caju*) cultivated on different agricultural wastes like wheat straw, paddy straw, sesame straw and sawdust. Grapevine sawdust had also been observed to exhibit the highest level of laccase activity (2144.6 ± 57.8 U/l) produced by *P. ostreatus* (Stajic *et al.* 2006a). *Datronia* sp., cultivated on SSF medium like sawdust and rice straw as substrate produced extracellular laccase and manganese peroxidase (Chedchant *et al.* 2009). Whereas Iqbal *et al*. (2011) reported maximum production of MnP (998 U/ml), LiP (620 U/ml) and laccase (49.7 U/ml) by *Trametes versicolor* in SSF medium containing rice straw.

In the past decade, many researchers have attributed the use of wheat straw for cultivating several fungal strains to produce ligninolytic enzymes (Maltseva *et al*. 1991a; Martinez *et al*. 1994; Vares *et al*. 1995; Lang *et al*. 1996; Gupte *et al*. 1998; Pandey *et al*. 1999; Arora *et al*. 2002; Zhang *et al*. 2008; Shrivastava *et al.* 2011). According to Stajic *et al.* (2011), wheat straw contains inducers of lignocellulolytic enzyme synthesis and a certain amount of soluble carbohydrates, and it is a very common agricultural residue available worldwide. Gupte *et al.* (2007), found that wheat straw is the best substrate for LiP, MnP and laccase production. High levels of laccase production were also reported by Valmaseda *et al*. (1991) when wheat straw was used as an SSF substrate for *Trametes versicolor* and *Pleurotus ostreatus*. Solid state fermentation on wheat straw by white rot Basidiomycete *Pleurotus ostreatus* resulted in lower variability of laccase activities (Baldrian and Gabriel 2002). Moreover, Kapoor *et al*. (2009) has also reported the potential of wheat straw as a natural support for the production of laccase from *Lentinus edodes*. Wheat straw was also the best suited substrate for production of manganese peroxidase, manganese independent peroxidase and laccase under SSF by *Phanerochaete chrysosporium* and *Irpex lacteus* (Koyani 2011). Laccase synthesis was reported only during the solid-state cultivation in wheat straw-enriched medium; similarly during solid-state fermentation, wheat straw proved to be a better carbon source for MnP and oak sawdust for MnIP production by *Trametes suaveolens* (Knezević *et al*. 2013). *Trametes trogii* produced high activity of laccase and manganese peroxidase when cultivated on wheat straw (Gai *et al*. 2014). Thus, the above mentioned information concludes that maximum production of enzymes depends upon the selection of substrate that is specific to fungal growth. In the present study, wheat straw and pigeon pea pod shells under SSF ensured significant enzyme production by *Trametes*

hirsuta and *Trametes versicolor* respectively (Fig. 11). Though, the use of pigeon pea pod shells as substrate for SSF is rarely reported. As per our knowledge, the only report by Prasad *et al*. (2011) is exists for laccase production under SSF using the husk of pigeon pea by *Pleurotus ostreatus*.

ii) Optimization of particle size

Specific surface area (i.e. particle size) available to the organism and its enzymes is a critical factor in the process of SSF (Couto and Sanroman 2006). Evaluation of different particle size of substrate may result in variation in enhanced production of enzymes; this variation may be associated with the surface area available to the fungi (Sanghvi *et al*. 2010). Therefore, appropriate particle size of wheat straw, i.e. 1, 1.40, 2.0, 2.80 and 4.0 mm was assessed to obtain maximum enzyme production. Compared to other substrates used, *T. hirsuta* produced highest activity of MnP (166.52 IU/ml), MnIP (170.32 IU/ml), laccase (221.27 IU/ml) and LiP (58.44 IU/ml) at a 1mm particle size of wheat straw (Table 9). Whereas in case of *T. versicolor*, the optimum activity of all the enzymes tested was recorded with peagen pea pod shells which were oven dried and crushed manually.

Particle Size (mm)	**Enzyme Activity (IU/ml)**			
	MnP	**MnIP**	**Lac**	**LiP**
1	166.52	170.32	221.27	58.44
1.40	157.27	162.58	190.33	43.85
2	126.13	115.71	178.44	57.58
2.80	148.22	98.82	170.08	52.17
4	99.81	94.29	183.83	54.91

Table 9: Optimization of particle size of wheat straw for ligninolytic enzyme production by *Trametes hirsuta.*

Bhattacharya *et al*. (2011), reported that increase in the laccase production can also be attributed to the partly anaerobic condition created by the decrease in particle size, ensuring increased nutrient availability to fungi. Aeration and nutrition availability are the two crucial factors for the production of any biomolecules by the microorganism. The smaller particle size may ensure increase in the ratio of accessible surface area to volume to the microorganism facilitating its growth

(Woiciechowski *et al.* 2014). However, large particle size can prevent the penetration of air and metabolite intermediates into the particles and also hamper accessibility of nutrients by fungi (Wan and Li 2010). In the present study also it is confirmed that the size of the carbon source is an important factor for the production of enzymes when the SSF method is used (Kalogeris *et al*. 1998; Koyani *et al*. 2013).

iii) Optimization of incubation time

Various white rot fungi have been reported to produce maximum ligninolytic enzymes after different time periods due to the composition of the substrates used, and genetic variation among the strains as well as nature (Heinzkill *et al*. 1998; Giardina *et al*. 2000; Patel *et al*. 2009; Irshad and Asgher 2011). In the present study, to conclude the optimum incubation period for maximum enzyme production; the enzyme activity was determined from the cultures harvested at an interval of every three days of incubation for 24 days (Fig. 14 and 15). *T. hirsuta* started production of MnP, MnIP on sawdust as a substrate of SSF media while Lac and LiP on wheat straw as a substrate. Similarly, *T. versicolor* showed initiation of MnP, MnIP and Lac production on pigeon pea pod shells and LiP on sugarcane bagasse as a substrate. It demonstrated an increasing trend of enzyme activity of all four enzymes i.e. MnP, MnIP, Lac and LiP from 6^{th} day and reached to its peak on 12^{th} day of incubation; after that, a gradual decrease in the enzymes activity of all four enzymes was observed (Fig. 14). In contrast, *T. versicolor* showed a peak of activity of laccase on the 9^{th} day, whereas MnP, MnIP and LiP attained their highest peak on the 12^{th} day of incubation. Subsequently, enzyme production declined after the 9^{th} day in laccase and after the 12^{th} day in MnP, MnIP and LiP (Fig. 15).

Similar to the current reports, Sivakumar *et al.* (2010) recorded maximum laccase activity in *Ganoderma* sp., on the 10^{th} day of incubation while the highest laccase and MnP activities were detected in *Pleurotus sajor-caju* on the 16^{th} day and LiP activity on the 9^{th} day of incubation by *Pleurotus djamore* (Velioglu and Urek 2014). In contrast, Niku-Paavola *et al*. (1990) observed maximum laccase production by *Phlebia radiata* on day 3-5 and it was rapidly disappeared before the increasing activities of manganese peroxidase and lignin peroxidase. There is no unanimous opinion about the maximal activity of ligninolytic enzyme production by *T. hirsuta* and *T. versicolor*. Couto *et al.* (2004), observed that laccase activity by *T. hirsuta* sharply increased up to maximum on the 9^{th} day of cultivation while its production

started on the 5th day and increased up to the 15th day of incubation (Moldes *et al*. 2003a). Similarly, Collins and Dobson (1997) recorded the maximum enzyme yield on the 10th day for *Trametes versicolor*. Schlosser *et al*. (1997), documented that *T. versicolor* produced the highest titre of ligninolytic enzymes within 14 days of incubation while Arora *et al*. (2002) and Zhang *et al*. (2008) stated the highest production of manganese peroxidase and laccase after 10 days of incubation on wheat straw as a substrate. Shrivastava *et al.* (2011), also studied *T. versicolor* and recorded that production of these enzymes reaches to its peak on the 5th day of inoculation.

The present study supports Tripathi *et al*. (2012) stating that nutritional and incubation conditions directly affect the enzymatic activity. Depletion of nutrients in response to the enhanced fungal biomass after a certain limit result in decreased enzyme production, which would result in a decreased metabolic activity (Kashyap *et al.* 2002). Hence, in the present investigation, peak enzyme activity by both the species occurs on the 12th day of incubation except for laccase of *Trametes versicolor* that peaked highest on the 9th day under SSF.

iv) Optimization of reaction time

Reaction time has also been considered as one of the important parameters for detection of the optimum enzyme activity as it is based on the amount of substrate oxidation over the period of time. In the present investigation, 5 to 45 minutes of reaction time was checked to find out the maximum enzyme activity by *Trametes hirsuta* and *Trametes versicolor*. Both fungal strains showed increased activity up to 10 minutes of reaction time after that a gradual decrease in activity of all the four enzymes was noticed. Therefore, reaction time of 10 minutes was considered as optimum to obtain potential results.

3.2.3 Production of ligninolytic enzymes by Trametes hirsuta and Trametes versicolor

Production of ligninolytic enzymes by white rot fungi varies within a wide range species depending on their physiological conditions and numerous cultivation factors (Stajic *et al*. 2006a, 2010; Songulashvili *et al*. 2007; Simonic *et al*. 2008; Cilerdzic *et al*. 2011). White rot fungi differ from other group of fungi with respect to their enzyme production patterns and produce various combinations of enzymes (Vares and Hatakka 1997). In the present study, both the fungal strains *T. hirsuta* and *T.*

versicolor produced all ligninolytic enzymes *viz*. Manganese Peroxidase (MP), Manganese Independent Peroxidae (MnIP), Laccase (Lac) and Lignin Peroxidase (LiP).

Enzyme activities of MnP, MnIP, Lac and LiP in crude extracts of *T. hirsuta* and *T. versicolor* varied depending on the selected agricultural wastes used. Under SSF, *T. hirsuta* showed highest activity for MnP (168.69IU/ml) and MnIP (177.64 IU/ml) when sawdust was used as substrate while laccase (221 IU/ml) and LiP (58.44IU/ml) showed the highest activity in wheat straw as a substrate (Fig. 12). In case of *T. versicolor* the highest MnP (171.91 IU/ml), MnIP (168.69 IU/ml) and Lac (203.61 IU/ml) were revealed in pigeon pea pod shells, whereas LiP (56.39 IU/ml) was highest in sugarcane bagasse (Fig. 13). Among all the four enzymes, both species showed highest activity of laccase subsequently followed by MnIP, MnP and LiP in *T. hirsuta* and MnP, MnIP and LiP in *T. versicolor*. Thus, with present experiments, laccase activity is highly expressed indicating that it is the predominating enzyme whereas LiP activities in both the strains were significantly lower compared to the other three enzymes.

Earlier, Cilerdzic *et al*. (2011) noted that *T. hirsuta* is the best producer of laccase among all the *Trametes* species studied so far. However, Remeshaiah and Reddy *et al*. (2015) reported *T. versicolor* as one of the best species that secretes various enzymes such as the phenol oxidase, laccase and perioxidase, which take part in the transformation of aromatic compounds. Contrary to our results obtained from *T. hirsuta and T. versicolor*, the results of numerous studies showed that the conditions of solid-state cultivation were not favorable for laccase production, but the same was appropriated for MnP synthesis (Sun *et al*. 2001; Jaszek *et al*. 2006; Dinis *et al*. 2009; Elisashvili *et al*. 2009). Jaszek *et al*. (2006) and Dinis *et al*. (2009) also reported that during solid-state fermentation of wheat straw, MnP was the predominant ligninolytic enzyme with maximum activity that was 10 times higher than the maximum level of laccase. Similar results are also documented by Hossain and Anantharaman (2005) that *T. versicolor* showed presence of all the three ligninolytic enzymes (MnP, Lac and LiP), from which LiP activity was maximum followed by MnP and laccase with bagasse powder. However, in the present study, laccase activity was more as compared to MnP and LiP. Perusal of literature indicates that different strains of white rot fungi predominantly produce MnP and laccase (Vyas *et al.* 1994; Hofrichter *et al.*

1999; Tekere *et al.* 2001; Arora *et al.* 2002; Koyani 2011). *T. trogii* BAFC 463 isolated from Argentina is a promising fungal strain producing high levels of laccase and MnP (Grassi *et al*. 2011) while *Pycnoporus cinnabarinus* produce laccase as the sole ligninolytic enzyme, which enables the fungi to degrade lignin (Eggert *et al.* 1996). The maximum LiP activities of the enzyme which were 5.46 and 6.39 U/ml was obtained at 30 °C in fungal strains *P. chrysosporium* and *P. ostreatus* respectively (Kheiralla *et al*. 2013) while LiP is not always detected (Tekere *et al.* 2001). Arora *et al*. (2002) and Vyas *et al*. (1994) detected LiP for *P. chrysosporium* and *T. versicolor* in SSF wheat straw medium.

3.2.4 Effect of physicochemical parameters

i) Effect of pH

Enzymes are highly sensitive to pH and are an important factor to control the activity of different ligninolytic enzymes (Koyani 2011). Therefore, the effect of pH on ligninolytic enzyme was investigated at the room temperature in the present study. The Na-acetate buffer (0.1 M) with a pH range of 3.5-6 for MnP and MnIP, while Na-acetate buffer (50 Mm) with a pH range of 3.5-6 for laccase and Na- tartarate buffer (5 mM) with pH range 2.5-5.0 for LiP was found to be more adaptive to the enzyme activity with their specific substrate. In case of *Trametes hirsuta* the highest activities of MnP, MnIP, Lac and LiP were recorded at pH 5, 3.5, 3.5 and 2.5 respectively (Fig. 16, 18 and 20). While in *Trametes versicolor* highest activities of MnP, MnIP, Lac and LiP was recorded at pH 3.5, 3.5, 4 and 2.5, respectively (Fig 17, 19 and 21).

Most constructive growth pH of ligninolytic fungi is around pH 3-5 (Fu and Viraraghavan 2001). According to previous studies, the optimum activities of MnP of various white rot fungi vary from 4-7 pH, laccase vary from pH range of 2-10 and LiPs vary between pH 2-5 (Bermek *et al.* 2004; Ürek and Pazarlioglu 2004; Yang *et al.* 2004; Baborová *et al.* 2006; Hakala *et al.* 2006; Asgher *et al.* 2007, 2008; Snajdr and Baldrian 2007). MnP from *P. chrysosporium* was stable in the pH range 4.5-6.0 (Urek and Pazarlioglu 2004) and MnP from *Lentinula edodes* had optimum activity at pH 4.5 when produced with SSF of corn cobs (Boer *et al.* 2006). *Trametes versicolor* produced a crude laccase having optimum pH 4.5 (Stoilova *et al.* 2010) while *Cerrena unicolor* 137 laccase displayed optimum activity at pH 7.0 (Cadimaliev *et al.* 2005; Mäkelä *et al.* 2006; Michniewicz *et al.* 2006; Zouari-Mechichi *et al.* 2006).

Whereas laccase from *Lentinula (Lentinus) edodes* was completely stable in a large pH range (4.0-6.0) and presented an optimum pH value of 4.5 (Boer *et al.* 2004).

ii) Effect of temperature

The effect of temperature on the production of ligninolytic enzyme by white rot fungi under SSF varies from one genus to another, depending on its physiology and type of substrate used (Isroi *et al.* 2011). Temperature affects the fungal growth, production, activity and stability of ligninolytic enzyme in white rot fungi (Snajdr and Baldrian 2007). In the present study, the enzyme activity of all four enzymes was estimated at varying temperature from 5-45 ºC. Both strains *viz*. *T. hirsuta* and *T. versicolor* showed fluctuations upon varying incubation temperatures (Fig. 22 and 23). All enzymes showed an increase in titres of activities up to 30 ºC, and enzyme activity gradually declined upon increasing temperature. Therefore, temperature optima for maximum ligninolytic enzyme production were found to be 30-35 ºC for MnP, MnIP, Lac and LiP by *T. hirsuta* and *T. versicolor*. It was also noticed that enzyme production in both fungal strains increased substantially with temperature up to the optimal value.

The temperature ranging from 25 to 37 ºC found to be optimum for ligninolytic enzyme production by different white rot fungus (Zadrazil *et al.* 1999; Arora and Gill 2001; Tekere *et al.* 2001; Tripathi *et al.* 2008). The highest rate of enzyme production by *Pleurotus ostreatus* was observed at 25 ºC and rapid enzyme inactivation occurred above 35 ºC (Shin *et al*. 1997). In support of our result, similar information, i.e. high laccase and MnP production by *Coriolus hirsutus* at 28 °C has been by reported Koroleva *et al.* (2002). According to Gill and Arora (2003) in *Coriolus vesicolor* and *P. chrysosporium* the optimal activity of the enzyme was expressed at 25-30 ºC, whereas no activity was observed above 30 ºC. The present study supports Iqbal *et al*. (2011) who revealed higher MnP, Lac and LiP activities at 30 ºC in *Trametes versicolor* IBL-04, as compared to other incubation temperatures. Similarly, Jordaan *et al.* (2004) recorded that *Trametes versicolor* exhibits a high level of laccase activity at temperature values 30 to 40 °C. For *Trametes modesta* and *Cyathus bulleri*, the optimal temperature for laccase production is described to be 30 °C (Nyanhongo *et al*. 2002, Vasdev *et al*. 2005). However Snajdr and Baldrian (2007) proved 30 °C and 35 °C as the most supporting temperature for the highest laccase

activity by *P. ostreatus* and *T. versicolor* respectively, although there are studies indicating that the optimal growth temperature for *T. versicolor* might be lower (Xavier *et al*. 2007). Patrick *et al*. (2010), reported maximum production of MnP at 30 ºC in *Trametes trogii*, while in *Neolentinus kauffmanii*, the highest level of peroxidase activity was obtained at 25 ºC and laccase at 30 ºC (Johnsy and Kaviyarasan 2014). On the other hand, it has been reported that the optimum temperature for LiP production by *P. chrysosporium* ATCC 24725 is at 37 ºC (Leisola and Fiechte 1985) and very supportively Bono *et al*. (1990) reported the production of lignin peroxidases by *P. chrysosporium* at 35 °C. Khiyami *et al*. (2006) also showed 25 to 39 °C as the most suitable temperature for LiP. Conversely, Badr el-Din *et al*. (2013) reported high LiP activity in *Pleurotus ostreatus* and *Phanerochaete chrysosporium* at 30 ºC. Also, Koyani (2011) reported maximum MnP, MnIP and Lac activity by *Irpex lacteus* and *Phanerochaete chrysosporium* at 35 ºC. The maximum MnP activity was obtained at 37 ºC by *Phanerochaete chrysosporium* (Urek and Pazarlioglu 2007).

However, exceptionally Zapata-Castillo *et al.* (2012) obtained maximum laccase by *T. hirsuta* at the optimal temperature of 40 to 60 °C with good stability up to 65 °C; while *Trametes versicolor* exhibited high enzyme activity at a broad range of temperature with highest laccase activity at 50 °C (Han *et al*. 2005). While in the present study decline of growth and enzyme activity at higher temperature may result from denaturation of metabolic enzymes of microorganisms.

iii) Effect of metal ions

During the growth on lignocellulosic substrates, different strains and species of Basidiomycetes differ in their sensitivity towards metals (Sathiya-Moorthi *et al.* 2007). In the present study, five different metal ions like Mn^{+2}, Zn^{+2}, Cu^{+2}, Ca^{+2}, and Mg^{+2} were examined for their ability to enhance the enzyme activity, wherein the activity of MnP, MnIP, Lac and LiP are not altered by the presence of metal ions in the enzyme reaction mixture. On the contrary, there are many studies revealing enhanced effect on ligninolytic activity of enzymes in presence of metal ions.

Available literature indicated that, the MnP production by the white rot fungus was enhanced by the addition of Mn^{+2} (Fujihara *et al.* 2010). It has been reported that metal ions stimulated laccase formation when added to actively growing culture of *Trametes pubescens* (Galhaup *et al.* 2002a; Mongkolthanaruk *et al.* 2012). The

addition of Mn^{2+} to the cultures of *C. subvermispora*, *T. versicolor*, *P. chrysosporium*, *P. ostreatus* is strictly required for production of MnP (Brown *et al*. 1991; Ruttimann *et al*. 1992; Johansson *et al*. 2002; Janusz *et al*. 2013). Mn^{+2} scaled up LiP activity in *Lentinus squarrosulus* and *Psathyrella atroumbonata* up to 11-fold and 14 fold at 80 mM respectively; while Ca^{+2} up to 14- fold at 40 mM in *Psathyrella atroumbonata*. Rosales *et al.* (2007) also found that *Trametes hirsuta* supplemented with 1mM copper sulphate increases laccase production. There are several reports on the metal ion requirements of laccases mentioning the activation effect caused by copper ions on laccase activity (Stajić *et al.* 2006b; Adamafio *et al.* 2012). Despite this fact, not all laccases are stimulated by copper ions. For instance, in *Trametes hirsuta* laccase was unstable at a concentration of 1 mM for 7 days against the metal ions tested Zn^{+2}, CrO_4^{-2}, Cd^{+2}, $Cr_2O_7^{-2}$, Fe^{+2}, Cu^{+2} and especially Hg^{+2} (Couto *et al*. 2005) in agreement with the present results.

LacII was strongly inhibited by Cd^{+2} followed by Cu^{+2}, Mn^{+2} and Zn^{+2} did not affect the enzyme activity at the concentrations tested in *Trametes versicolor* (Lorenzo *et al*. 2005). The results of the present study can be compared favorably with data reported in the literature for laccases purified from other white-rot fungi. In *Trametes versicolor,* $CaCl_2$, $FeSO_4$ and KCl were found to be inhibitory to fungal growth and laccase synthesis (Asgher *et al*. 2012).

Baldrian and Gabriel (2002) and Baldrian (2004) reported that Mn^{2+} caused 91 % inhibition at 1 mM concentration and efficiently inhibited laccase from the fungus *Daedalea quercina.* Moreover, they also reported that the addition of Zn^{2+} decreased laccase activity in cultures of *Pleurous ostreatus* and among several heavy metals, Fe^{+2} highly inhibited the enzyme activity in *Ganoderma lucidum* (Murugesan *et al*. 2009). In *Trametes trogii,* MnP and laccase retained more than 40 % of their activities at a concentration 0.1 M of Cu^{2+}, Co^{2+} and Mn^{2+}; with further decrease in concentration to 10 mM, after one day MnP retained 62, 100, 44 and 17 %, with Cu^{2+}, Fe^{2+}, Cd^{2+} and Pb^{2+} of its activity, while laccase activity was 90, 80, 54 and 20 % (Grassi *et al*. 2011). According to Johnsy and Kaviyarasan (2014), in *Neolentinus kauffmanii* compared to the control conditions, laccase activity remain stable for Fe^{+2} and decreased in $ZnSO_4$ and $CaCl_2$; while MnP activity was decreased on addition of aluminium oxide and calcium chloride.

The strong negative effect of heavy metals on the growth of wood-rotting basidiomycetes is already well documented *in vitro* (Baldrian and Gabriel 1997; Mandal *et al*. 1998, Baldrian *et al*. 2000). Thus, the turnover rate of extracellular enzymes can be altered by the activation or inhibition of proteolytic enzymes by metals (Palmer *et al.* 2001). Though, earlier studies reported enhanced effect of metal ions, in the present study both the strains showed no effect.

3.3 Partial purification of crude extracts

3.3.1 Ammonium sulphate precipitation

Considering the high amounts of laccase produced by *T. hirsuta* and *T. versicolor*, ammonium sulphate precipitation was carried out at different percent saturation (20 to 80 %) described by Dawson *et al.* (1969) and the fraction with highest laccase activity was subjected to molecular weight determination. Crude extract of laccase obtained from *T. hirsuta* (221.27 IU/ml) and *T. versicolor* (203.61 IU/ml) exhibited high laccase activity at 60 % and 20 % saturated fraction respectively (Fig. 24 and 25). These fractions were further dialyzed with dialysis membrane having 12000-14000 Da cut off value.

3.3.2 Molecular weight determination

The resulted partially purified laccase of both the strains was resolved on SDS-PAGE and stained with CBB dye for distinct bands. *T. hirsuta* produce laccase of molecular mass 68 kDa and laccase of *T. versicolor* has molecular mass of 29 kDa. (Fig. 26).

Thurston (1994) and Wong (2009), reported that laccase have a molecular mass ranging from 50 to 110 kDa. In *Polyporus pinisitus*, laccase of 65 kDa was obtained (Claus *et al*. 2002) while Baldrian (2004) revealed purified laccase from *Daedalea quercina* to be a monomeric protein of 69 kDa. Molecular mass of *Lentinus squarrosulus* MR13 determined by SDS-PAGE was found to be of 66 kDa (Mukhopadhyay and Banerjee 2014), whereas laccase purified from *Pleurotus ostreatus* showed a molecular mass of 85 kDa (Othman *et al*. 2014). On the other hand, laccases obtained from most of the white rot fungi have been reported to be extracellular glycosylated proteins with molecular weights ranging from 50-90 kDa on SDS-PAGE (Baldrian 2006; Quaratino *et al*. 2007; Asgher *et al*. 2008, 2012). Laccases from the same or related species of *Trametes* or other fungi, range from 61 ~ 81 kDa (Yaver *et al.* 1996; Garzillo *et al.* 1998; Périé *et al.* 1998; Shin and Lee 2000;

Min *et al.* 2001; Jung *et al.* 2002; Iyer and Chattoo, 2003; Xiao *et al.* 2003; Han *et al.* 2005). *Trametes sanguinea* M85-2 has laccase of molecular mass 62 kDa (Nishizawa *et al*. 1995) while two to three laccase isoforms with molecular masses of 64–70 kDa were described in *T. trogii* (Vares and Hatakka 1997) and *T. hispida* (Rodriguez *et al.* 1999), *T. gibbosa, T. hirsuta* (Levin *et al*. 2002). Moreover, laccase from *Trametes multicolor* has molecular mass of 63 kDa (Leitner *et al.* 2002) and two isoenzymes of laccase were obtained from *Trametes trogii* of molecular weight around 62 kDa (Zouari-Mechichi *et al.* 2006). Similarly Si *et al.* (2013) also obtained laccase in the same range i.e.68 kDa molecular mass from *Trametes pubescens.*

However, the molecular mass of the laccase in *Trametes hirsuta* determined from SDS-PAGE analysis was 55.0 kDa (Chaurasia *et al*. 2014). In support to our result, Shleev *et al*. (2004) reported the molecular mass of laccases from *Trametes hirsuta*, *Trametes ochracea*, *Coriolopsis fulvocinerea*, and *Cerrena máxima* within a range of 64 to 70 kDa. Purified laccase of moloecular mass 66 kDa was obtained from *Trametes hirsuta* (Lim and Yoon 2004) and Zapata-Castillo *et al*. (2012) also reported major laccase from *Trametes hirsuta* Bm-2, with an apparent molecular mass of 65 kDa (SDS-PAGE), which is very much similar to the present investigation.

Laccase from *Trametes versicolor* with the molecular weight as low as 29 kDa, which has never been recorded before. In contrast to previous research, where some basidiomycetes such as *Trametes versicolor* and *Fomitella fraxinea*, has the molecular weight of the laccases ranging from 97 to 80 kDa (Park and Park 2008; Zapata-Castillo *et al*. 2012). Han *et al*. (2005), also reported 97 kDa molecular mass of denatured laccase from *T. versicolor* 951022. Zhu *et al*. (2011) revealed 60 kDa molecular mass of laccase from *Trametes versicolor* sdu-4. According to Zapata-Castillo *et al*. (2012), these variations in laccase size may be attributed to the glycosylation degree of the protein.

3.4 Decolourization and degradation experiments

3.4.1 Dye decolourization in liquid medium by Trametes hirsuta and Trametes versicolor

Several white rot fungi (e.g. *Phanerocheate chrysosporium, Pleurotus ostreatus, Bejerkandera adusta, Trametes versicolor*, etc.) have been intensively studied in connection with their dye decolourization ability (Rodríguez *et al*. 1999; Borchert and

Libra 2001; Moreira *et al*. 2001; Conneely *et al*. 2002; Jarosz-Wilkolazka *et al*. 2002; Martins *et al*. 2003; Moldes *et al*. 2003b). Fungal nutrition has repeatedly been shown to be of enormous importance in the effectiveness of fungal decolourization systems using live mycelium (Knapp *et al.* 2001).

The present study investigated decolourization of five textile dyes (Reactive Red HE8B, Reactive Orange 2R, Reactive Black B, Reactive Red ME4BL and Reactive Yellow FG) by *Trametes hirsuta* and *Trametes versicolor.* Initially series of experiments were performed by using the liquid culture method to evaluate the rate of dye decolourization; wherein different concentrations from 1, 10, 50, 100, 250 and 500 mg/L dye were checked. Decolourization was measured at the wavelength of maximum absorbance (λmax,nm) of respective dyes. With the increasing concentration, time delay was observed in rate of decolourization. It is also conferred that there is substrate inhibition to fungal decolourization when initial dye concentration is greater than 100 mg/L (Venkatachalam and Venkatachalam 2008).

The colour change in all the five dyes was observed from 3rd day of incubation in both the fungal strains. Pronounced decolourization by both *T. hirsuta* and *T. versicolor* was found in 10 mg/L concentration wherein all five dyes showed complete decolourization at the end of 13 days of incubation (Fig. 27-31). *T. hirsuta* decolourized all the five dyes on the 13th day of incubation. Similar to former species, *T. versicolor* also showed complete decolourization on the 13th day of Reactive Red HE8B, Reactive Orange 2R, Reactive Black B but Reactive Red ME4BL and Reactive Yellow FG were decolourized up to 97.9 % and 92.3 % respectively at the end of 13 days and complete decolourization was observed on the 15th day of fungal inoculation. This indicates that Reactive Red ME4BL and Reactive Yellow FG were more difficult to be decolourized as compared to all other three dyes (Fig. 32-36). Decolourization efficiency of both species differed which showed that rate of decolourization by *Trametes hirsuta* was relatively faster than that of *Trametes versicolor.*

Previous studies mentioned 95 % removal of HRB 8 dyes by *T. versicolor* in four days (Heinfling *et al.* 1997) and 92.17 % removal of Blue CA by *Trametes hirsuta* in 10 days of incubation (Sathiya-Moorthi *et al*. 2007). Swamy and Ramsay (1999) reported complete decolourization of dye Reactive Black 5 within 2 days.

Trametes sp. was also found to decolourize 89 % Congo red, 54.5 % Rhodamine 6G and 76.1 % Malachite green at 50 μM concentration on the fifth day (Selvam *et al*. 2012). With the exception of Acid Red (97–99 %), other azo dyes (Congo Red, Fast Blue R R salt (FBRR), Amido Black 10 B and Orange G) and anthraquinonic dye (RBBR) were degraded by *Trametes* sp. SQ01 in 7 days (Yang *et al*. 2009). Similar to our result, *T. versicolor* G-99 was slightly less effective, decolourizing Reactive Black B less than 60 % on the 8th day (Mohorcic *et al*. 2006). However, the high decolourizartion percentage was obtained in a short time for indigo carmine (96 %) and phenol red (69 %) in 24 hr indicating suitability for synthetic dye decolourization by *Trametes hirsuta* (Dominguiz *et al*. 2005). The white rot fungus *Coriolus versicolor* could decolourize reactive dye Remazol Brilliant Violet to almost 90 % (Sanghi *et al*. 2006) while it showed maximum decolourization of Cibacron Yellow S-3R (90 %), a recalcitrant azo reactive textile dye at the optimized conditions (Venkatachalam and Venkatachalam 2008).

Apart from *Trametes* sp., many other species of white rot fungi have shown potential for decolourizing dyes in liquid medium. Banat *et al.* (1996) also reported that other white rot fungi like *Hirschioporus larincinus, Inonotus hispidus, Phlebia tremellosa and Coriolus versicolor* can be used to decolourize dyes. Heinfling *et al.* (1997) reported that *Bjerkandera adusta* removed 95 % of HRB 8 dyes within four days. *Thelephora* sp., has a superior potential to decolourize some azo dyes such as Congo red or Amido Black 10 B (Selvam *et al*. 2003). *Dichomitus squalens* and *Irpex flavus* were found to be competitive industrial dye decolourizers (Chander and Arora 2005).

At a lower concentration of 25 mg/L *Pleurotus florida* showed 93.54 % and 83.70 % decolourization of Blue CA and Corazol Violet SR respectively on the 10th day of incubation (Sathiya-Moorthi *et al*. 2007). *Phanerochaetae chrysosporium* removed 85 % of azo dye Orange II in 7 days (Sharma *et al*. 2009) while *Irpex lacteus* decolourized 100 % of Reactive Yellow FG, Reactive Violet 5R, Reactive Magenta HB, and Reactive Yellow MERL by after the 11th day of inoculation (Koyani 2011).

Figure 11: Solid State fermentation A) Growth of *Trametes hirsuta* on 1 mm wheat straw after 12 days of incubation B) Growth of *Trametes versicolor* on Pigeon pea (*Cajanus cajun*) pod shells after 9 days of incubation.

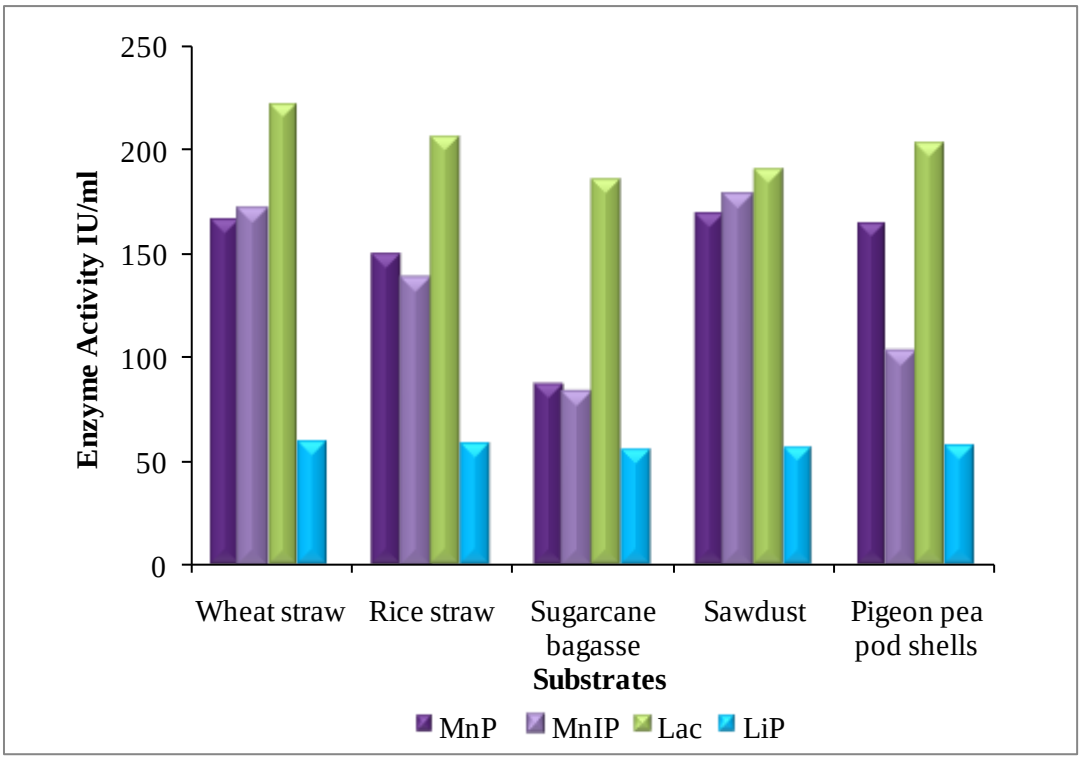

Figure 12: Optimization of agro-industrial waste used as substrates for ligninolytic enzyme production by *Trametes hirsuta*.

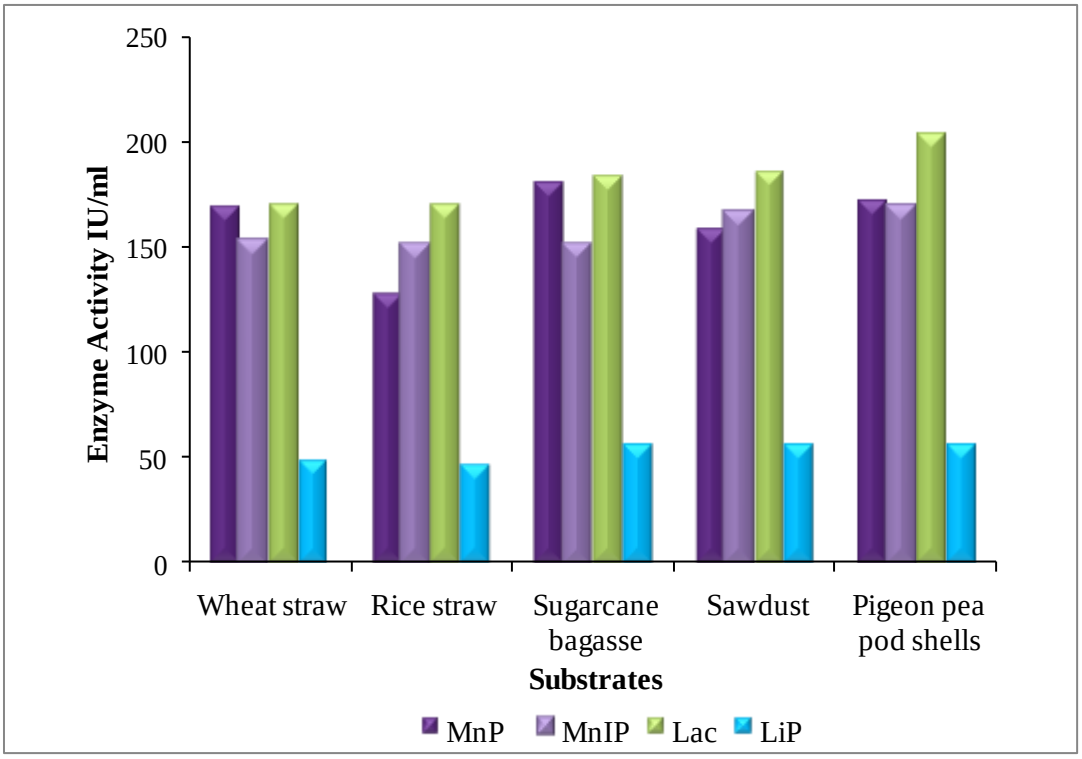

Figure 13: Optimization of agro-industrial waste used as substrates for ligninolytic enzyme production by *Trametes versicolor*.

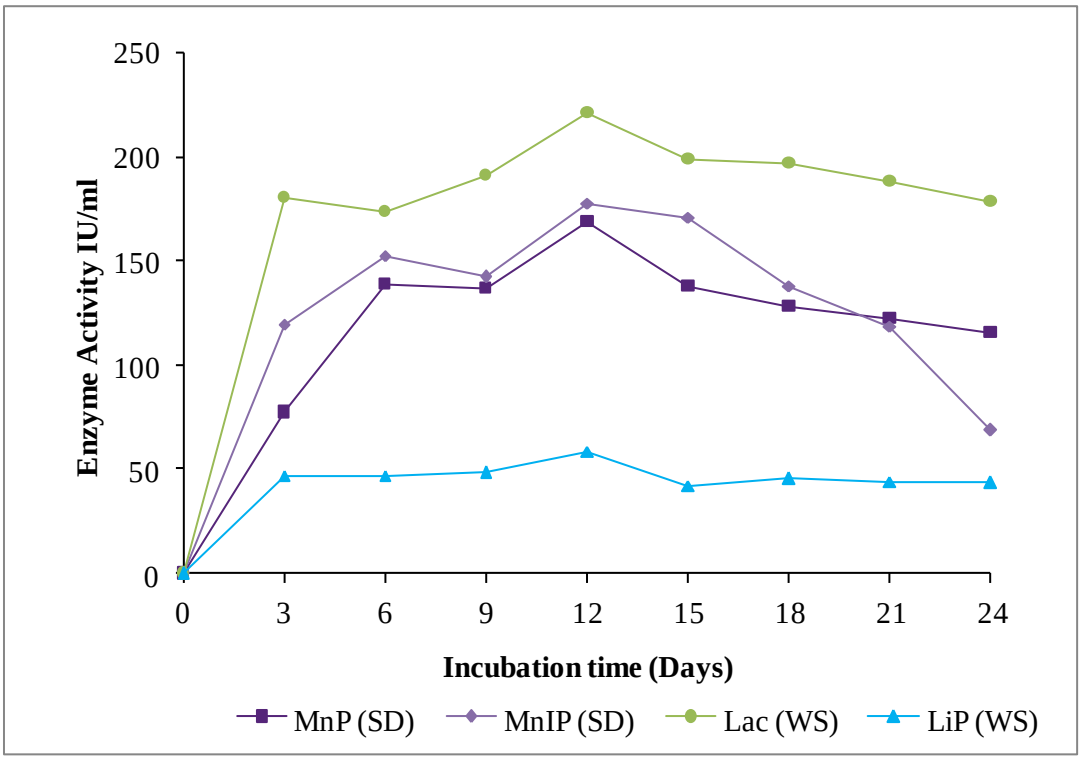

Note: SD- Sawdust, WS- Wheat straw

Figure 14: Optimization of incubation time for ligninolytic enzyme production with respect to their specific substrates by *Trametes hirsuta.*

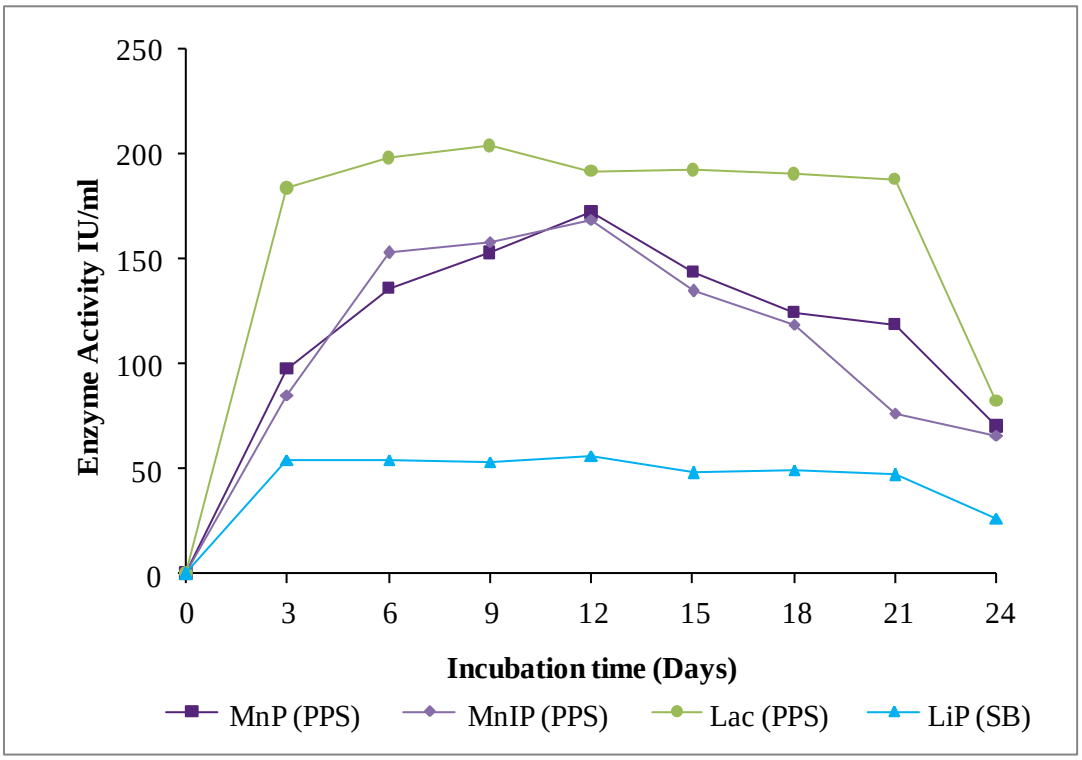

Note: PPPS- Pigeon pea pod shells, SB- Sugarcane bagasse

Figure 15: Optimization of incubation time for ligninolytic enzyme production with respect to their specific substrates by *Trametes versicolor.*

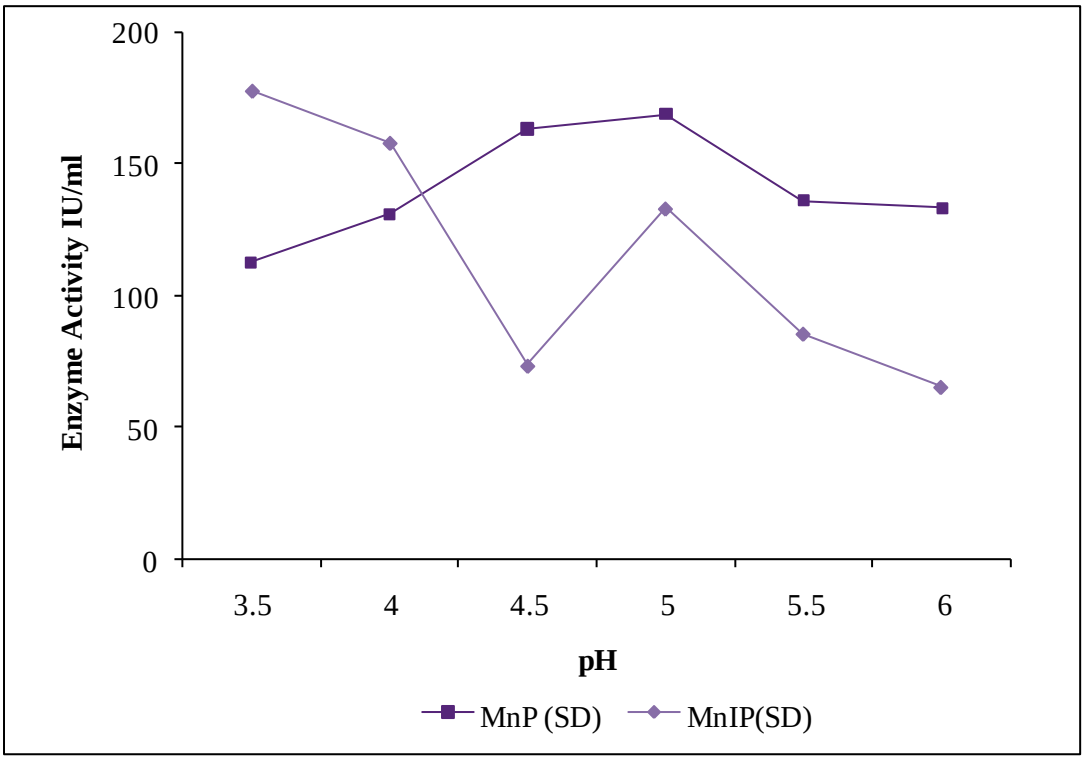

Note: 0.1 M Na-acetate buffer, SD- Sawdust

Figure 16: Effect of pH on MnP and MnIP enzyme activity produced by *Trametes hirsuta*.

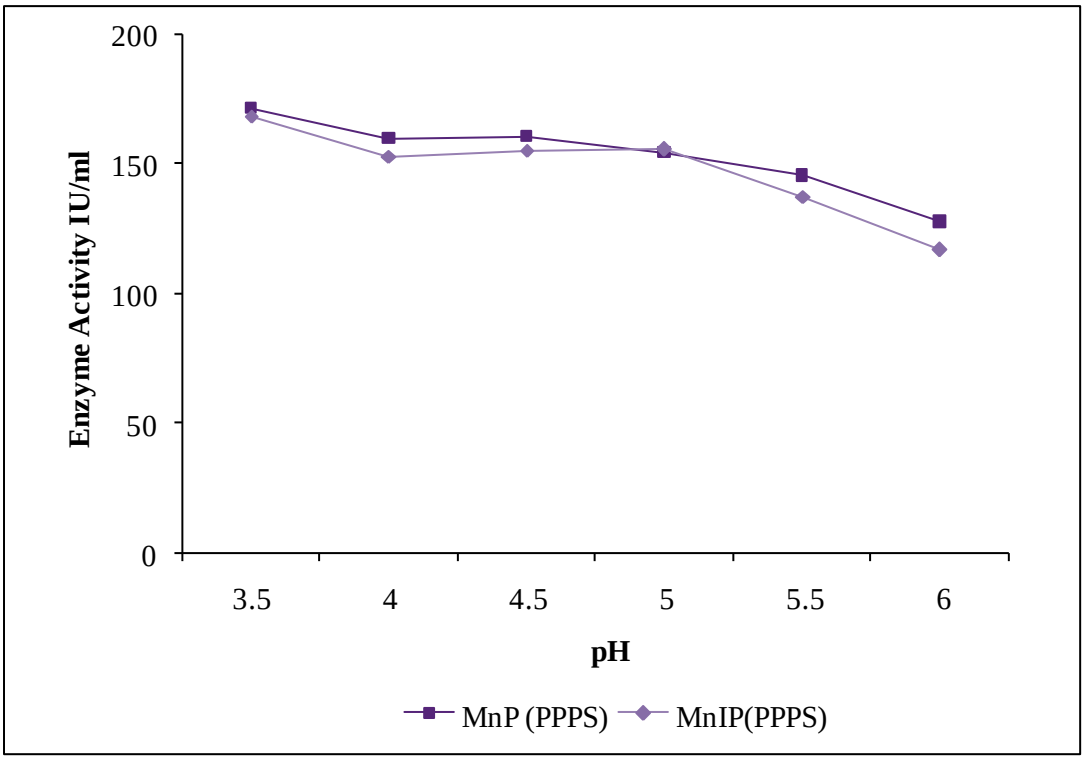

Note: 0.1 M Na-acetate buffer, PPPS- Pigeon pea pod shell

Figure 17: Effect of pH on MnP and MnIP enzyme activity produced by *Trametes versicolor.*

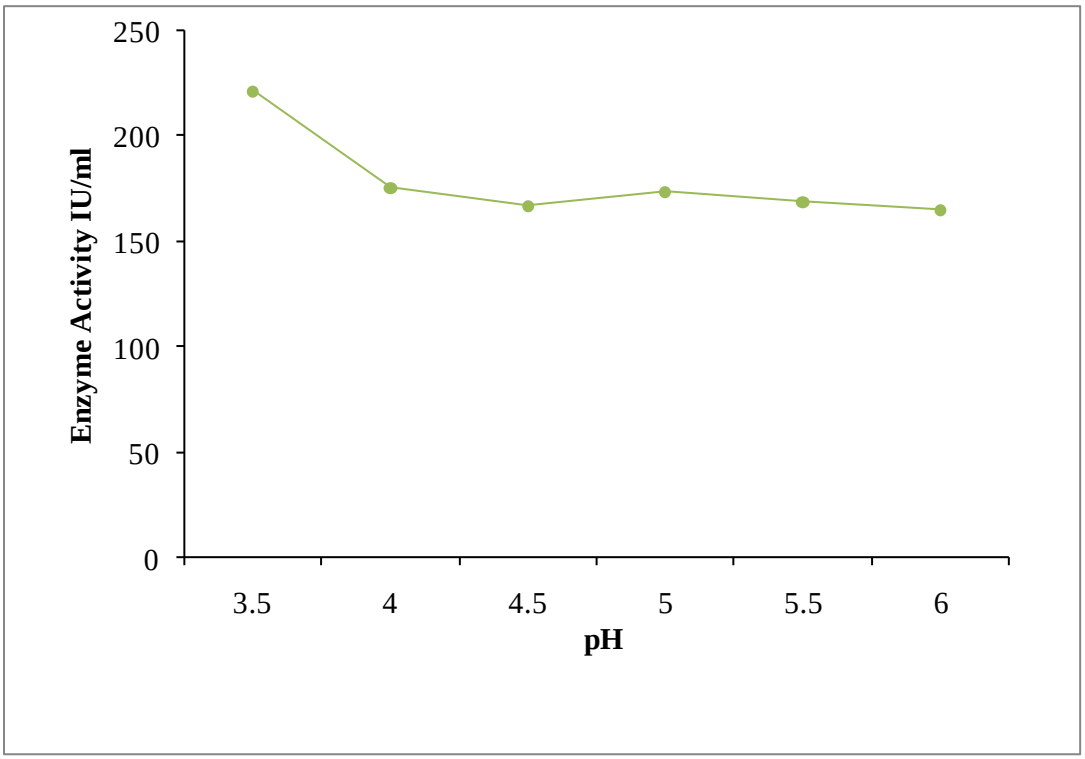

Note**:** 50 mM Na-acetate buffer

Figure 18: Effect of pH on laccase enzyme activity produced by *Trametes hirsuta.*

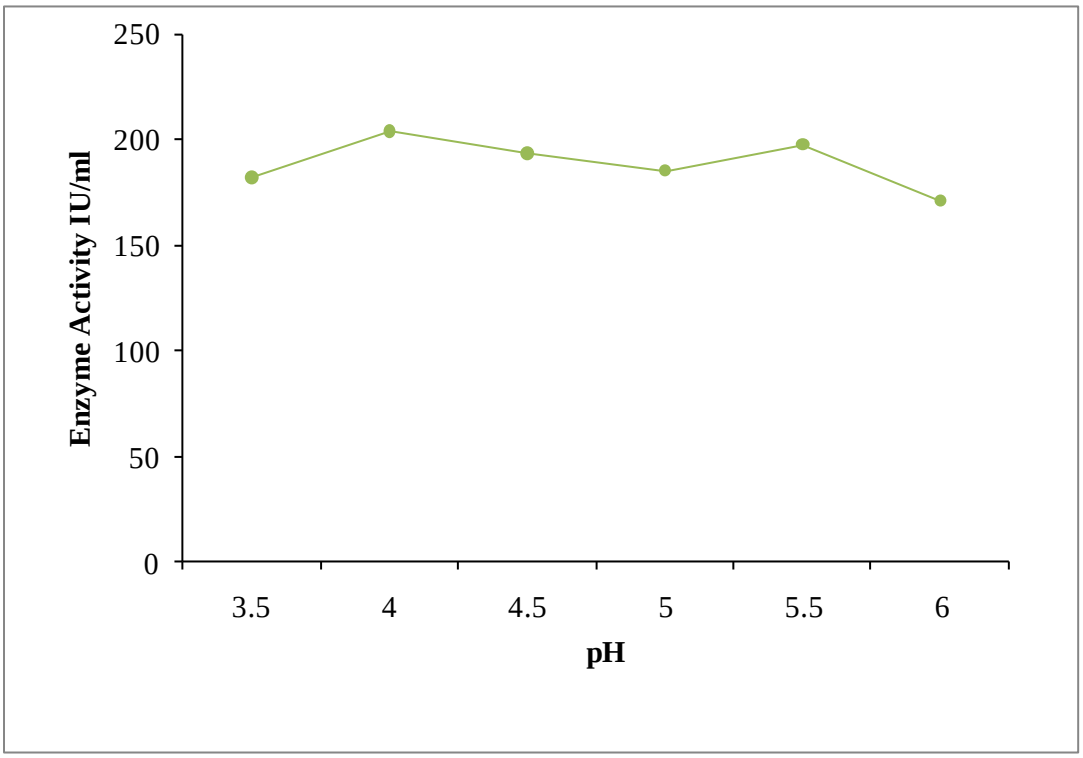

Note**:** 50 mM Na-acetate buffer

Figure 19: Effect of pH on laccase enzyme activity produced by *Trametes versicolor.*

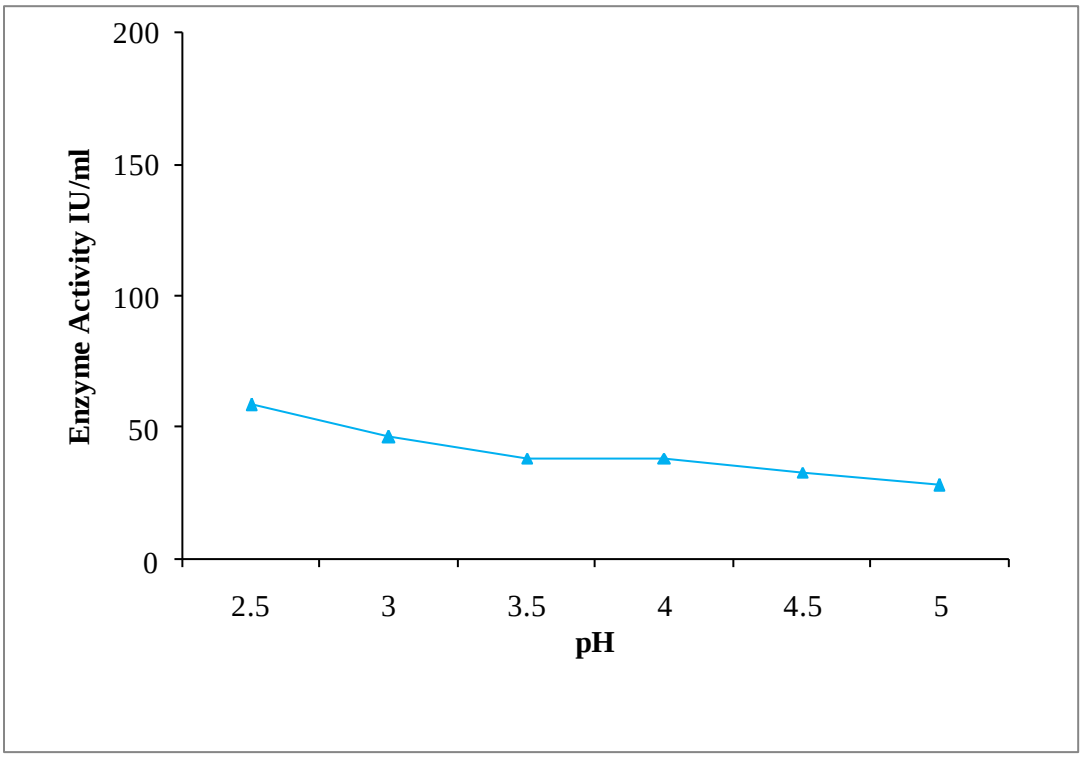

Note**:** 50 mM Na- tartarate buffer

Figure 20: Effect of pH on LiP enzyme activity produced by *Trametes hirsuta.*

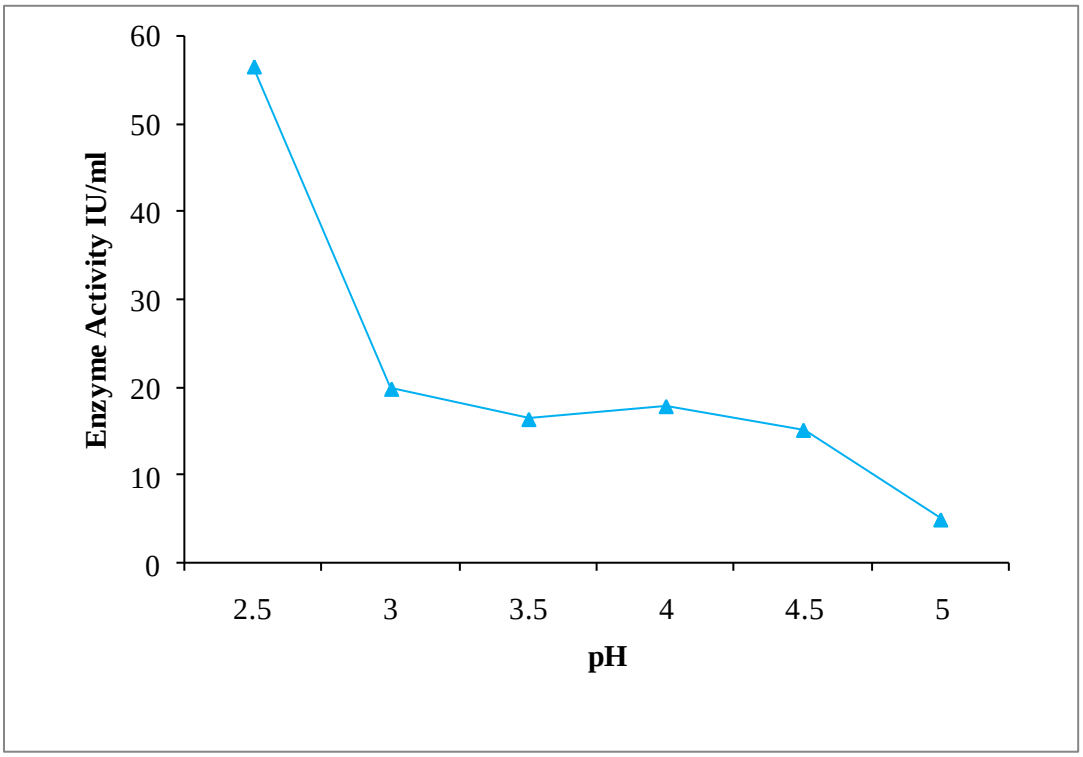

Note: 50 mM Na- tartarate buffer

Figure 21: Effect of pH on LiP enzyme activity produced by *Trametes versicolor.*

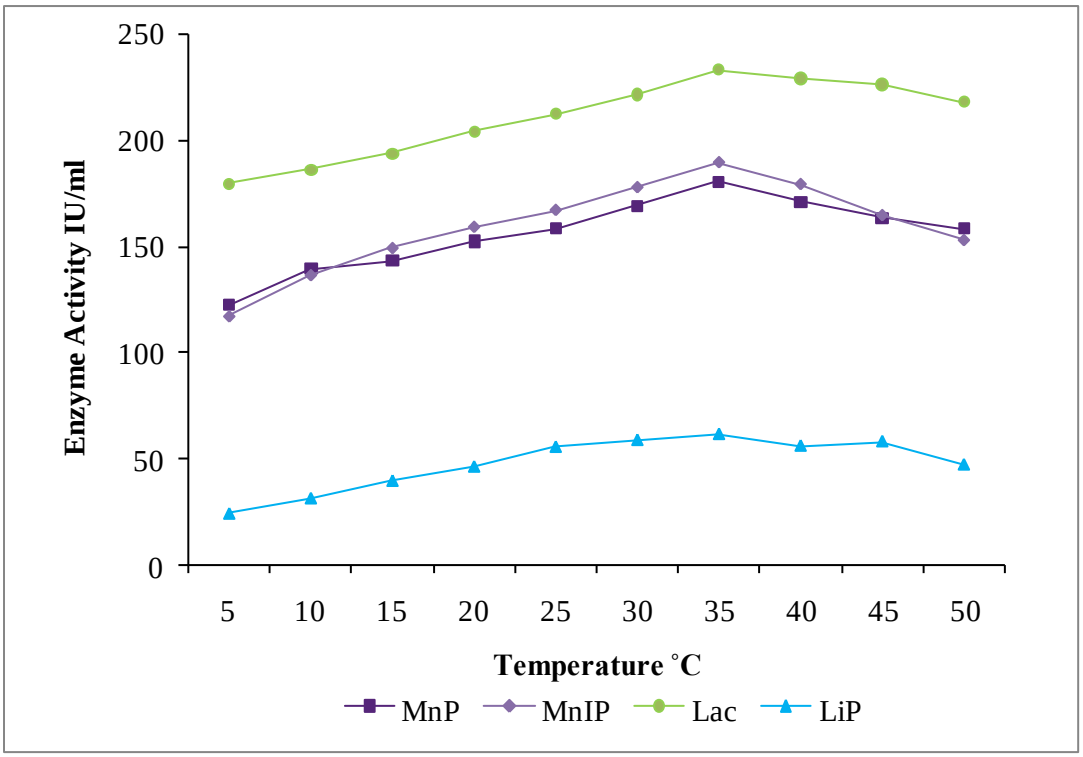

Figure 22: Effect of temperature on ligninolytic enzyme production by *Trametes hirsuta.*

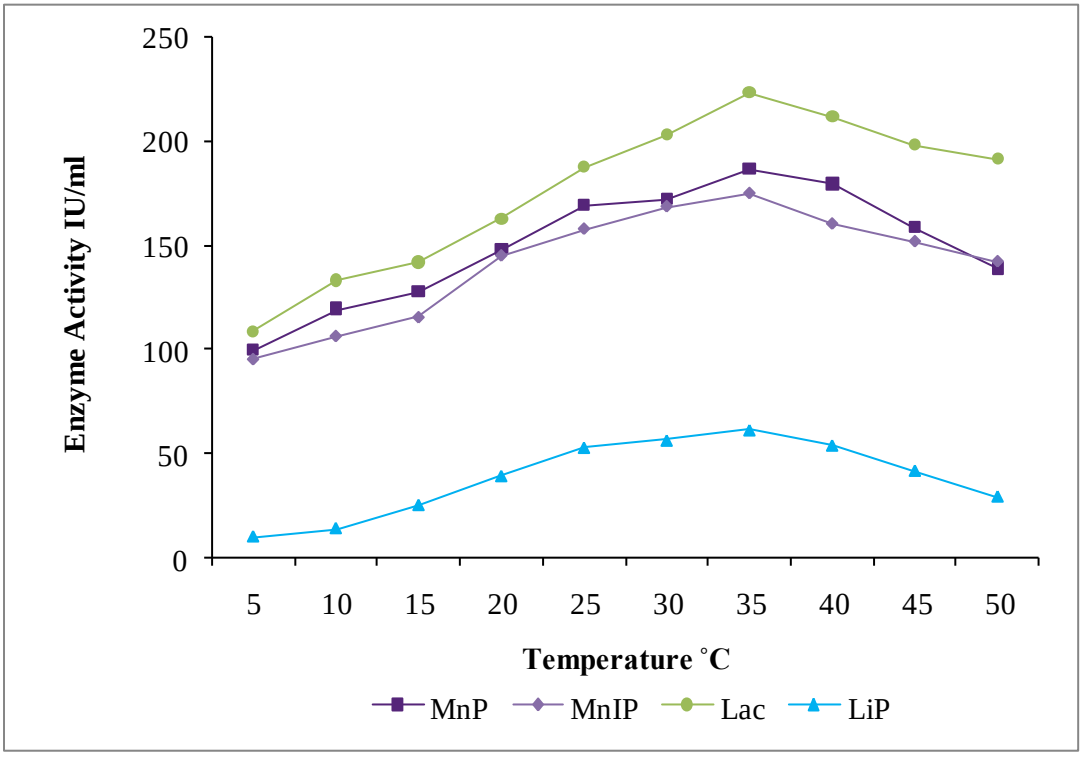

Figure 23: Effect of temperature on ligninolytic enzyme production by *Trametes versicolor.*

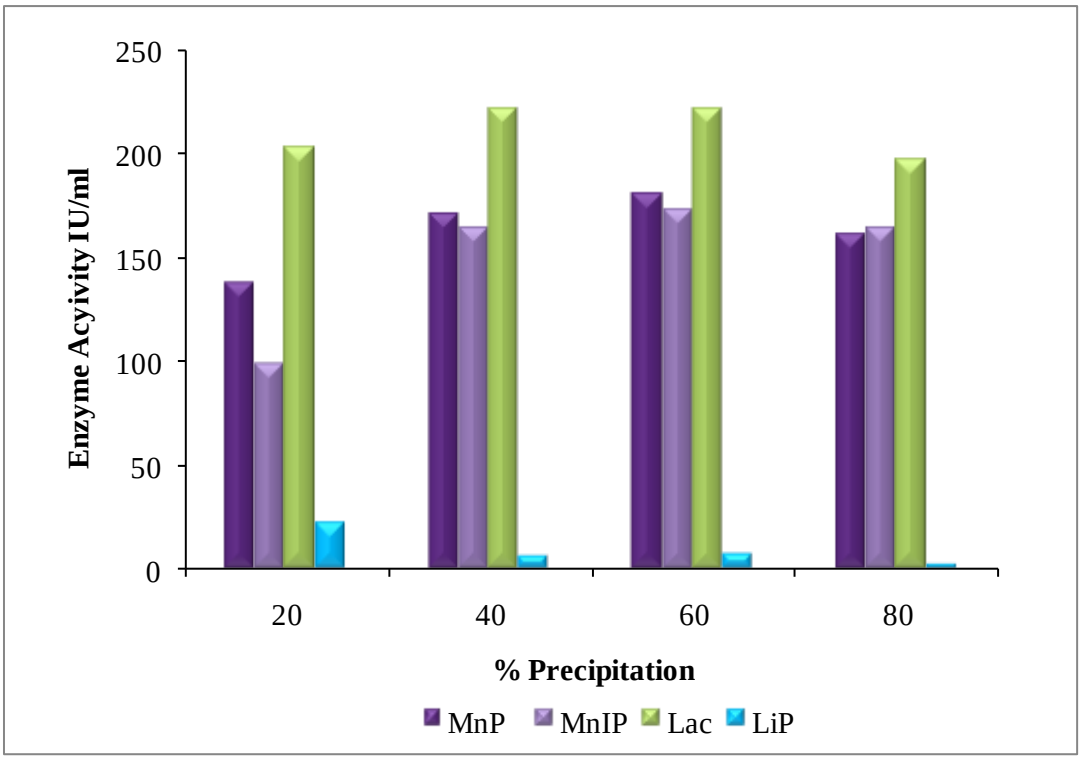

Figure 24: Production profile of ligninolytic enzymes after partial purification with ammonium sulphate precipitation produced by *Trametes hirsuta.*

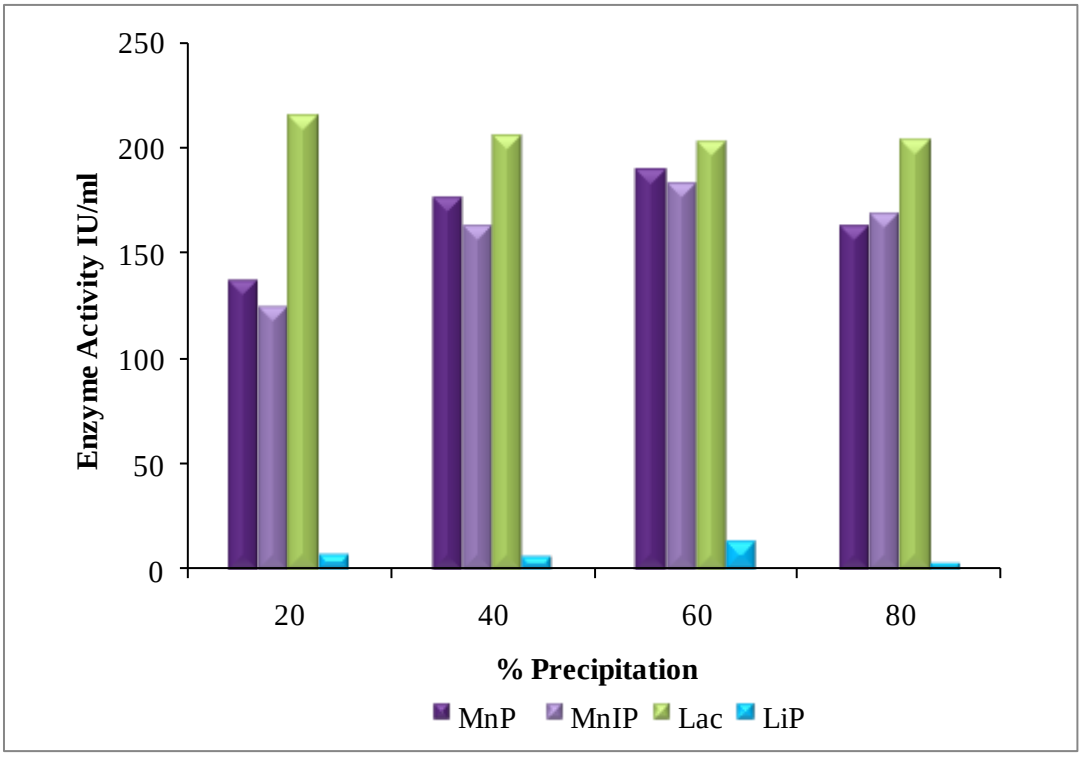

Figure 25: Production profile of ligninolytic enzymes after partial purification with Ammonium sulphate precipitation produced by *Trametes versicolor.*

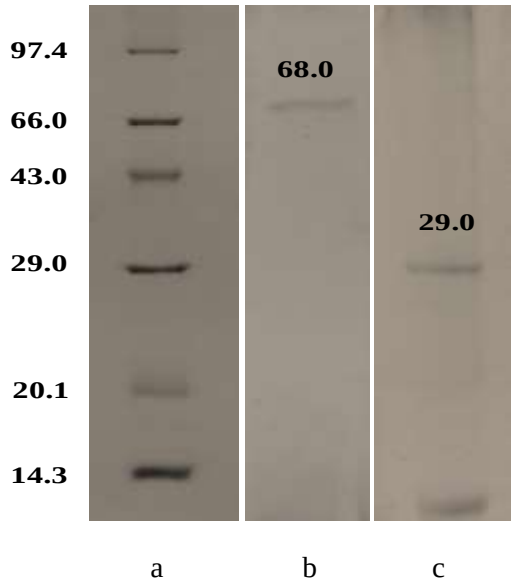

Figure 26: SDS-PAGE of the purified Laccase from fungal strains a) marker b) *Trametes hirsuta and* c) *Trametes versicolor.*

Figure 27: Decolourization of dye Reactive Red HE8B in liquid medium by (left to right) *Trametes hirsuta*, Control and *Trametes versicolor*.

Figure 28: Decolourization of dye Reactive Orange R in liquid medium by (left to right) *Trametes hirsuta*, Control and *Trametes versicolor*.

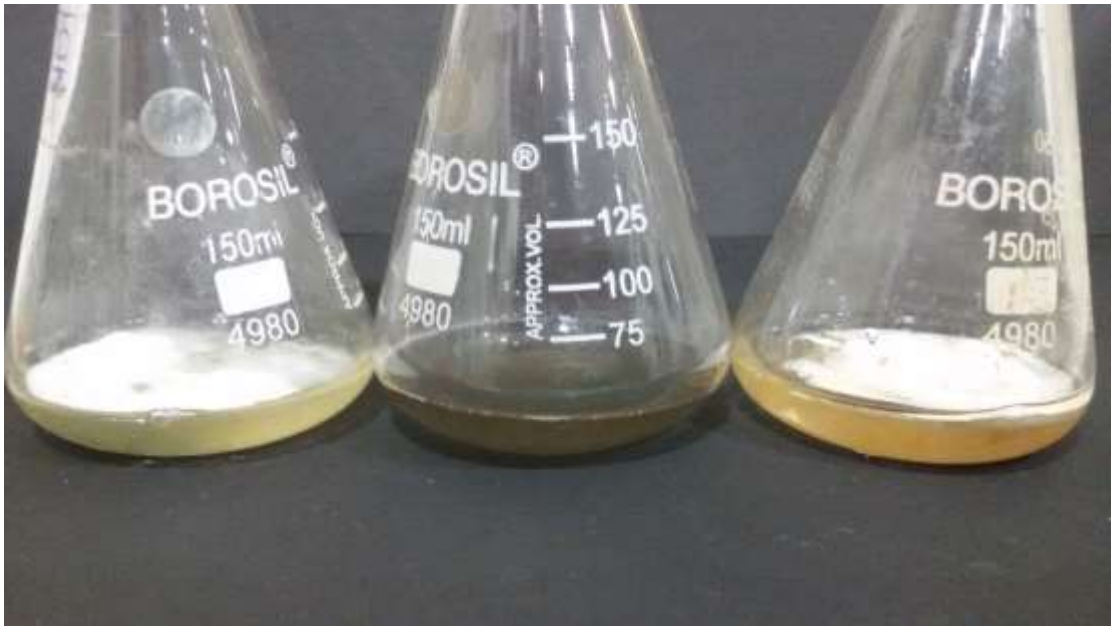

Figure 29: Decolourization of dye Reactive Black B in liquid medium by (left to right) *Trametes hirsuta*, Control and *Trametes versicolor*.

Figure 30: Decolourization of dye Reactive Red ME4BL in liquid medium by (left to right) *Trametes hirsuta*, Control and *Trametes versicolor*.

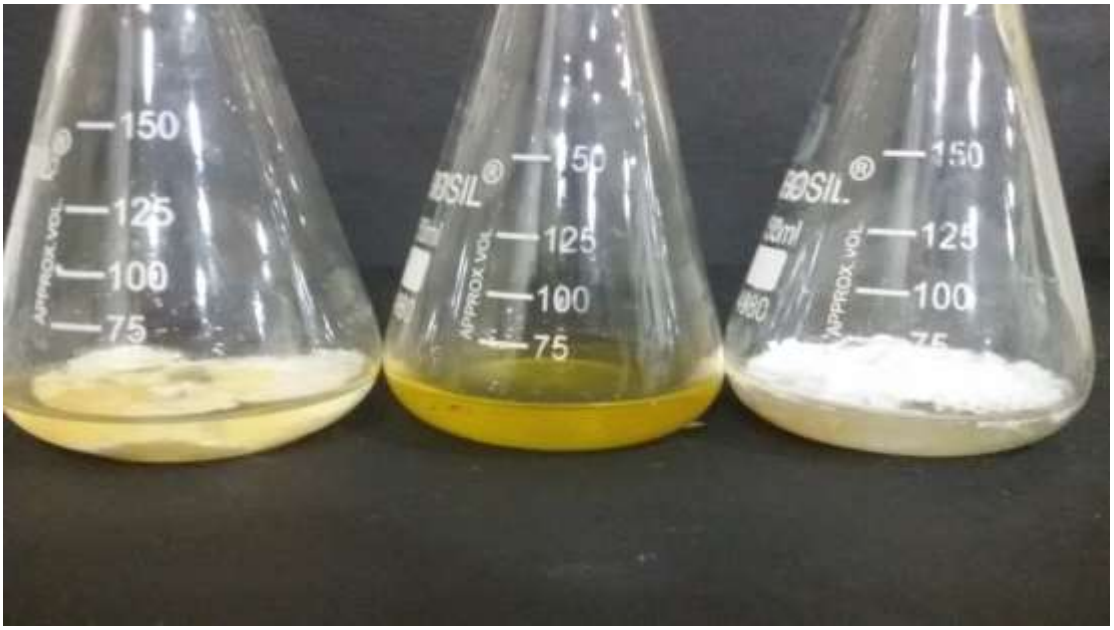

Figure 31: Decolourization of dye Reactive Yellow FG in liquid medium by (left to right) *Trametes hirsuta*, Control and *Trametes versicolor*.

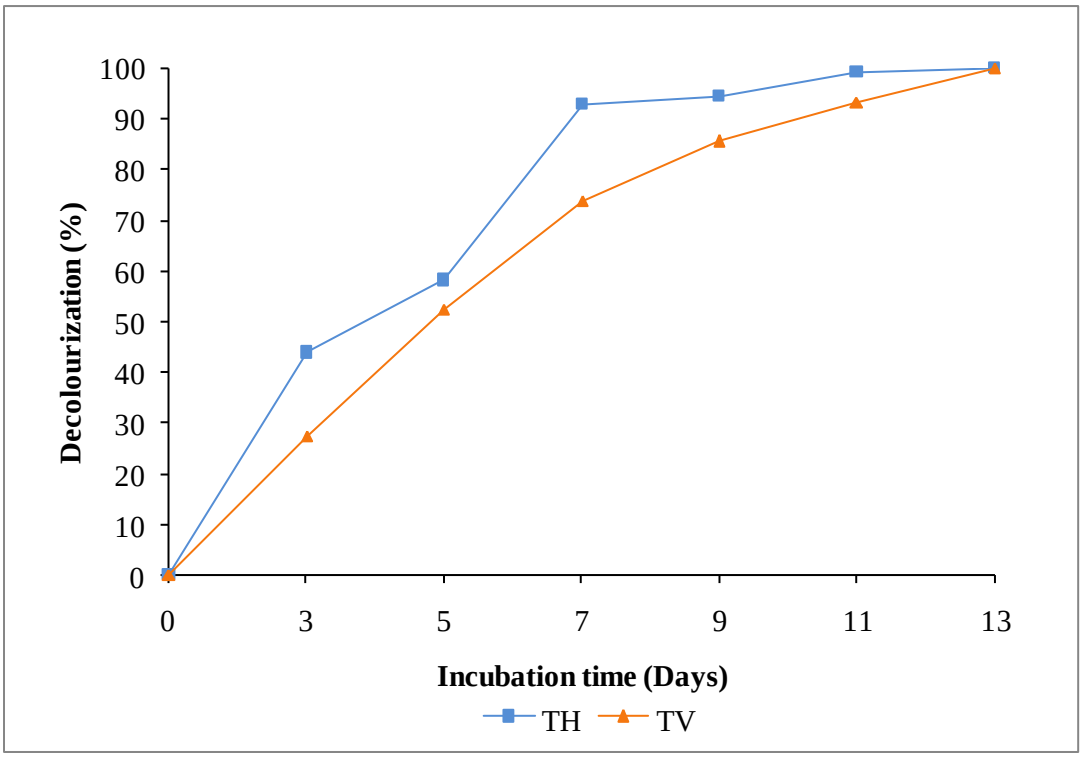

Figure 32: Percent decolourization of dye Reactive Red HE8B in liquid medium by *Trametes hirsuta* (TH) and *Trametes versicolor* (TV).

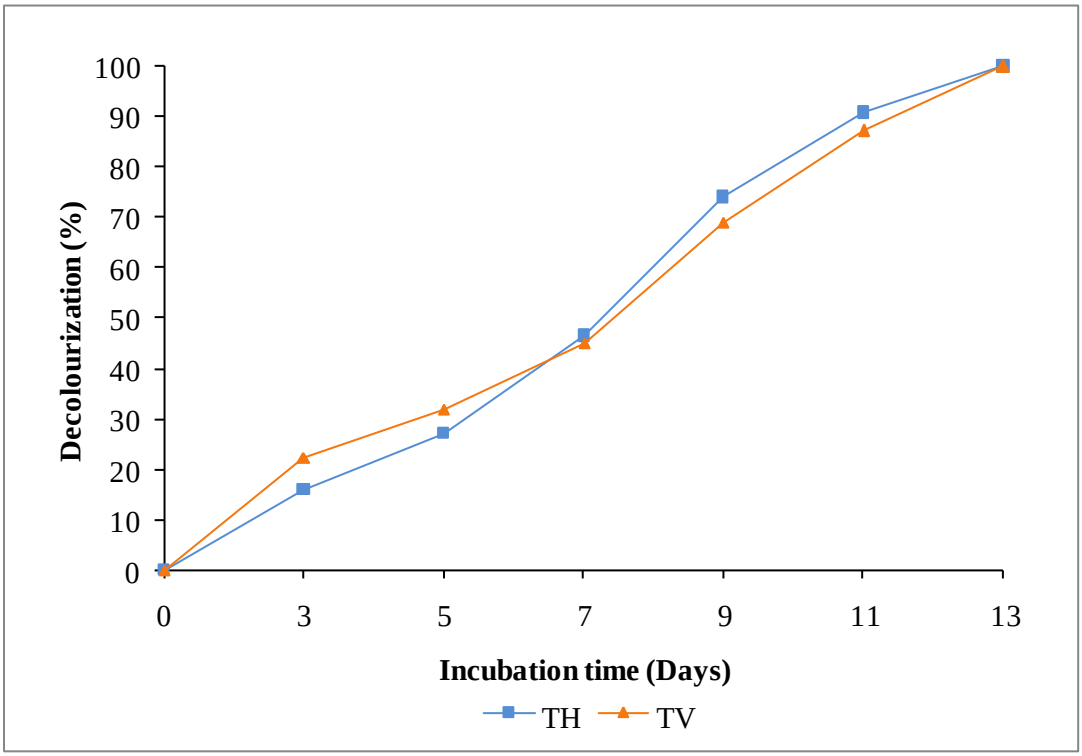

Figure 33: Percent decolourization of dye Reactive Orange 2R in liquid medium by *Trametes hirsuta* (TH) and *Trametes versicolor* (TV).

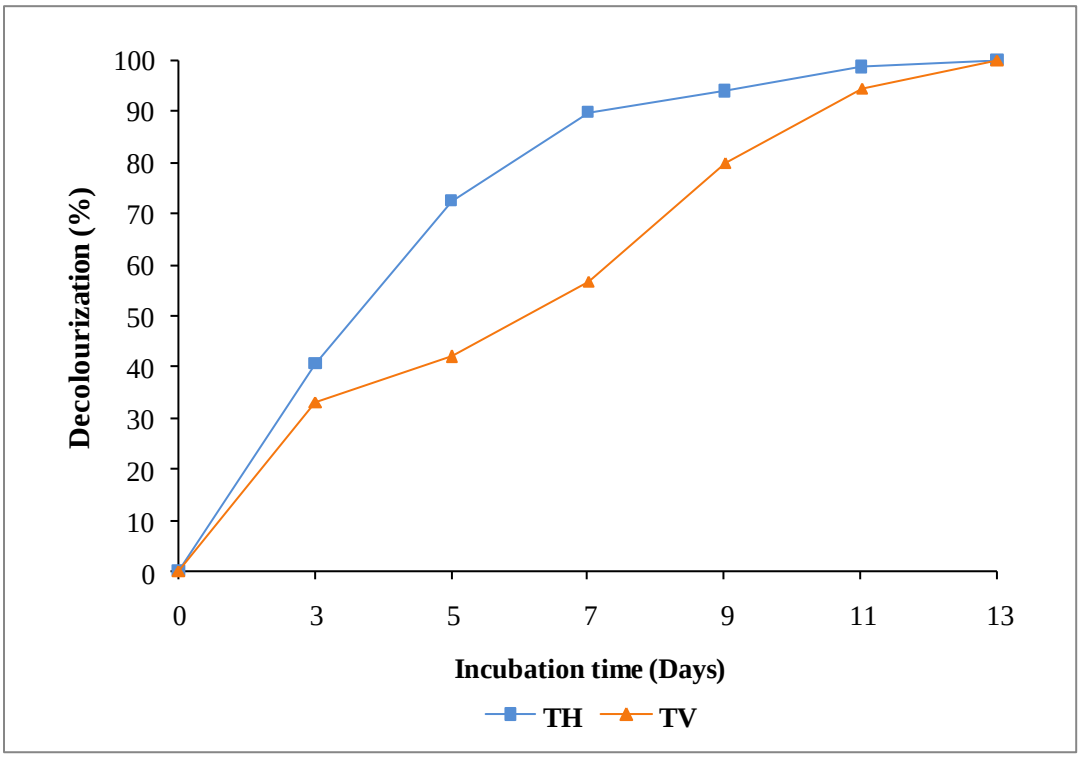

Figure 34: Percent decolourization of dye Reactive Black B in liquid medium by *Trametes hirsuta* (TH) **and *Trametes versicolor*** (TV).

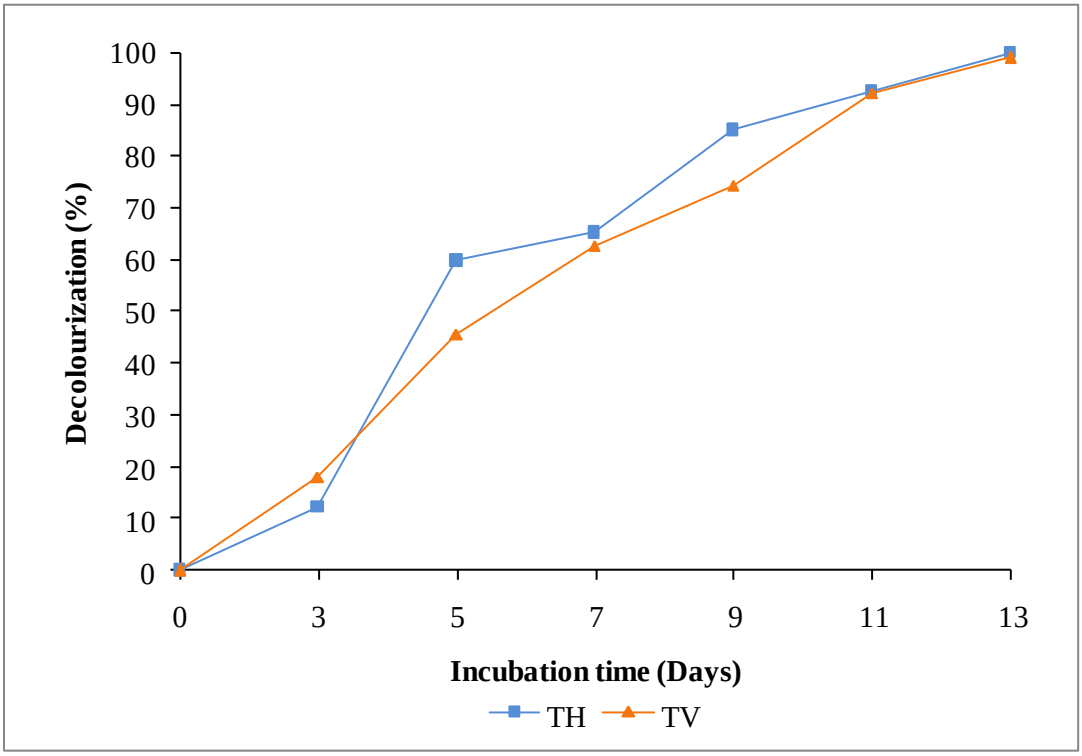

Figure 35: Percent decolourization of dye Reactive Red ME4BL in liquid medium by *Trametes hirsuta* (TH) **and *Trametes versicolor*** (TV).

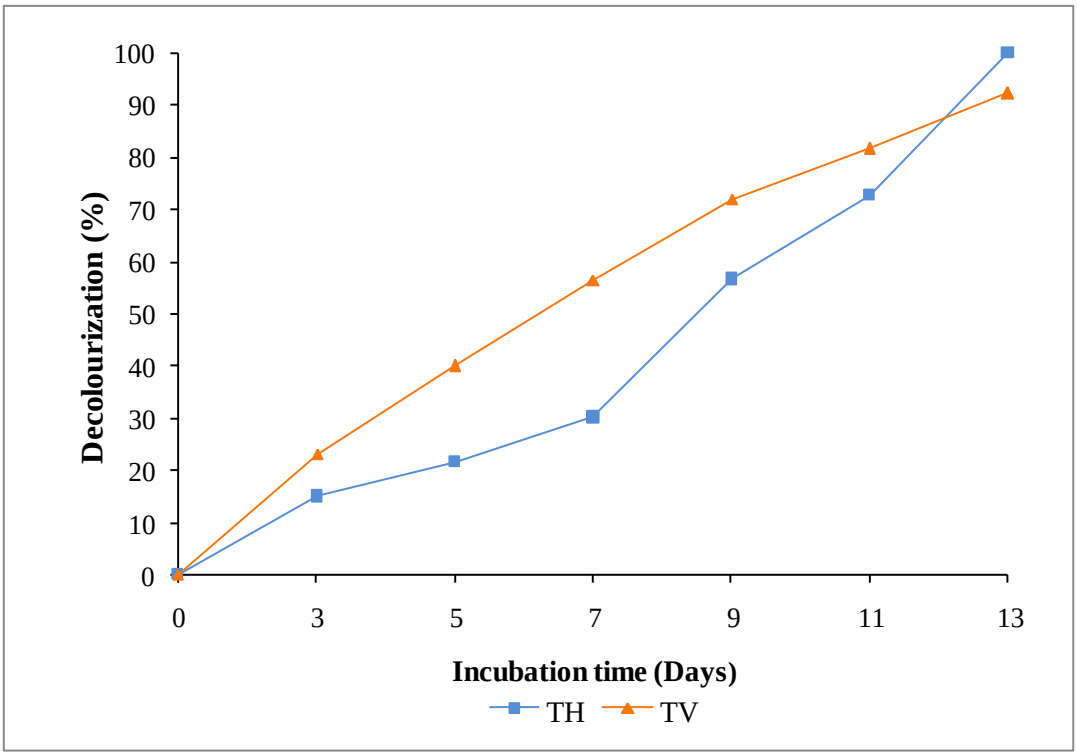

Figure 36: Percent decolourization of dye Reactive Yellow FG in liquid medium by *Trametes hirsuta* (TH) **and *Trametes versicolor*** (TV).

3.4.2 FTIR (Fourier Transform Infrared) Spectroscopy Analysis

In recent years, characterization of the different samples by vibrational spectroscopies such as Fourier transform infrared (FTIR) are very common (Goodacre *et al.* 2000; Oberreuter *et al.* 2002; Gomare *et al.* 2009). Owing to non-specific characteristics of the extracellular ligninolytic enzymes of white rot fungus, they have the ability to degrade a wide spectrum of recalcitrant organo-pollutants such as chlorinated phenols and various xenobiotic compounds including synthetic dyes, pesticides, PCBs and PAHs (Heinfling *et al.* 1997; Novotny *et al.* 2001; Rigas and Drista 2005; Gao *et al.* 2006). Therefore, FTIR analysis was carried out to confirm the biodegradation of these compounds by ligninolytic enzymes, (Parshetti *et al.* 2006; Kalme *et al.* 2007; Dhanve *et al.* 2009; Ghodake *et al.* 2009, Koyani *et al*. 2014).

The UV-VIS spectrometry allows us to evaluate the biodegradation process via absorbance ratio (Glen and Gold 1983) while with FTIR, differences in the dye structure can be distinguished by comparing the spectra of the treated and untreated dyes (Rathod and Archana 2013). Therefore, UV-VIS spectrometry coupled with FTIR spectroscopy is an important tool in the analysis of biodegradation of recalcitrant compounds (Santos *et al*. 2014). FTIR analysis points out the structural alterations/degradation of the dye molecule which leads to the decolourization and investigates the changes in surface of functional groups of the extracted metabolites before and after microbial decolourization (Lade *et al.* 2012). In the present investigation, the FTIR spectra of all the tested control dyes and its treatment with fungi *Trametes hirsuta* and *Trametes versicolor* showed the specific peaks in specific region of stretching (4000 to 500 cm^{-1}), which clarifies the degradation of the dyes with fungal enzymes over decolourization.

i) Reactive Red HE8B dye

FTIR spectrum of control Reactive Red HE8B dye (Fig. 37a and 38a) displayed a wide peak at 3454 cm^{-1} representing -N-H stretching and small peaks at about 2915 cm^{-1} and 2840 cm^{-1} are in aromatic and aliphatic –C-H bonds. Stretching at 1611cm^{-1}, 1476 cm^{-1}, and 1211 cm^{-1} demonstrates the presence of aromatic –C=C–, azo –N=N– and SO_2 groups respectively while peak at 1411 cm^{-1} is of ring vibrations. However peaks at 1040 cm^{-1} for C-N stretching and 976 cm^{-1} for C-H bend clearly confirmed its chemical structure and nature of reactive dye.

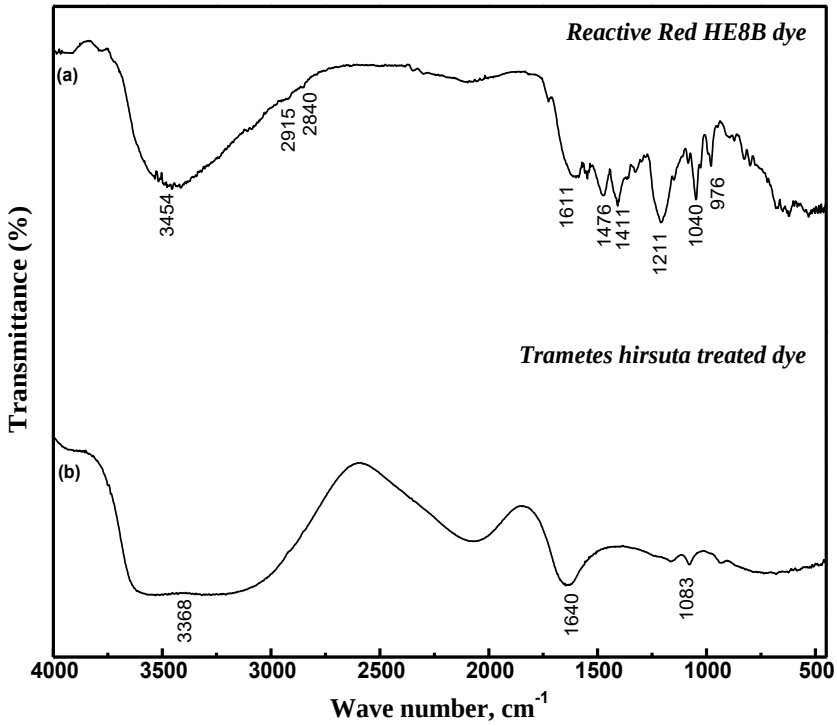

Figure 37: FTIR spectra of a) control dye Reactive Red HE8B and b) its degradation product treated by *Trametes hirsuta.*

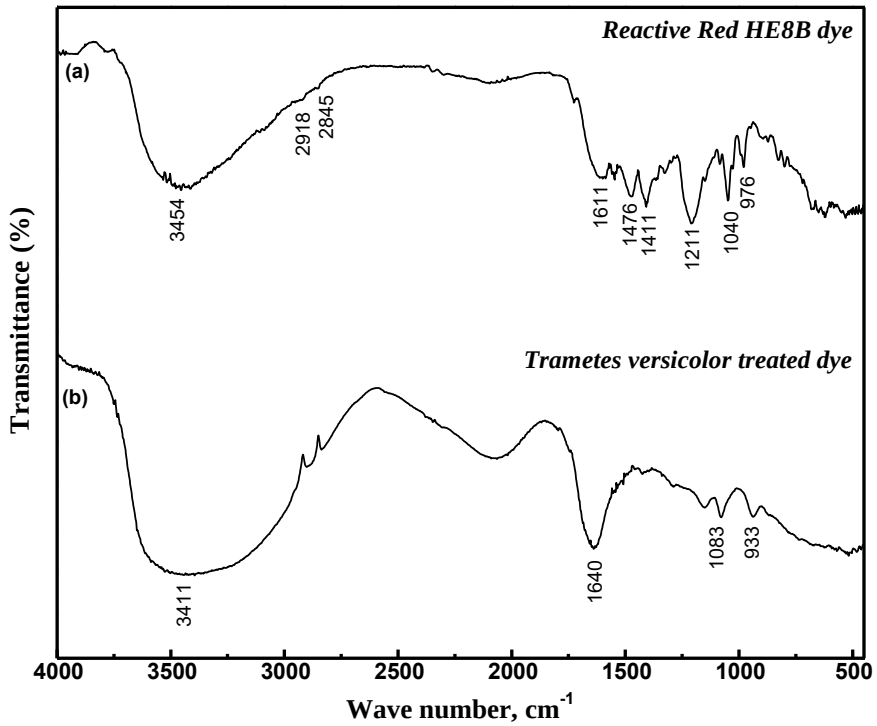

Figure 38: FTIR spectra of a) control dye Reactive Red HE8B and b) its degradation product treated by *Trametes versicolor.*

FTIR spectrum of Reactive Red HE8B dye treated with *Trametes hirsuta* (Fig. 37b) and *Trametes versicolor* (Fig. 38b) showed complete disappearance of a peak at 1476 cm^{-1} for an azo stretching. Broadband was observed at peak 3368 cm^{-1} (*Trametes hirsuta)* and 3411 cm^{-1} (*Trametes versicolor)* for-N-H stretch and peak at 1083 cm^{-1} (*Trametes hirsuta)* and 1083 cm^{-1} (*Trametes versicolor)* for C-N stretch of Ar-NH-R indicates the degradation.

ii) Reactive Orange 2R dye

FTIR spectrums of control Reactive Orange 2R dye (Fig. 39a and 40a) displayed peaks, i.e. 3446 cm^{-1} for -N-H stretching, 2925 cm^{-1} and 2852 cm^{-1} for aromatic and aliphatic –C-H stretching, 1628 cm^{-1} for aromatic –C=C– stretching, 1513 cm^{-1} for –N-N- stretching, 1382 cm^{-1} for ring vibrations, and 1136 cm^{-1} for SO_2 stretching. While peaks at 1049 cm^{-1} for C-N stretch and at 700 cm^{-1} for C-H bend clearly suggested the nature of dye and confirmed its chemical structure.

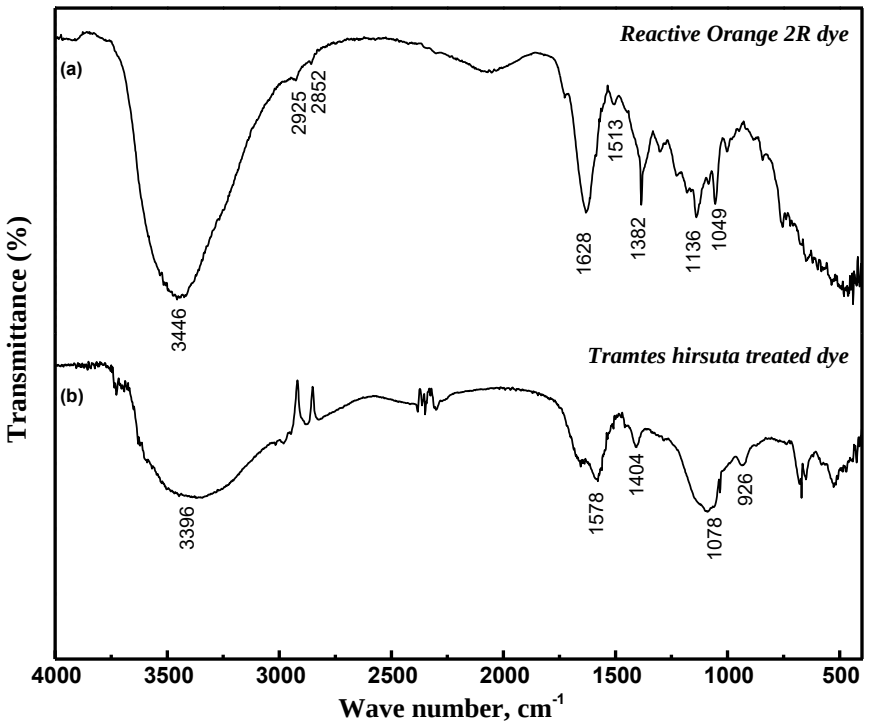

Figure 39: FTIR spectra of a) control dye Reactive Orange 2R and b) its degradation product treated by *Trametes hirsuta.*

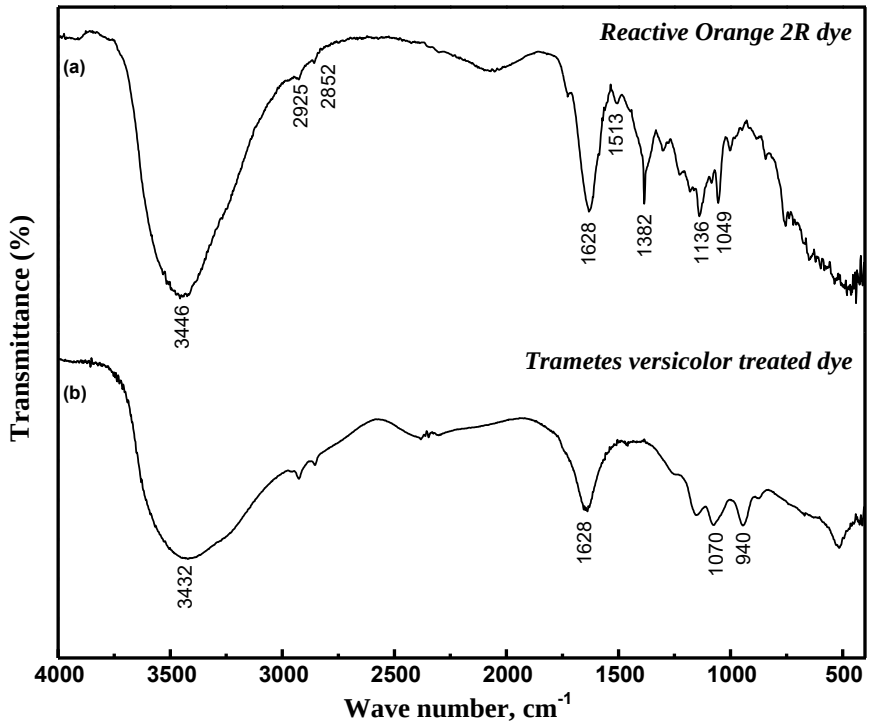

Figure 40: FTIR spectra of a) control dye Reactive Orange 2R and b) its degradation product treated by *Trametes versicolor.*

FTIR spectrum of Reactive Orange 2R dye treated with *Trametes hirsuta* (Fig. 39b) and *Trametes versicolor* (Fig. 40b) showed complete disappearance of a peak at 1513 cm^{-1} for an azo stretch. Broadband was observed at peak 3396 cm^{-1} (*Trametes hirsuta)* and at 3432 cm^{-1} (*Trametes versicolor)* for-N-H stretch, peak at 926 cm^{-1} (*Trametes hirsuta)* and at 940 cm^{-1} (*Trametes versicolor)* for C-H bend and peak at 1078 cm^{-1} (*Trametes hirsuta)* and at 1070 cm^{-1} (*Trametes versicolor)* for C-N stretch of Ar-NH-R with shifting indicated the degradation of dye.

iii) Reactive Black B dye

FTIR spectrum of control Reactive Black B dye (Fig. 41a and 42a) displayed a peak at 3454 cm^{-1} for -N-H stretch, smaller peaks at about 2900 cm^{-1} and 2800 cm^{-1} for aromatic and aliphatic –C-H stretching, 1618 cm^{-1} for aromatic –C=C– stretching, 1483 cm^{-1} for –N=N- stretching, 1290 cm^{-1} for ring vibrations, and 1126 cm^{-1} for SO_2 stretching. While peaks at 1047 cm^{-1} for C-N stretch and at about 847 cm^{-1} for C-H bend clearly suggested the nature of dye and confirmed its chemical structure.

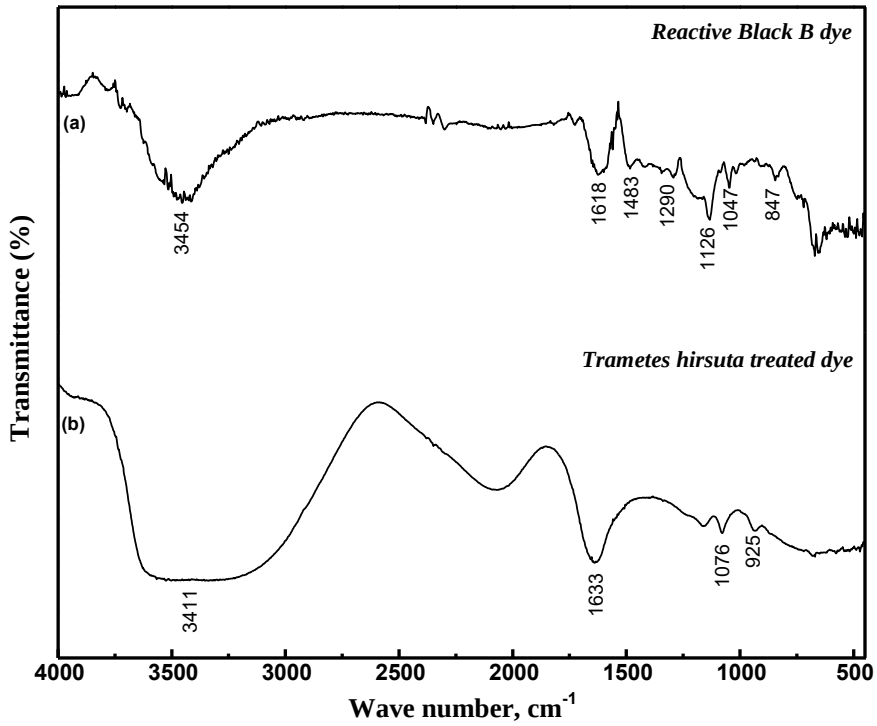

Figure 41: FTIR spectra of a) control dye Reactive Black B and b) its degradation product treated by *Trametes hirsuta.*

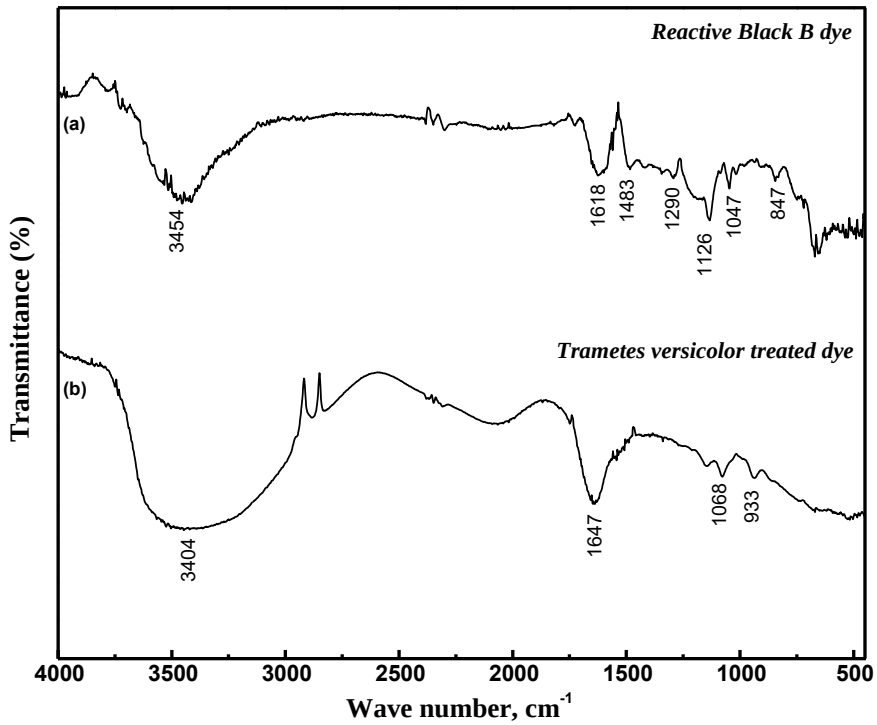

Figure 42: FTIR spectra of a) control dye Reactive Black B and b) its degradation product treated by *Trametes versicolor.*

FTIR spectrum of Reactive Black B dye treated with *Trametes hirsuta* (Fig. 41b) and *Trametes versicolor* (Fig. 42b) showed complete disappearance of a peak at 1483 cm^{-1} for an azo stretch. Broad band was observed at peak 3411 cm^{-1} (*Trametes hirsuta)* and at 3404 cm^{-1} (*Trametes versicolor)* for-N-H stretch, a peak at 925 cm^{-1} (*Trametes hirsuta)* and at 933 cm^{-1} (*Trametes versicolor)* for C-H bend and peak at 1076 cm^{-1} (*Trametes hirsuta)* and at 1068 cm^{-1} (*Trametes versicolor)* for C-N stretch of Ar-NH-R with shifting also proved breaking of dye structure.

iv) Reactive Red ME4BL dye

FTIR spectrum of control Reactive Red ME4BL dye (Fig. 43a and 44a) displayed a peak at 3456 cm^{-1} for -N-H stretch, small peaks at about 2900 cm^{-1} and 2800 cm^{-1} for aromatic and aliphatic –C-H stretching, 1626 cm^{-1} for aromatic –C=C– stretching, 1540 cm^{-1} for –N=N– stretching, 1404 cm^{-1} for ring vibrations, and 1210 cm^{-1} for SO_2 stretching. While peaks at 1033 cm^{-1} for C-N stretch and at about 700 cm^{-1} for C-H bend clearly suggested the nature of dye and confirmed its chemical structure.

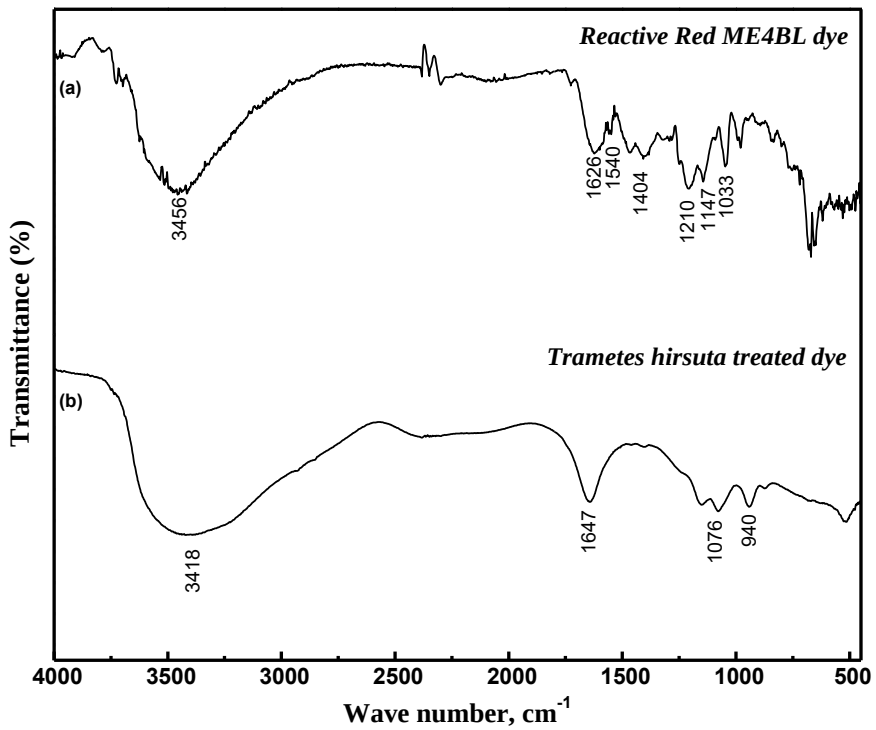

Figure 43: FTIR spectra of a) control dye Reactive Red ME4BL and b) its degradation product treated by *Trametes hirsuta.*

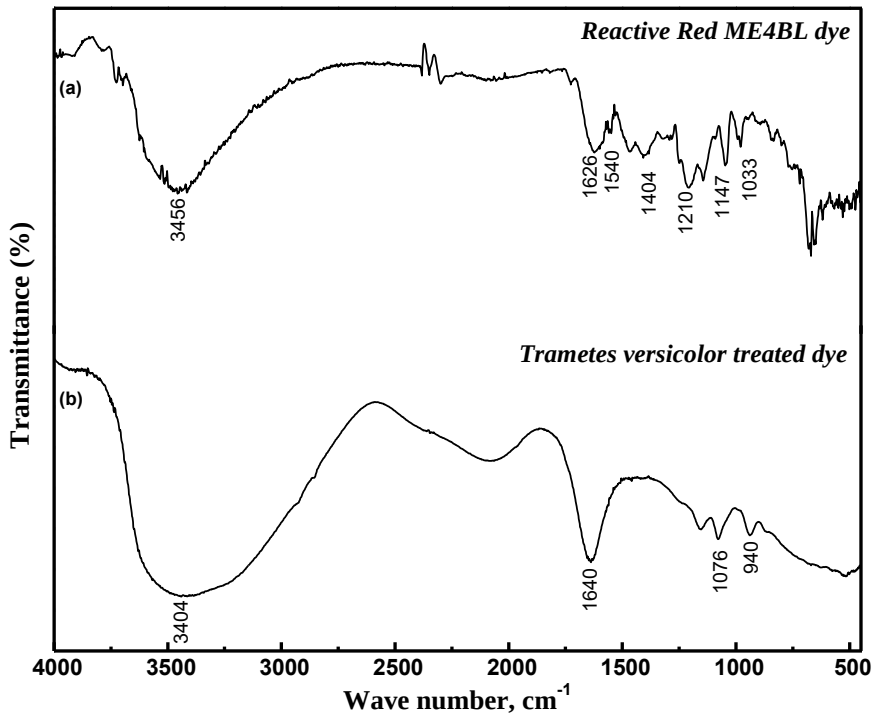

Figure 44: FTIR spectra of a) control dye Reactive Red ME4BL and b) its degradation product treated by *Trametes versicolor.*

FTIR spectrum of Reactive Red ME4BL dye treated with *Trametes hirsuta* (Fig. 43b) and *Trametes versicolor* (Fig. 44b) showed complete disappearance of a peak at 1540 cm^{-1} for an azo stretch. Broad band was observed at peak 3418 cm^{-1} (*Trametes hirsuta)* and at 3404 cm^{-1} (*Trametes versicolor)* for-N-H stretch, peak at 940 cm^{-1} (*Trametes hirsuta)* and at 940 cm^{-1} (*Trametes versicolor)* for C-H bend and peak at 1076 cm^{-1} (*Trametes hirsuta)* and at 1076 cm^{-1} (*Trametes versicolor)* for C-N stretch of Ar-NH-R indicated the degradation.

v) Reactive Yellow FG dye

FTIR spectrum of control Reactive Yellow FG dye (Fig. 45a and 46a) displayed a peak at 3613 cm^{-1} for -N-H stretching, 2976 cm^{-1} and 2896 cm^{-1} for aromatic and aliphatic –C-H stretching, 1693 cm^{-1} for aromatic –C=C– stretching, 1549 cm^{-1} for –N=N– stretching, 1339 cm^{-1} for ring vibrations, and 1222 cm^{-1} for SO_2 stretching. While peaks at 1042 cm^{-1} for C-N stretch and at 723 cm^{-1} for C-H bend clearly suggested the nature of dye and confirmed its chemical structure.

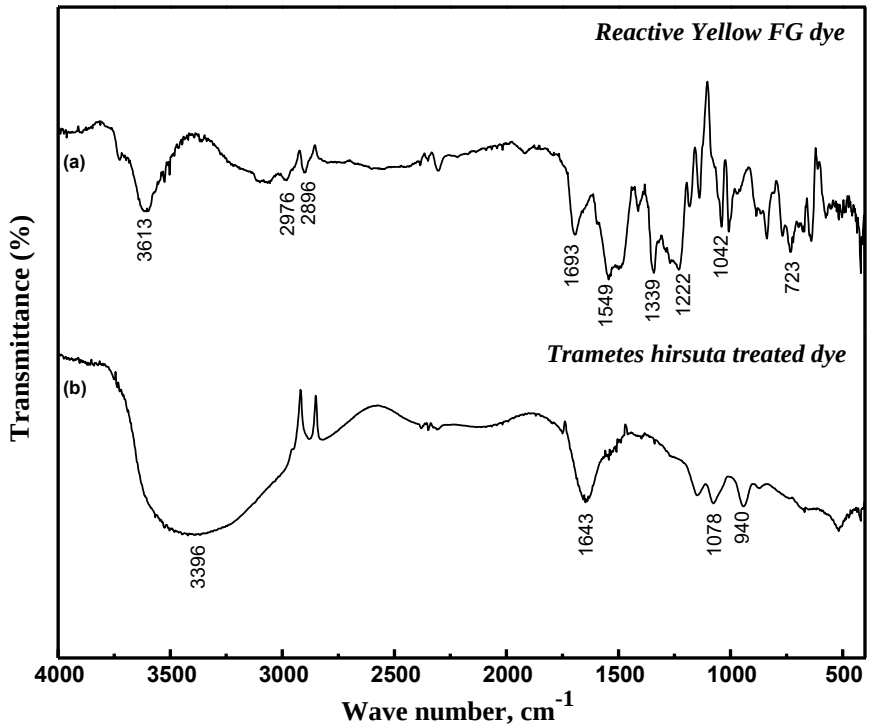

Figure 45: FTIR spectra of a) control dye Reactive Yellow FG and b) its degradation product treated by *Trametes hirsuta.*

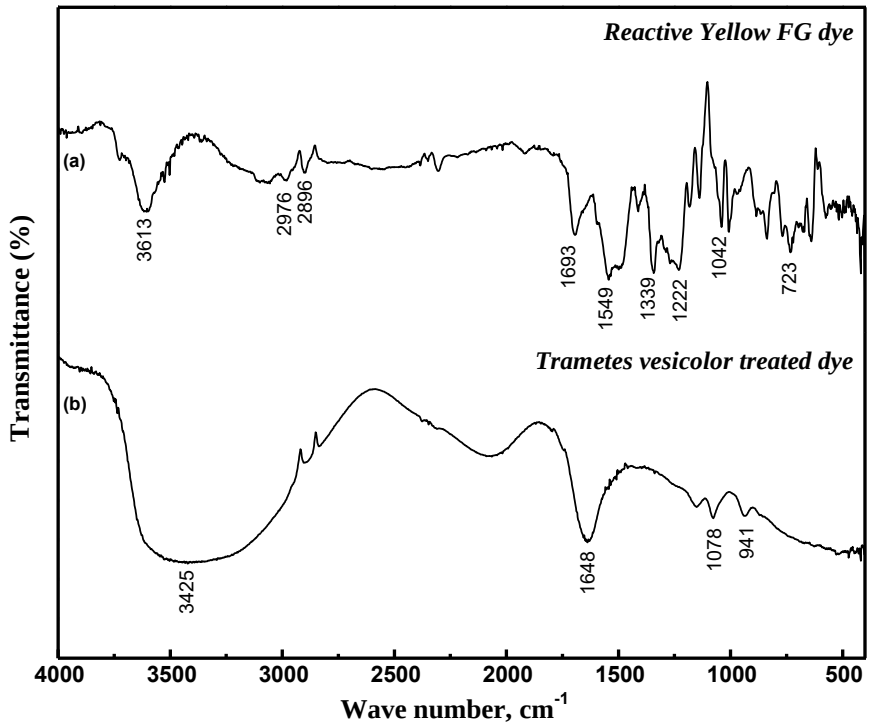

Figure 46: FTIR spectra of a) control dye Reactive Yellow FG and b) its degradation product treated by *Trametes versicolor.*

FTIR spectrum of Reactive Yellow FG dye treated with *Trametes hirsuta* (Fig. 45b) and *Trametes versicolor* (Fig. 46b) showed complete disappearance of a peak at 1549 cm^{-1} for an azo stretch. Broadband was observed at peak 3396 cm^{-1} (*Trametes hirsuta*) and at 3374 cm^{-1} (*Trametes versicolor*) for-N-H stretch, peak at 940 cm^{-1} (*Trametes hirsuta)* and at 926 cm^{-1} (*Trametes versicolor)* for C-H bend and peak at 1078 cm^{-1} (*Trametes hirsuta)* and at 1078 cm^{-1} (*Trametes versicolor)* for C-N stretch of Ar-NH-R with shifting confirmed the degradation of the dye.

Thus, in the present study the disappearance of a peak for an azo stretch clearly indicates the breaking of azo bond by *Trametes hirsuta* and *Trametes versicolor* that would be an essential and foremost step for the color removal. Broadband for-N-H stretching was the evidence for the aromatic amine group present in the parent dye compound; whereas peaks for C-H bend, and for C-N stretching of Ar-NH-R suggests the formation of aromatic amine. Comparison between the spectrum of control and treated dyes exhibited the changes in the positions of these peaks. The shifting of peaks from their original positions clearly indicates the degradation of the original molecular structure of the dye. Similar changes in the peak of different dyes has already been reported by earlier workers (Field *et al.* 1993; Parshetti *et al.* 2006; Kalme *et al.* 2007; Dhanve *et al.* 2009; Ghodake *et al.* 2009; Gomare *et al.* 2009; Koyani *et al.* 2013).

II. HISTOLOGICAL STUDY

Several species of *Trametes* are reported to have potential of biological delignification due to the presence of well-developed ligninolytic enzymes such as laccase and Mn dependant peroxidase (Nakagame *et al.* 2006; Gutierrez *et al*. 2012). The modification of *Eucalyptus* chemi thermo mechanical pulp (CTMP) fibres using *Trametes hirsuta* resulted in a 32 % increase of fibre internal bond strength and significant improvements in hand sheet tensile and tear properties (Wong *et al.* 2000). These improvements were largely due to modification of fibre wall, particularly loosening of fibre wall fine structure and a reduction in extent of middle lamellae remaining on the fibre surface. However, it is known that the same species of white rot fungi shows a different pattern of delignification depending upon the wood species (Schwarze *et al.*

1997; Schwarze and Fink 1998; Bhatt *et al.* 2015). On the other hand, heterogeneity in decay pattern was shown by several white rot fungi, i.e. the same species cause selective degradation of lignin in one tree species, and simultaneous pattern of degradation in another (Agosin *et al*. 1990).

Available literature also indicates that a particular species may show selective delignification in early stage of wood decay and may shift over simultaneous rot pattern (Bhatt *et al*. 2015). The genus *Trametes* is known to show both selective and simultaneous mode of decay with respect to species variation within genera and wood type (Anagnost 1998; Levin and Castro 1998). Hence it is important to investigate the decay pattern exhibited by the fungi in the wood species of specific commercial applications.

Trametes hirsuta and *Trametes versicolor* are known to possess strong ligninolytic activity such as manganese peroxidase, laccase and lignin peroxidase. In the present study, wood decay pattern caused by *Trametes hirsuta* and *Trametes versicolor* is investigated on four different commercially important timber species *viz.* 1) *Eucalyptus globulus* Labill. 2) *Azadirachta indica* A. Juss 3) *Tectona grandis* L.f., and 4) *Leucaena leucocephala* (Lam.) de Wit.

The genus *Eucalyptus* (Myrtaceae) is mainly cultivated for paper, pulp, pharmaceutical and cosmetics industries (Silva *et al*. 2003). In recent years, many studies have revealed the potential of *E. globulus* in the production of timber, pulpwood and for the production of bioethanol (Whittock *et al*. 2007; Romani *et al*. 2012). Due to the growing economic importance, *Eucalyptus* spp. is also used in the fungal decay studies (Fernandes *et al*. 2005).

Azadirachta indica A. Juss (Meliaceae), popularly known as Neem is one of the most versatile medicinal plants. According to Biswas *et al*. (2002), Neem has been used in Indian medicine system for more than 2000 years, each part of Neem is highly valued for its antimicrobial and medicinal properties not only for household remedy but it is also documented in Ayurveda, Unani and Homoeopathic medicines. Azadirachtin, isolated from its seed has strong antimalarial property while the flavonoid quercetin present in the Neem attributes hypoglycaemic activity (Daniel, 1991). Although, *A. indica* reported to produce different chemical constituents that are reported as an antimicrobial and anti-fungal in nature (Patel and Trivedi 1962; Biswas

et al. 2002); little information is available on its sensitivity to wood decay by rot fungi.

Tectona grandis L. f., (Lamiaceae) is the most priced commercial timber, which is widely used in India for more than 2000 years (Nagadesi *et al*. 2013). Teak wood is highly valued for its use in general carpentry, shipbuilding and furniture. According to Browning (1963) *T. grandis* consist of 31 % of lignin that cements cellulose and hemicelluloses within thus endows rigidity and stiffness to the wood. In terms of durability, teak wood has extraordinary durability against pathogen or insect attack like termite, fungi and insects, which is rendered by its antidecay compound tectoquinone (Haupt *et al.* 2003; Thulasidas and Bhat 2007). On the other hand, the heartwood extractives reported to play a major role in the natural durability of plantation-grown teakwood (Haupt *et al.* 2003). Due to its extraordinary quality American Society for Testing Material (1981) placed it in durability Class I (highly resistant) of the general classification system (Bhat *et al*. 2005; Koyani *et al.* 2014).

Leucaena leucocephala (Subabul), is a tropical, evergreen hardwood tree species belongs to Fabaceae. It is one of the most versatile, fast growing commercially important species widely cultivated for paper and pulp industry in India; it contributes nearly 25 % of total raw material (Pramod and Rao 2012). Tropical biodiversity is known for a number of tree species having medicinal value, but their response to wood rot fungi have received little attention. The propensity of trees to wood decay is important as decay leads to breakdown of cellular structure of wood and the defense response of the plant leads to increased deposition of lignin content in the wood which will reduce pulp yield (Pearce 1996). The non-specific enzyme system of wood-degrading fungi with the ability to completely degrade lignin has tremendously contributed the biotechnological researches to their potential in bioremediation of organic pollutants, ethanol production, and bio-pulping of wood in paper industry (Maciel *et al*. 2010).

Hence it is important to investigate the decay pattern exhibited by the fungi in the wood species for its specific commercial applications. Therefore, the present study is aimed to investigate the delignification pattern of *T. hirsuta* and *T. versicolor* and associated alternations in the wood cell wall structure of *Eucalyptus globulus* Labill.,

A*zadirachta indica* A. Juss, *Tectona grandis* L.f. and *Leucaena leucocephala* (Lam.) de Wit.

3.5 Structure of secondary xylem

***Eucalyptus globulus*:** Wood is diffuse porous with indistinct growth rings. Vessels appear solitary and as a radial or tangential multiples with simple perforation plates with an alternate arrangement bordered pits on lateral walls. Vessels are associated with scanty paratracheal parenchyma cells. Rays are uni-triseriate. Fibres are thick walled with numerous simple pits on the lateral wall.

Azadirachta indica: Secondary xylem is diffuse porous with indistinct growth rings. Vessels are solitary and in radial multiples of 2-6 vessels associated with vasicentric sparse paratracheal parenchyma cells. Vessel elements possess alternate bordered pits on lateral walls and simple perforation plate on transverse end walls. Xylem rays were uni-multiseriate, compound and homocellular. Apotracheal parenchyma appears as banded multiceriate.

Tectona grandis: Secondary xylem of *T. grandis* is ring porous with distinct growth rings. Sapwood is pale yellow while heartwood is light golden brown in fresh and brown to dark brown in dry condition. In early wood, vessels are large, oval to circular in outline. They are chiefly solitary but sometimes occur in radial multiples of two to three vessels. Parenchyma cells form a thin sheath around the vessels which are distinct in the early wood. Rays are uni-multiseriate with oval to polygonal ray cells.

Leucena leucocephala: Wood in *Leucaena* is diffuse porous, growth rings indistinct. Vessels are solitary and in radial multiples of 2-3 with an oblique simple perforation plate. Axial parenchyma cells are vasicentric and scanty paratracheal. Apotracheal parenchyma cells often show accumulation of rhomboidal crystals. Xylem rays are uni-multiseriate and homocellular. Fibres are septate and living.

3.6 *Invitro* decay test

After the inoculation of wood blocks of all the timber species, every alternate day petri plates were observed for visual interpretation. At the end of the first week, fungal mycelia began to ramify on wood blocks which were completely covered with a mycelial mat after 12-15 days of inoculation. At the end of the third week, mycelial

mat appeared as a uniform mass of fungi completely masking the wood blocks and petri plates. Thus, it became difficult to make out the presence of wood block in the Petri dish. There was minimal weight loss, even when wood blocks were completely covered with fungal mycelia after 30 days of incubation. The percent weight loss of test blocks was found to be more in all four wood blocks inoculated with *T. hirsuta* as compared to *T. versicolor*.

3.7 General mechanism of hyphal invasion

After 10-15 days of fungal inoculation, mycelia ramified completely over wood blocks. At the end of 30 days, all the cell types of secondary xylem were invaded by both the species of *Trametes* through vessels and vessel-associated axial parenchyma. From the vessels, hyphae traversed into neighboring rays and gradually extended in all directions covering xylem fibres and adjacent axial and ray parenchyma cells. At this stage, no visual damage in cell walls was observed within 30 days of incubation. Fungal mycelia moved from one cell to the next through pits present on the cell wall. However, initiation of cell wall separations at cell corners was observed occasionally in some of the sections.

3.8 Decay pattern of *Trametes hirsuta and Trametes versicolor* in the cell wall of wood species

1. *EUCALYPTUS GLOBULUS* Labill.

The weight loss pattern was gradual in case of both the fungi. In *T. hirsuta* more than 50 % weight loss was evident at the end of 120 days. However, in *T. versicolor*, initial weight loss was rapid but a gradual difference in weight loss was noticed during advanced stages of decay (Fig. 47) and reached about 45 % after 120 days of incubation.

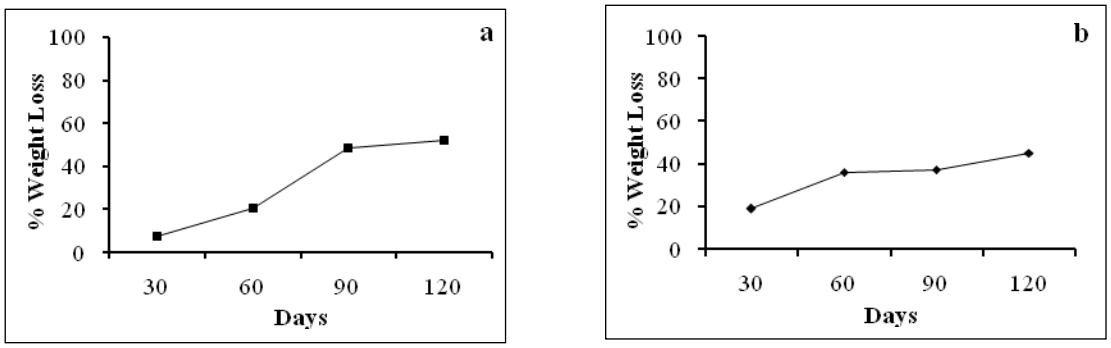

Figure 47: Average percentage of weight loss in *Eucalyptus globulus* after different incubation periods of the woods with a) *T. hirsuta* and b) *T. versicolor.*

Anatomical Changes Induced by *Trametes hirsuta*

The transverse sections obtained from the wood blocks after 30 days of inoculation revealed that all the cell types of secondary xylem were invaded by the mycelia and showed initiation of cell wall separation due to dissolution of middle lamellae (Fig. 48a). Fungal mycelia traversed into adjacent cells through the bordered pits present on the lateral walls of the vessels and fibre tracheids (Fig. 48b). Formation of wall erosion channels around the pit aperture (Fig. 48c) was also observed at this stage. The longitudinal sections also showed a blue colored tangential wall of fibres due to cellulose rich cell wall following selective delignification (Fig. 48d). Extensive pit erosion in fibre tracheids was noticed after 60 days of inoculation (Fig. 48e). The selectively delignified and eroded regions in the wall often appeared oval-oblong in shape (Fig. 48e). The majority of the fibre tracheids were stained with astra blue because of advancement of selective delignification (Fig. 48f). The separation of ray cells and fibres due to delamellation became more prominent after 60 days of fungal incubation (Fig. 48g-i). Vessel wall damage initiated with erosion channels between bordered pits and the complete erosion of larger areas was observed in the later stages of decay (Fig. 48j, k).

After 90 days of inoculation, fibres often showed merging of erosion patches and formed large unstained areas (Fig. 48l). The complete removal of cell wall polymers in the S_2 region of the secondary wall resulted in large hollow space in the fibre tracheids (Fig. 48m). At the end of 120 days, the migration of fungal mycelia from contact rays into vessel led to collapse of vessels and the subsequent degradation of its wall (Fig. 48n). Erosion of pit margin around the bordered and simple pits was common in the secondary wall of fibre (Fig. 48o) and tracheids respectively. The degradation of both radial and tangential walls of ray cells resulted in the large hollow region in the tangential sections (Fig. 48p).

Anatomical Changes Induced by *Trametes versicolor*

In contrast to the selective delignification pattern shown by former species, the wood colonized by *T. versicolor* showed thinning of fibre wall in two patterns. In the first case, formation of localized erosion occurred from inner wall layer (S_3) and progressed further into the middle layer of the wall, while the second pattern showed initiation of delignification from the outer layers of secondary wall (S_1+S_2) leaving compound middle lamellae and S_3 layer intact (Fig. 49a). Fungal mycelia moved

through the cell lumen and invaded adjacent cells by eroding bordered pits located on the lateral walls of fibre tracheids (Fig. 49b, c, e). In tangential sections, the radial walls of fibres also showed separation (Fig. 49d). The analysis of pit erosion under high magnification revealed mycelia penetration through the pit (Fig. 49e), which may then enter into an adjacent cell (Fig. 49f) or bend and pass vertically through middle lamella (Fig. 49g), leading to the separation of cells (Fig. 49h). Simultaneous degradation of wall material around and between pits in the fibres appeared as patches of unstained region in their tangential wall (Fig. 49i, j). One of the characteristic of simultaneous rot (i.e. the 'U' shape notch and appearance of erosion channels) was apparent in the tangential walls of fibres (Fig. 49k).

Separation of cells and formation of erosion channels from the cell lumen became more apparent after 60 days of inoculation (Fig. 49l). Separation of both axial and radial elements by dissolution of middle lamellae in all the cell types was also observed (Fig. 49m). Vertical tunneling along the cell axis appeared as unstained regions due to the simultaneous pattern of decay (Fig. 49n). In case of ray cells, dissolution of middle lamellae in both radial and tangential wall resulted in separation and isolation of ray cells (Fig. 49o). The fungal mycelia passing through contact rays into vessels, axial parenchyma cell and vessel wall often showed erosion near the bordered pit regions (Fig. 49p). The presence of fungal mycelia within the erosion channels formed between bordered pits in the vessel wall also seen frequently in several sections (Fig. 49q). Migration of fungal hyphae between rays and fibre tracheids through simple and bordered pits respectively was a common feature (Fig. 49r). Presence of artificially stained (blue colored) hyphae was often observed in the erosion channels in the radial wall of rays (Fig. 49s). After 120 days of inoculation, thinning of the wall and dissolution of middle lamellae became more pronounced during the advanced stage (Fig. 49t). At this stage fungal mycelia also formed chlamydospores (Fig. 49u).

Confocal Microscopy of *Eucalyptus* wood infected by *T. hirsuta and T. versicolor*

The vessel wall and compound middle lamellae of fibres showed high intensity of fluorescence even after 120 days of incubation. At this stage, wood blocks inoculated with *T. hirsuta* showed gradual loss of fluorescence from the inner secondary wall layer of the vessel (Fig. 50a, b) while compound middle lamellae of fibres showed separation and absence of auto-fluorescence due to strong delignification from this

region (Fig. 50c). Ray parenchyma also showed enlarged pit fields due extension of pit erosion from adjacent lignified region of the cell wall (Fig. 50d). Delignification of vessel walls and compound middle lamellae of fibres were also apparent in the wood infected with *T. versicolor* (Fig. 50f, g). Delignification of cell wall adjacent to pits in the fibre wall appeared as non-fluorescent regions in middle lamellae and outer layers of secondary wall (Fig. 50h).

2. *AZADIRACHTA INDICA* A. Juss.

The pattern of weight loss was rapid during four different intervals of wood decay by *T. hirsuta* and *T. versicolor*. However, percentage of weight loss was high in *T. hirsuta* compared to *T. versicolor* (Fig. 51).

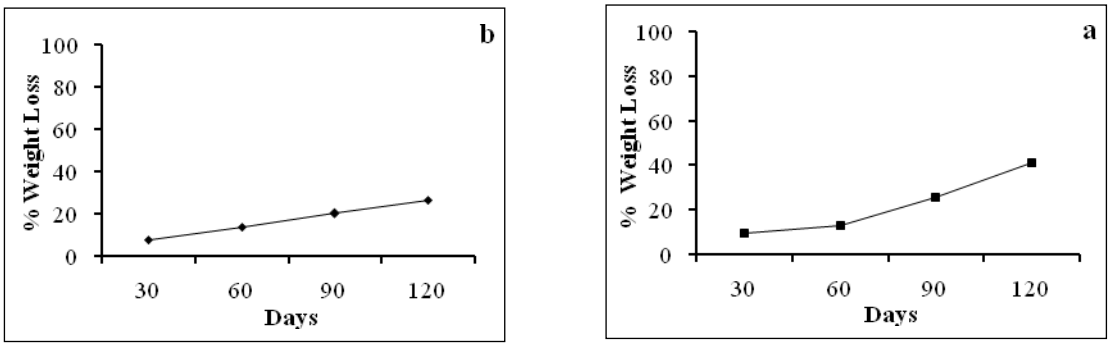

Figure 51: Average percentage of weight loss in *Azadirachta indica* after different incubation periods of the woods with a) *T. hirsuta* and b) *T. versicolor.*

<u>Anatomical Changes Induced by *Trametes hirsuta*</u>

After 30 days of incubation, fungal mycelia masked over whole test blocks and invaded vessel lumen and ray cells (Fig. 52a). At this stage, the hyphal movement was enabled through the simple pits between adjacent rays and axial elements (Fig. 52a, b) and within fibres (Fig. 52c). The diameter of these pits increased due to removal of lignin by extracellular enzymes produced by the fungus. Formation of boreholes and their fusion with adjacent boreholes resulted in the formation of large sized oval to circular holes on lateral walls (Fig. 52d). Defibration in response to dissolution of middle lamellae occurred consistently (Fig. 52e), while formation of erosion channels from the lumen surface towards middle lamellae in the localized regions of fibres becomes distinct at this stage (Fig. 52b). The axial parenchyma showed thinning of cell walls (Fig. 52f) and the formation of erosion channels across the wall led to breaking of the cell wall which provided path for the migration of mycelia between

adjacent cells (Fig. 52g). Similar thinning of the ray cell wall adjacent to axial parenchyma formed large erosion channels (Fig. 52g, h).

After 60 days of inoculation, the delamellation of the fibres became more pronounced and 'U' shaped erosion channels often noticed during tangential spreading of hyphae between cells (Fig. 53a). Mycelia traverse from one cell to another by boring through the middle lamellae of ray cell and fibres or through the pits on lateral walls (Fig. 53b). Increase in diameter of the simple pits of fibres indicates that the cell wall erosion begins from this region and spreads into secondary walls of fibres (Fig. 53c). Formation of erosion troughs with round to oval shaped edges were observed at this stage in the tangential walls of fibres (Fig. 53d). The simultaneous degradation of lignin from radial and tangential walls of fibres often resulted in large erosion channels with irregular shape and size (Fig. 53d, e). The tunnel formed in the tangential and radial walls often showed the presence of fungal hyphae (Fig. 53f). The delignification and separation of cells, particularly at cell corners was evident from the Astra blue staining. Part of the delignified wall stains with Astra blue instead of safranin (Fig. 53g). After 120 days, the majority of fibres became separated and patches of secondary wall with erosion channels were more manifested in the transverse sections (Fig. 53h). The separation of compound middle lamella and delignification of secondary wall of parenchyma cell increased in advanced stages of decay (Fig. 53i). At this stage, most of the ray cells were collapsed completely and appeared hollow due to complete degradation/removal of the cell walls in the central portion of the rays (Fig. 53j).

Anatomical Changes Induced by *Trametes versicolor*

Mycelia moved in both horizontal and vertical directions through lateral pits present on the lateral walls of radial and axial elements respectively (Fig. 54a). After 30 days of inoculation, the selective delignification pattern became evident by defibration and the removal of cell wall polymers from the middle lamellae region, resulting in gap between secondary walls of adjacent cells (Fig. 54b, c). However, the delignification became more severe and noticeable after 60 days of fungal incubation. It was apparent from the unstained portions of the cell walls that delignification not only occurred in fibres, but also takes place in the secondary walls of axial parenchyma and vessel elements (Fig. 54d). Separation of vessels and delignification of walls affect its rigidity which consequently led to collapse of vessels (Fig. 54e). Like former species,

formation of 'U' shaped notch in the fibre walls became more frequent at this stage (Fig. 54f). Due to dissolution of middle lamella, outer layer of the fibre walls became separated and showed large gaps between the adjacent cells (Fig. 54g, h, i). Features of cell wall degradation at this stage of decay (after 90 days) remained similar to former species except removal of lignin along the cellulose microfibrils (Fig. 54j). After 120 days, defibration of the fibres became more severe and patches of localized wall erosion were apparent in the transverse sections (Fig. 54k). The fungal mycelia became narrow when passing through the pits in the rays while their diameter increased in cell lumen and produced chlamydospores after entry into the cell lumen (Fig. 54l).

Confocal Microscopy of *Azadirachta* wood infected by *T. hirsuta and T. versicolor*

Alterations in the delignification pattern of cell wall polysaccharides in the secondary xylem of *A. indica* inoculated with *T. hirsuta* and *T. versicolor* were also studied under confocal laser scanning microscope. *In vitro* test blocks incubated with *T. hirsuta*, showed lack of auto-fluorescence in the eroded region of the cell walls of vessels, rays and fibres (Fig. 55a-c). At an advanced stage of decay, though cell corners of fibres remained intact and unaltered, but radial and tangential walls showed apparently no fluorescence signals due to an extensive delignification (Fig. 55b). The cell wall of a vessel associated parenchyma cells and vessels showed several delignified regions without any fluorescence signals (Fig. 55c, d). Similarly, the pit region in the tangential wall between ray cells and secondary wall adjacent to pit region of fibres inhabited by fungal hyphae often showed complete lack of fluorescence indicating the initiation of erosion channels in the pit and subsequent degradation of adjacent secondary wall of fibres (Fig. 55e, f). In test blocks inoculated with *T. versicolor*, the vessel wall showed similar features as described for above mentioned species (Fig. 55g-j).

3. *TECTONA GRANDIS* L.f.

Both the strains completely invaded the wood blocks after 30 days of incubation, but there was no appreciable weight loss. Thereafter, weight loss was rapid in the succeeding days, wherein T. *hirsuta* showed 43.23 % and T. *versicolor* showed about 30 % weight loss after 120 days of inoculation (Fig. 56).

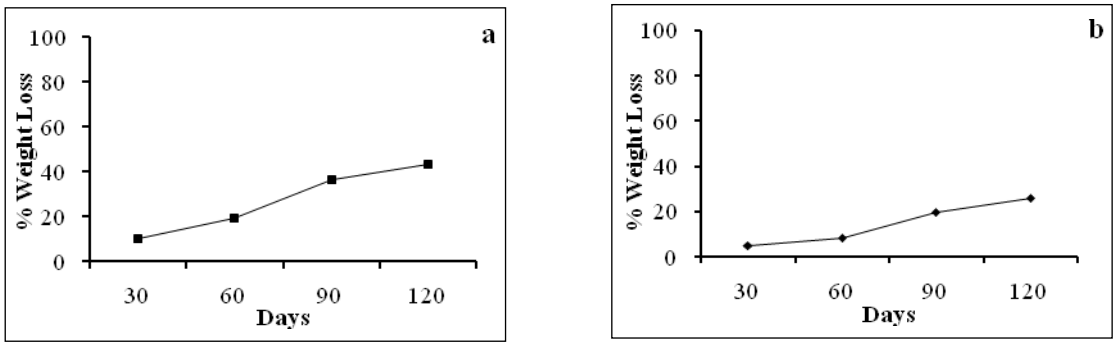

Figure 56: Average percentage of weight loss in *Tectona grandis* after different incubation periods of the woods with a) *T. hirsuta* and b) *T. versicolor*.

Anatomical Changes Induced By *Trametes hirsuta*

Formation of erosion troughs and separation of secondary wall near the compound middle lamellae of all the cell types of the secondary xylem was observed after 30 days of infection (Fig. 57a). The compound middle lamellae remain intact during this stage indicating cell wall separation may occur from the outer layer (S_1) of secondary wall (Fig. 57a). However, after 60 days, cell separation through dissolution of middle lamellae indicates a typical selective white rot mode of decay pattern in both transverse and tangential sections of wood (Fig. 57b, c). Colonization pattern of fungi remains similar as described for other wood samples (Fig. 57d). Extensive degradation of ray cell walls results in the formation of large hollow pockets within the rays (Fig. 57e). The fibres adjacent to heavily degraded ray showed large erosion channels on the walls from where hypha enters into their lumen (Fig. 57e).

As the time passed, boreholes became larger in the fibre wall and were more apparent after 90 days (Fig. 57f, g). Not only the size of the boreholes increased, but merging of adjacent boreholes also resulted in the formation of large erosion channels (Fig. 57h). Apart from the typical borehole formation and its merging, another pattern of erosion channel formation was also observed along the angle of cellulose microfibrils (Fig. 57i, j). In case of vessels, wall degradation started from the side of cell wall facing the paratracheal parenchyma cells that were already invaded by the fungus (Fig. 57k). In tangential sections vessel wall showed erosion of bordered pits and its extension between adjacent pits led to the formation of large eroded regions on the cell wall (Fig. 57l). At this stage, fibres often showed erosion channels within S_2 wall layer resembling boreholes in soft rot decay by progression of erosion channel parallel to middle lamella on upper and lower side as the decay progressed further

(Fig. 57m). Even at the advanced stage of decay, i.e. after 120 days, fungal mycelia were observed throughout the cell lumen of all the cell types (Fig. 57n). At this stage, separation of fibres was more common features (Fig. 57o). The secondary wall of fibre became heavily eroded and typical 'L' bending pattern become distinct across and along the length of cell wall (Fig. 57p, q).

Anatomical Changes Induced by *Trametes versicolor*

Similar to *T. hirsuta*, separation of secondary wall from its outer layer was also noticed in the wood blocks after 30 days of inoculation with *T. versicolor* (Fig. 58a). The erosion channel moved through fibre walls (Fig. 58b). Thinning of fibre walls is one of the typical simultaneous white-rot features noticed at this stage (Fig. 58c). Vessel showed progression of erosion channel in the wall region between the adjacent bordered pits (Fig. 58d). Formation of erosion troughs from the lumen side towards middle lamellae and separation of inter-vessel wall starts after 90 days (Fig. 58e). At an advanced stage of decay, thinning and collapse of fibre wall was a distinct feature (Fig. 58f). In tangential sections, the eroded region of wall appeared as unstained patches within the lignified secondary walls of fibres (Fig. 58g).

Confocal Microscopy of *Tectona* wood infected by *T. hirsuta and T. versicolor*

The variation in fluorescence pattern corresponding to delignification and structural changes in the cell wall during wood decay was revealed by confocal microscopy. The wood blocks infected with *T. hirsuta* showed erosion of secondary wall and expansion of pit fields appeared as larger non-fluorescent regions in the cell wall (Fig. 59a). During the early stage of decay, the separation of cell wall from outer layers of secondary wall (i.e. S_1) and existence of compound middle lamellae was also confirmed by confocal imaging (Fig. 59b). Absence of fluorescence from the later areas during the advanced stage indicated the delignification of compound middle lamellae and collapse of cells during late stages of decay (Fig. 59c). Thinning of secondary wall and formation of erosion troughs in the vessel and adjacent cells resulted in absence of fluorescence from these regions (Fig. 59d, e). The wood blocks infected with *T. versicolor* also showed large, non-fluorescent erosion troughs in secondary wall (Fig. 59f). Erosion from cell lumen into compound middle lamellae and subsequent delignification of cell corner region indicates the strong ligninolytic properties of *T. versicolor* (Fig. 59f). Dissolution of middle lamellae and separation of fibres was observed frequently (Fig. 59g). Occurrence of penetration hyphae within

the separated region was noticed in the bright field combined image of the same region (Fig. 59h). Extensive thinning and erosion of fibres and ray cells wall was apparent at this stage which indicates complete delignification and formation of erosion in the cell wall (Fig. 59i-l). The cell wall of vessel and associated parenchyma showed weak fluorescence due to thinning and erosion of their secondary wall (Fig. 59m).

4. *LEUCAENA LEUCOCEPHALA* (Lam.) de Wit.

At the end of 30 days, both the strains i.e. *T. hirsuta* and *T. versicolor* showed a lower percentage of weight loss of 7.2 % and 4.7 % respectively. Thereafter, the weight loss was rapid in *Leucaena* by both the fungal strains *viz*. *T. hirsuta* 43.03 % and *T. versicolor* 32.18 % at the end of 120 days (Fig. 60).

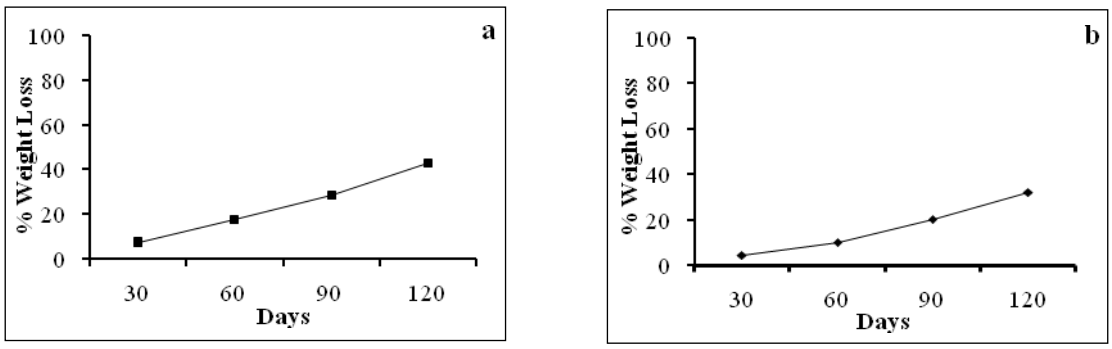

Figure 60: Average percentage of weight loss in *Leucaena leucocephala* after different incubation periods of the woods with a) *T. hirsuta* and b) *T. versicolor*.

<u>Anatomical Changes Induced by *Trametes hirsuta*</u>

T. hirsuta showed anatomical characteristics which are specific to the simultaneous pattern of white-rot during degradation of *Leucaena* wood. The appearance of 'U' shaped notches and merging of boreholes during extension of erosion channels along the axis of fibres indicated the typical simultaneous decay features (Fig. 61a, b). On the other hand, separation of fibres and ray cells by degradation of outer secondary wall region (i.e. S_1 layer) leaving S_3 layer and middle lamella region intact was a conspicuous feature observed during the initial stages of cell wall degradation (Fig. 61c-f). The degraded region appeared as large eroded pockets within the secondary wall (Fig. 61g-h). Large erosion channels through the wall between adjacent fibres (Fig. 61i) and thinning of cell wall (Fig. 61j) during an advanced stage of decay confirmed the simultaneous decay by *T. hirsuta* in *Leucaena* wood after 120 days of

inoculation. Rays are severely degraded at this stage and showed complete removal of ray cell wall at several places within the section (Fig. 61j).

Anatomical Changes Induced by *Trametes versicolor*

Transverse sections of the fibres showed two distinct types of cell wall thinning; one was characterized by the localized degradation of the cell wall and separation of middle lamellae (Fig. 62a) while the second pattern showed general erosion of the cell walls adjacent to hyphae growing in the lumen surface. Tangential sections also revealed the thinning of secondary wall and formation of erosion troughs from the lumen surface towards middle lamella during advancement of decay indicating typical simultaneous white rot (Fig. 62b). Large erosion channels formed through simultaneous degradation along the cell axis and merging of boreholes were detected after 60 days of infection (Fig. 62c). In fibres, colonization of fungal mycelia occurred through the formation of penetration hyphae passing through the simple pits between adjacent cells (Fig. 62d). The tangential walls of fibre showed progression of erosion channels appeared with 'U' shaped notches (Fig. 62e, g, h). The fungal hypha within the erosion channel was contrasted with Astra blue staining (Fig. 62f). Multi-seriate rays often showed the hollow region because of complete degradation of cell wall constituents of some of the cells (Fig. 62i). Separation of fibres dissolution from cell corners and compound middle lamellae was also evident during advanced stages of decay (Fig. 62j). Large voids formed due to the progression of bordered pit erosion were detected in inter-vessel walls (Fig. 62k). Radial sections revealed the extensive degradation of the ray cell resulting in unstained patches of cell wall regions often inhabited by fungal mycelia (Fig. 62l).

Confocal Microscopy of *Leucaena* wood infected by *T. hirsuta and T. versicolor*

Transverse section of infected wood samples observed under a confocal microscope also revealed a simultaneous white rot pattern of delignification during degradation of wood cell walls in *Leucaena* by *T. hirsuta* and *T. versicolor*. In wood inoculated with *T. hirsuta* showed formation of erosion channels from the intercellular spaces into cell lumen while it was represented as non-fluorescent gap regions in the radial wall of ray parenchyma (Fig. 63a, b). Weak fluorescence from the wall region surrounding the bordered pits of the vessels indicated delignification of these regions following the pit erosion (Fig. 63c). Severe degradation was also noticed in the cell wall of paratracheal

parenchyma cells (Fig. 63c). Severely affected wood showed removal of compound middle lamallae of fibres (Fig. 63d) while removal of lignin from secondary wall region adjacent to eroded pits in the fibres appeared as large non-fluorescent gap regions (Fig. 63e). In *T. versicolor*, lignin degradation from the cell corners was detected, particularly in fibre walls adjacent to ray cells (Fig. 63f). The absence of fluorescence from the degraded regions of the vessel wall, vessel associated parenchyma and ray cell wall indicates the strong ligninolytic activity of *T. versicolor* (Fig. 63f). The delignification from cell corner region towards compound middle lamellae was observed in the cell wall region between fibre and parenchyma cell (Fig. 63g, h). Thinning of fibre walls in response to lignin removal from inner layer towards the middle lamellae resulted in reduction in auto-fluorescence intensity of these cell walls (Fig. 63g). The erosion channels formed across the fibre appeared non-fluorescent due to delignification (Fig. 63i, j). Erosion and expansion of simple pits resulted in large boreholes in the ray cell wall (Fig. 63k).

Discussion

Wood is the main renewable source of material on terrestrial earth and is a predominant commercial product from forests which is largely used as building materials, pulp and paper products (Martinez *et al*. 2005). Wood is formed by three main polymeric constituents, cellulose, hemicelluloses and lignin (Higuchi 1997; Evert 2006). Among these, lignin is highly resistant towards chemical and biological degradation; its highest concentration is found in the middle lamella, where it acts as cement between wood fibres conferring mechanical resistance to wood (Fengel and Wegener 1984; Fazio *et al*. 2010; Sanghvi *et al*. 2013). In terrestrial ecosystems, lignocellulose degradation is a central step for carbon recycling (Martinez *et al*. 2005). Wood is subject to attack by microorganism subsequently when in use and even in a standing tree, decays by these microorganism cause principal economic losses by weakening the cell wall components of wood. Among the microorganisms concerned, fungi are the main wood rotters due to their ability to degrade or modify lignin (Savory 1954).

Each group of fungi express characteristic chemical and micro-morphological pattern of wood degradation and accordingly they are classified into white-rot, soft-rot and brown rot fungi (Liese 1970; Eaton and Hale 1993; Blanchette 1991, 2000; Boddy and Watkinson 1995; Schwarze 2007; Koyani *et al*. 2010; Koyani and Rajput

2015). White rot fungi are unique in their ability to efficiently degrade lignin from wood cell walls by secreting extracellular oxidative enzymes. Fungal decay of wood in service results in billion-euro losses. Moreover, these extracellular enzymes are of promising biotechnological uses. White rot fungi have two types of degradation patterns, selective and simultaneous degradation (Schwarze and Fink 1998; Schwarze and Baum 2000; Schwarze 2007; Lehringer *et al.* 2010; Koyani *et al.* 2010, 2011). In the present study, two fungal species viz. *Trametes hirsuta* and *Trametes versicolor* were utilized to investigate the pattern of wood decay and structural alterations induced in the wood cell wall of *Eucalyptus globulus* Labill., *Azadirachta indica* A. Juss, *Tectona grandis* L.f. and *Leucaena leucocephala* (Lam.) de Wit. The growth of fungal species induces anatomical changes in wood cell walls as a result of their inhabitation in or on the wood. This may further result in weight loss affecting the timber properties of wood.

Our results show variation in the percentage of weight loss depending upon different wood and the fungal species. Even though, both the strains completely ramify the wood blocks within the first fifteen days, no appreciable weight loss was observed by *T. hirsuta* and *T. versicolor* in all four woods at the end of first month. According to Koyani and Rajput (2015), presence of several low molecular weight compounds in wood cells might be acting as a source of carbon during this stage which consequently results in no weight loss. No appreciable weight loss at the end of one month indicates that the fungus either requires unusual conditions or the decay may develop slowly (Worrall *et al*. 1997). However, after 120 days of incubation, the highest percent of weight loss occurred in *Eucalyptus* wood 51.9 % by *T. hirsuta* compared to samples of other wood samples. Similar to former fungal species, the percent of weight loss was highest in *Eucalyptus* 44.8 % incubated with *T. versicolor* whereas it was least in teak wood. Thus, percent weight loss was relatively more by *T. hirsuta* than *T. versicolor.* Increase in weight loss indicates greater removal of cell wall polysaccharides and lignin. According to Adaskaveg *et al*. (1995) the rate and extent of polysaccharides and lignin removal differs among different white-rot fungi. Extensive weight loss of wood blocks following infection suggests that both the species of *Trametes* are aggressive wood degrading fungi. In contrast to experimental wood blocks, no appreciable weight loss was observed in control blocks. Weight loss of 2 % was considered as threshold of decay initiation by Fengel and Wegener (1989)

and Worrall *et al.* (1997). In the present study, control samples showed weight loss less than 1 % which may be handling error. Earlier studies have also reported similar results in minor weight loss of control samples (Worrall *et al.* 1997; Anagnost 1998; Koyani and Rajput 2015).

Patterns of degradation may also depend on environmental factors which directly or indirectly contributes to the efficiency fungi. Among them temperature, humidity and pH are important factors (Eriksson *et al*.1990; Eaton and Hale 1993; Koyani *et al*. 2010). However white rot fungi show tremendous variability in pattern of wood degradation. Some species can cause selective removal of lignin at one location and simultaneous removal of both lignin and cellulose at another location in the same wood sample (Srebotnik and Messner 1994); also same white rot fungi seem to switch from selective to simultaneous degradation (Otjen and Blanchette 1985; Worrall *et al*. 1997; Koyani *et al*. 2010) and even different strains of a single species can show considerable variation (Blanchette *et al*. 1992; Bhatt *et al.* 2015). In the present study, both *T. hirsuta* and *T. versicolor* showed the decay pattern typical to white rot type. Based on the pattern of delignification of cell wall polymers by the fungus, white rot decay is categorized into two types 1) selective delignification and 2) simultaneous degradation of all cell wall constituents (Schwarze and Fink, 1998; Schwarze 2007; Koyani *et al*. 2010; Pramod *et al*. 2015).

During the early stages of wood decay, i.e. after 30 days of incubation in *Eucalyptus* and *Azadirachta* wood, *T. hirsuta* exhibited selective delignification causing dissolution of the middle lamella between the adjacent cells followed by cell separation at an early stage of degradation. Such separation of cells is considered to be the best sign of selective delignification (Anagnost 1998). A similar pattern of wood degradation by *Inonotus hispidus* in *Ailanthus* is reported wherein, degradation commences at the corner of middle lamellae in xylem fibres causing dissolution of middle lamellae which is remarkable feature for selective delignification (Koyani *et al*. 2010; Pramod *et al*. 2015). In *Eucalyptus*, advancement in the selective delignification of secondary wall of fibre tracheids has been evident from its blue colored appearance after safranin-astra blue staining. Astra blue is specific for cellulosic polysaccharides and widely used as a best indicator for delignification studies (Kraus *et al*. 1998). In *Azadirachta*, the formation of erosion channels, pit erosion and thinning of cell wall was also evident during the advanced stages of

decay. Similar to *Azadirachta*, during the initial stage of decay in *Tectona* formation of erosion troughs and separation of secondary wall near the compound middle lamellae of all the cell types of secondary xylem was observed. Further with the advancement of decay in *Azadirachta*, and in the initial stage of delignification in *Leucaena*, appearance of 'U' shaped notches in fibre wall due to extension of erosion channels along the axis of fibres indicated the typical simultaneous decay features. The important white rot features associated with simultaneous decay are the appearance of erosion troughs with their 'U' shaped notch, erosion of lumen surface resulting in the cell wall thinning and localized removal of middle lamellae (Anagnost 1998). Therefore, majority of anatomical features observed during the wood decay by *T. hirsuta* used in the study suggest selective delignification in *Eucalyptus* and in *Azadirachta* (at an initial stage); whereas simultaneous degradation was evident at a later stage in *Azadirachta* and at an initial stage in *Eucalyptus, Tectona* and *Leucaena* wood.

Trametes versicolor is demonstrated to be a typical simultaneous rot fungus (Eriksson *et al*. 1990). In the present study also it causes typical simultaneous degradation of lignin in *Eucalyptus, Tectona* and *Leucaena* wood during the initial stage of decay. In case of *Eucalyptus*, it revealed erosion channels around the pit chamber which extended laterally forming tunnels and often forms U-notch appearance in tangential sections. On the other hand, in other three woods, it shows conspicuous thinning of cell wall in the fibres. Typical localized cell wall thinning was noticed in *Eucalyptus* and *Leucaena*. Moreover *Leucaena* showed two distinct pattern during advancement of decay where the first one in localized and the other is a generalized degradation from lumen surface of the cells towards the primary wall. This observation is in agreement with Yilgor *et al.* (2013) who reported similar features during degradation of *Liquidambar orientalis* heartwood by *T. versicolor.* In case of *Trametes versicolor* in decay of *Azadirachta* wood after 30 days of inoculation, the selective delignification pattern was evident by separation of fibres. Separation of xylem cells has been demonstrated to be one of the key anatomical features to identify the pattern of selective delignification (Anagnost 1988).

Similar to *Eucalyptus* and *Azadirachta*, cell separation by dissolution of middle lamellae (a typical selective white rot mode of decay pattern) was evident in *Tectona* after 60 days of incubation with *T. hirsuta*. Delay in the cell separation

suggests that *Tectona* shows high resistance to decay as compared to *Eucalyptus* and *Azadirachta*. *Tectona* wood is known for its durability and belongs to durability Class I (highly resistant) of the general classification system (ASTM 1981). However, natural durability of wood depends on the toxic polyphenolic compounds encrusted in the cell wall and lumen; often, the individual extractive compounds may contribute decay resistance (Haupt *et al*. 2003, Windeisen *et al*. 2003, Thulasidas and Bhat 2007; Koyani *et al.* 2015), which could be the reason behind the variation in cell wall damage. Similar patterns of resistance of teak wood to *Schizophyllum commune* has been demonstrated in our previous studies. In the later stage, i.e. after 60 days of fungal incubation in *Eucalyptus* and *Tectona* wood, *T. hirsuta* showed formation of erosion channels revealing transition from selective delignification to simultaneous degradation parallel to that in *Azadirachta*. Further decay by *T. hirsuta* resulted in the severity of formation of erosion troughs and erosion channels were common in wood of all wood species investigated. It has been reported that the presence of erosion troughs and channels, thinning of cell wall, boreholes, round or oval shaped pit erosion are characteristic features associated with simultaneous degradation by white rot fungi (Schwarze *et al.* 1995; Anagnost 1998; Luna *et al*. 2004; Yilgor *et al*. 2013). In case of *Eucalyptus*, formation of erosion channels and tunnels has been observed in the secondary wall of fibres indicating a transition from selective delignification to removal of cellulosic polysaccharides during the advanced stage of decay. Although internal cavity formation in cell walls is generally regarded as characteristic of soft rots, there are some evidences that it can also associated with white rot type of decay (Schwarze *et al*. 1995).

In the present study *Eucalyptus*, *Azadirachta* and *Tectona* show that these processes occur during different stages of degradation (initial and advanced) rather than a side by side. *Ganoderma pfeifferi* caused both selective and simultaneous rot in beech and oak wood suggesting both mode of decay can be caused by single fungus and the two processes can be occur side by side (Blanchette 1980; Schwarze 2007). Similar observations were also documented in the wood of *Ailanthus excelsa* caused by *Inonotus hispidus* (Koyani *et al*. 2011, 2015). Our results are in agreement with Levin and Castro (1998) who observed a combined pattern of selective and simultaneous white rot in Poplar by *Trametes trogii* during early and late stages of decay respectively.

Unlike wood of other three species, the degradation by *T. hirsuta* after 60 days of incubation in *Leucaena* wood was characterized by cell separation without degrading compound middle lamellae, rather the outer layer of secondary wall preferentially underwent degradation. This forms an unusual pattern as the erosion of outer layer of secondary wall do not show any structural similarities to that of white rot, where degradation commence from S_3 layer leaving compound middle lamellae till the advanced stage of decay (Yilgor *et al*. 2013).

After 60 days of *T. versicolor* incubation in all the four wood samples indicates that it causes the simultaneous rot. Structural alterations induced by *T. versicolor* includes thinning of cell wall in *Tectona*, boreholes formation in case of *Azadirachta* and *Leucaena* and apparent erosion channels formation all the four species. In the advance stage of decay *Leucaena* also showed formation of 'U' shaped notches. Separation of cells by dissolution of middle lamellae is frequently observed in all the four wood samples also indicates it's ability of selective mode of delignification. This feature also forms a common link between *T. hirsuta* and *T. versicolor* for their ability of a selective delignification process where former retains the selective mode of decay for extended periods. Apart from these white rot features, the present study also showed the multiple branching of hyphae within the cavities which is reported as a characteristic of soft rot decay by earlier workers (Schwarze *et al*. 2000b). Worall *et al*. (1997) postulated that evolution wood decay fungi began with a soft rot pattern from which white rot and subsequently brown rot have been evolved. Therefore, similarities in features of different groups of the two related species of fungi could plausibly due to their phylogenetic relationship with ancestral group.

On the other hand, decay in *Azadirachta* by *T. versicolor* after 60 days of incubation also featured collapse of vessels. The vessel and parenchyma cells often resist rapid degradation due to lignin concentration and phenolic accumulation respectively (Blanchette *et al*. 1987; Schwarze and Fink 1997). The vessel wall resists degradation by *T. trogii* in the wood of Poplar and Salix (Levin and Castro, 1998). The present study shows no such resistance from parenchyma or vessel and collapse of vessels after extensive wall degradation has been noticed from earlier stage of infection. The living trees of *A. indica* are known for their large diversity of secondary metabolites with antimicrobial properties (Biswas *et al*. 2002; Verma *et al*. 2007). Our

in vitro experiment results suggest that these compounds may be effective to protect the wood when trees are living but in dead wood blocks, both species of fungi i.e. *T. hirsuta* and *T. versicolor* easily penetrated within wood and caused drastic alteration, including the collapse of the vessels at the end of 120 days of incubation. .

After 90 days of incubation, severity of decay increased and majority of structural alterations in wood cell walls occurred during this period. At this stage *Trametes hirsuta* revealed simultaneous degradation pattern in all wood species. In *Eucalyptus*, oval shaped selectively delignified regions in the fibre wall that appeared during early stages of decay are coalesced and formed larger patches of erosion. Such large patches are characterized by complete removal of cell wall polymers (unstained regions) during this stage of decay. Erosion in oval patches extending from lumen to the middle lamellae has been demonstrated to be a specific feature associated with selective delignification in birch wood by *Phellinus pini* (Anagnost 1998). This further suggests loss of oval shape of erosion channels could be an anatomical feature during transition from selective to the simultaneous mode of decay by *T. hirsuta* in *E. globulus* (Anagnost 1998). In case of *Azadirachta*, severity of fibre wall thinning, increase in defibrillation and formation of borehole through middle lamellae and secondary wall was noticed frequently in most of the samples investigated. Moreover, delignification of ray cell walls was evident from the unstained region within the cell wall. In *Tectona* fibres often showed erosion channels within the S_2 wall layer resembling boreholes like soft rot decay by the progression of erosion channel (in the vertical axis) parallel to middle lamella on the upper and lower side. On the other hand, in *Leucaena*, our results showed large erosion channels progressing sidewise in the transverse sections to cover the partial circumference of cells. Ruel *et al*. (1981) reported that in the wood of spruce (*Picea abies*) degradation by *Phanerochaete chrysosporium* originated at the pit membrane and degradation was evident across the transition between the S_1 and S_2 layers. A lateral progression of degradation occurred within the secondary wall and disintegration became evident in the transition area between the S_1–S_2 and S_2–S_3 layers, while the middle lamella was degraded after the secondary wall was severely eroded. Therefore, the decay pattern by *T. hirsuta* during degradation of *Leucaena* wood showed structural similarities to that of *P. chrysosporium* in spruce wood.

Similar to *Trametes hirsuta*, *T. versicolor* also depicted structural changes showing the simultaneous type of wood degradation in *Eucalyptus*, *Azadirachta* and *Tectona* except *Leucaena*. Thinning of the wall and dissolution of middle lamellae resulted in appearance of thin walled isolated fibre tracheids during an advanced stage of decay in *Eucalyptus*. In *Azadirachta*, the simultaneous degradation of secondary wall during advanced stage of decay resulted in large boreholes with irregular shape. Such formation of boreholes in secondary wall is a feature of soft rot. Moreover, the secondary wall of fibre in *A. indica* showed cavities along the angle of cellulose microfibrils. This feature reported to be soft rot characteristics in which cavities resembles like tunnels and are formed along the orientation of cellulose microfibrils in secondary wall (Courtois 1963). However, this feature has also been described for a range of wood decay caused by basidiomycetes (Daniel *et al*. 1992; Worrall *et al*. 1997; Schwarze and Fink 1998). In case of *Tectona*, also the formation of erosion troughs in vessel wall was noticed. Rest of the features as discussed for simultaneous degradation by *T. hirsuta* is also revealed by *T. versicolor*.

In *Leucaena*, multiseriate rays appeared hollow due to complete removal of ray cell walls in the central region. Degradation of pectin rich middle lamellae commenced after the delignification of secondary walls resulted in conspicuous hollowing multi-seriate xylem rays in beech wood (Schwarze and Fink 1998). On the other hand, the separation of fibre cell walls through degradation of middle lamellae by *T. versicolor* indicates its ability for selective mode of decay also. Obst *et al.* (1994) reported that *T. versicolor* caused preferential degradation of cell corners and middle lamellae of fibre wall in seven species of hard wood. *T. versicolor* removed lignin first in the fibre wall of Poplar and subsequent biochemical changes of cell wall polymers suggests that it may facilitate access to the cell wall carbohydrates (Skyba *et al*. 2013). Similar feature is observed in *Eucalyptus*, *Azadirachta* and *Tectona* wood wherein in early stage of degradation in these wood species showed that selective and simultaneous degradation occur during different stages of degradation (initial and advanced) rather than a side by side process.

During the advanced stage of decay (after 120 days) by *Trametes hirsuta* simultaneous type of degradation was prevalent in *Eucalyptus*, *Tectona* and *Leucaena* while *Azadirachta* at this stage revealed selective delignification. Collapse of the vessel was observed following the migration of fungal mycelia from contact rays into

vessel and wall erosion around the bordered pits was common in the secondary wall of fibre tracheids causing subsequent degradation of its wall. The axial alignment xylem fibres and vessels and the radial arrangement of xylem ray parenchyma make easy access into the wood and allow widespread distribution of hyphae within the xylem (Schwarze *et al*. 2004). This resembles to the collapse of vessel wall of *Azadirachta* by *T. versicolor* after 60 days of incubation. Although localized removal of middle lamellae has been the feature associated with simultaneous rot (Anagnost 1998). In *Azadirachta*, complete removal of middle lamellae after 120 days resulted in isolated, separated cells were evident from Fig. 3i. This suggests the affinity of both the fungal species towards the selective delignification pattern. In *Tectona* during this stage, the fibre secondary wall became heavily eroded and typical L-bending pattern become distinct across and along the length of the cell wall. with the advancement of decay by *Trametes hirsuta* simultaneous degradation further proceeded forming large erosion channels through the wall between adjacent fibres and thinning of the cell wall.

Chlamydospore formation has also been observed during the advanced stage of decay in *Eucalyptus* and *Azadirachta* wood by *T. versicolor* suggesting its potential of spread and capacity of new host colonization (Robles *et al*. 2014). Formation of chlamydospores has been one of the conspicuous features during advanced stage of decay by *T. versicolor*. Chlamydospore formation may be crucial to survive under dry or moist condition which allows the survival in time rather than space for a range of wood decay fungi (Powell 2002; Schwarze 2007). On the other hand, similar to *T. hirsuta*, complete removal of middle lamellae in *Azadirachta* by *T. versicolor* resulted into cell separation, suggesting affinity towards the selective delignification pattern. The blue colored staining of cell wall during advancement of decay due to the presence of cellulosic polysaccharides stained with astra blue also suggests that lignin might have removed during the early stage of decay. In Poplar, the enzymatic system of white rot fungus *T. versicolor* removes lignin first facilitating access to the cell wall carbohydrates resulted in significant weight loss and greater extent of lignocellulose composition (Skyba *et al*. 2013). Our result also suggest the selective removal of lignin from the cell wall during initial stage, facilitating access to cell wall polysaccharides and simultaneous degradation of cellulosic polysaccharides proceeds at an advanced stage resulting in thinning of the wall.

In *Tectona*, the fibre wall collapsed due to increase in the wall thinning. In case of *Leucaena* formation of boreholes occurred in the inter vessel walls. Moreover, ray cell inhabited by fungal mycelia revealed extensive degradation. In hardwoods, vessels and ray parenchyma considered to be resistant to fungal degradation due to the presence of more guaiacyl lignin units and polyphenolic substances respectively (Blanchette 1984; Schwarze 2007).

Confocal microscopy also revealed the extensive degradation of lignin from the cell wall of all types of wood elements undergoing fungal degradation. During advanced stages of decay in all wood species investigated, degradation of fibres and vessel wall delignification in cell wall components was evident supporting the light microscopy observations. These results indicate the strong ligninolytic activity of *T. hirsuta* and *T. versicolor* as well as vulnerability of lignin composition to their enzymatic mechanism against all the four wood species.

In *Eucalyptus*, the collapse of the vessels in the advance stage of decay by both *T. hirsuta* and *T. versicolor* through erosion channels formed between the bordered pits. Large voids in the tangential wall by lateral merging of erosion channels has also been noticed in the vessel during advanced stages of decay indicating removal of polysaccharides and strong ligninolytic activity during this stage. In *Azadirachta*, the cell corners of fibres and parenchyma showed resistance to decay even during advanced stages of decay while rest of wall regions underwent extensive erosion of wall erosion. The decay resistances of cell corners of hard wood fibres have been attributed to the relatively more lignin concentration and guaiacyl monomeric units compared to secondary wall rich in syringyl units (Obst *et al*. 1994). On the contrary, the present study also showed that the vessel wall with similar lignin characteristics undergoing degradation during advanced stages of infection. The lignin distribution pattern in vessel and parenchyma cells also supports our light microscopic observation on degradation of wall polymers in these cell types, suggesting strong ligninolytic activity shown by both the species of *Trametes* used in this study. Although *T. hirsuta* in *Azadirachta* and as well as *T. versicolor* in *Tectona* induced selective delignification during the initials stages of decay, removal of cellulosic polysaccharides resulting in thinning and formation of erosion channels has been noticed in the advanced stage of decay. Our results are in agreement with Levin and Castro (1998), who observed a combined pattern of selective and simultaneous white

rot. In *Leucaena*, the fluorescence intensity greatly diminished during the degradation of these cell wall/regions during advanced stages of decay.

According to Robles *et al*. (2014), high concentration of lignin in the vessel wall makes it resistant to attack by some white rot fungi. Both vessel wall and compound middle lamellae of fibres generally resist degradation due to the presence of more condensed guaiacyl lignin monomers in these regions (Blanchette 1984; Grunward *et al*. 2002; Pramod *et al*. 2012). Species of *Trametes* are considered to be most efficient degraders in which the ligninolytic enzyme system is comprised of laccase and Mn dependant peroxidase (MnP) as well as a series of cellulases and cellobiose dehydrogenase (Nakagame *et al*. 2006).

In general, both the species *T. hirsuta* and *T. versicolor* in *Eucalyptus*, *Azadirachta* and solely *T. hirsuta* in *Tectona* showed a combined pattern of degradation of selective and simultaneous rot. Whereas in *Leucaena* both the species and exclusively *T. versicolor* in *Tectona*, showed the typical simultaneous mode of decay during initial and advanced stage of decay.

T. hirsuta induced selective delignification in *Eucalyptus* that is evident from the typical anatomical features like cell separation, formation of oval shaped cavities rich in cellulosic polysaccharides and pit erosion while degradation of all wall constituents was noticed in advanced stages of decay resulting in transformation of oval cavities into large void areas. *T. versicolor* showed distinct simultaneous white rot decay pattern in the early stages of wood decay leading to formation of erosion channels across the wall and tunnels within the secondary wall. Although *T. versicolor* showed simultaneous rot, its ability for selective delignification was evident from the dissolution of middle lamellae and separation of cells, and this also forms a similar white rot feature exhibited by both the species of *Trametes* used in this study. Hence our results suggest that both the species of *Trametes* possesses ability for selective and simultaneous modes of decay with a specific difference in its duration of former decay mode in the wood of *E. globulus*.

In case of *A. indica* during initial stages of decay, *T. hirsuta* showed selective delignification while removal of carbohydrates during advanced stage of infection resulted in erosion of the cell wall. *T. versicolor* showed a typical simultaneous pattern of white rot with characteristic anatomical features such as erosion channels

with ‘U’shaped notch appearance and separation of cells. Confocal microscopy revealed the removal of lignin from cell types including vessels and parenchyma which often resist degradation.

In case of *Tectona* wood, *T. hirsuta* showed simultaneous degradation during the early stage of decay by formation of erosion troughs. On the other hand, further decay caused cell separation and dissolution of middle lamella indicating a typical selective mode of delignification which was also confirmed in confocal microscopy. In contrast, at the advanced stage formation of borehole, erosion channels and degradation of vessel and fibre wall depicted characteristic feature of simultaneous degradation. Also a typical L-bending pattern which is a distinct soft rot feature was also noticed. On other hand, *T. versicolor* showed a majority of features characteristic to simultaneous rot with the formation of erosion channels, erosion troughs and thinning of fibre wall leading to collapse of fibres.

In *Leucaena*, present study revealed that both *T. hirsuta* and *T. versicolor* cause anatomical changes in the cell wall specific to the simultaneous mode of decay. Many of the structural changes during advanced stages of decay such as thinning of the fibre cell wall in two distinct patterns, formation of boreholes and pit erosion were similar for both the species of *Trametes*. However, cell separation without degrading the compound middle lamellae with preferential degradation of outer secondary wall layer during the initial stages of decay was an unusual pattern showed by *T. hirsuta*. A detailed investigation on enzymatic activity with respect to the timing of structural alternation in the cell wall will be helpful to understand the physiology of the unusual degradation pattern shown by *T. hirsuta* in *Leucaena* wood.

Figure 48(a-p): Transverse (a, i, m and n), tangential (b, d-h, j-l, o and p) and radial longitudinal (c) sections of *Eucaltyptus globulus* wood blocks infected with *Trametes hirsuta* for 30 (a-d), 60 (e-k), 90 (l and m) and 120 (n-p) days.

a. Separation of cells (arrowhead) and blue colored regions (cellulose stained with astra blue) of secondary wall (arrows) indicating the selective delignification.
b. Branching of mycelia and migration into adjacent fibre through the pit (arrow).
c. The erosion channels showing blue to white color due to selective delignification (arrow).
d. Fibre wall showing selective delignification (arrow).
e. The secondary wall of fibres adjacent to pit showing selective delignification (arrow).
f. Extensive delignification of fibre wall showing cellulose rich secondary wall.
g. The ray cell showing separation (arrow). Note the selective delignification of adjacent fibre.
h. Separation of ray cells.
i. Fibre showing dissolution of middle lamellae followed by cell separation (arrow).
j. The erosion channels formed across the bordered pits in the vessel (arrow).
k. The advanced stage of erosion vessel wall (asterisk).
l. Fibre wall showing patches of unstained regions representing the degraded wall (arrow).
m. The middle layer of secondary wall showing whitish space formed after delignification (arrows).
n. Collapse of vessel (V) during advanced stage of decay. Note the fungal mycelia (arrow) passing through the erosion channels in the contact rays (R).
o. Pits in the fibre showing enlargement following erosion and joining of adjacent ones (arrows).
p. Ray cells (R) showing separation from the axial elements and formation of erosion channels.

Scale bar: (a-p) = 10µm

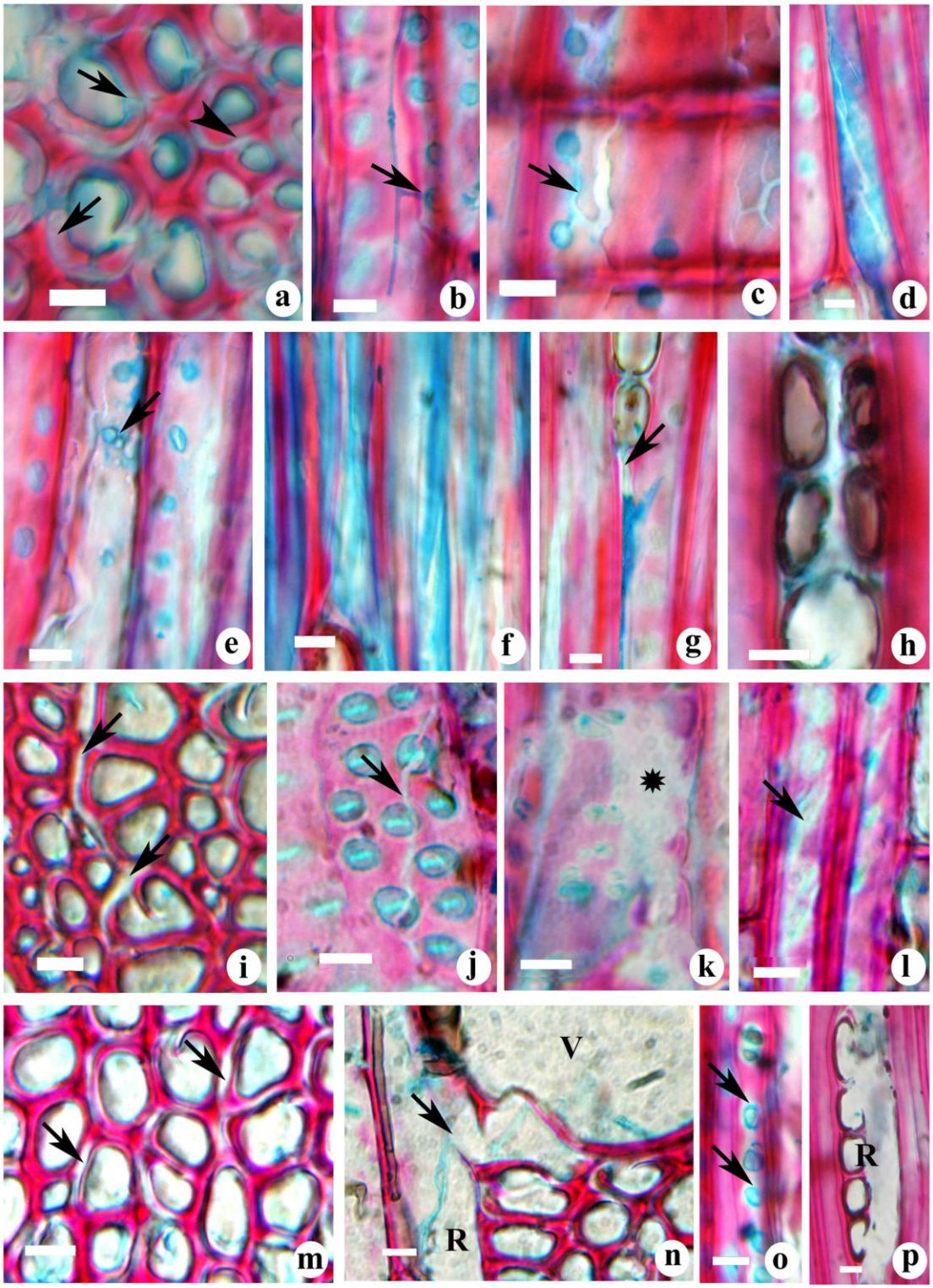

Figure 48

Figure 49 (a-u): Transverse (a, l, p and t) tangential (b-k, m, n, o, q and r) and radial longitudinal (s and u) sections of *Eucalyptus globulus* wood blocks infected with *Trametes versicolor* for 30 (a-k), 60 (l-o), 90 (p-s) and 120 (t and u) days.

a. Thinning of secondary wall (arrow) and separation of s. Note the preferential degradation of outer layers of fibre secondary wall and its lateral expansion.
b. Mycelia migrating into adjacent cells through pits in the tangential wall (arrow).
c. Branching of mycelia with thin cell lumen of fibre (arrow).
d. Erosion channels formed in the radial wall of fibre (arrow). Note the large bordered pit on the tangential wall of adjacent fibre tracheid.
e. Fungal mycelia entering into pit (arrow).
f. Mycelia passing through the pit (arrow).
g. Vertical growth of fungus within cell wall through middle lamellae (arrow).
h. Separation of cells after dissolution of middle lamellae (arrow).
i. The wall around the pit showing erosion of secondary wall (arrow).
j. Enlargement of erosion channels in the fibre tracheids (arrow).
k. The 'U' notch appearance of erosion channels in tangential sections of fibre tracheids (arrow).
l. Separation of cells (arrow) and formation of large erosion channels (arrowheads) in the fibre secondary wall.
m. Separation of wall between fibre tracheids and ray cell beneath the fibre (arrow).
n. Progression of erosion of fibre wall in vertical direction (arrow).
o. Separation of ray cells after dissolution of middle lamellae in both radial and tangential walls (arrow).
p. Delignification followed by collapse of vessel wall (V). Arrow indicates eroded region of secondary wall of vessel. Note the mycelia passing through the contact rays (R) and erosion channels in the parenchyma cell.
q. Vessel wall showing erosion channels formed pit between adjacent bordered pits. Note the blue colored mycelia within the erosion channel (arrow).
r. Mycelia (arrow) passing through the bordered pits in the fibre tracheids (F) and simple pits in the ray cell (R).
s. The fungal mycelia passing through erosion channel in the ray cell wall (arrow).
t. The thinning of secondary wall (arrow) and separation of fibre tracheids during advanced stage of decay.
u. The chlamydospore formation in the fungal mycelia within the cell lumen (arrow).

Scale bar: (a-u) = 10µm

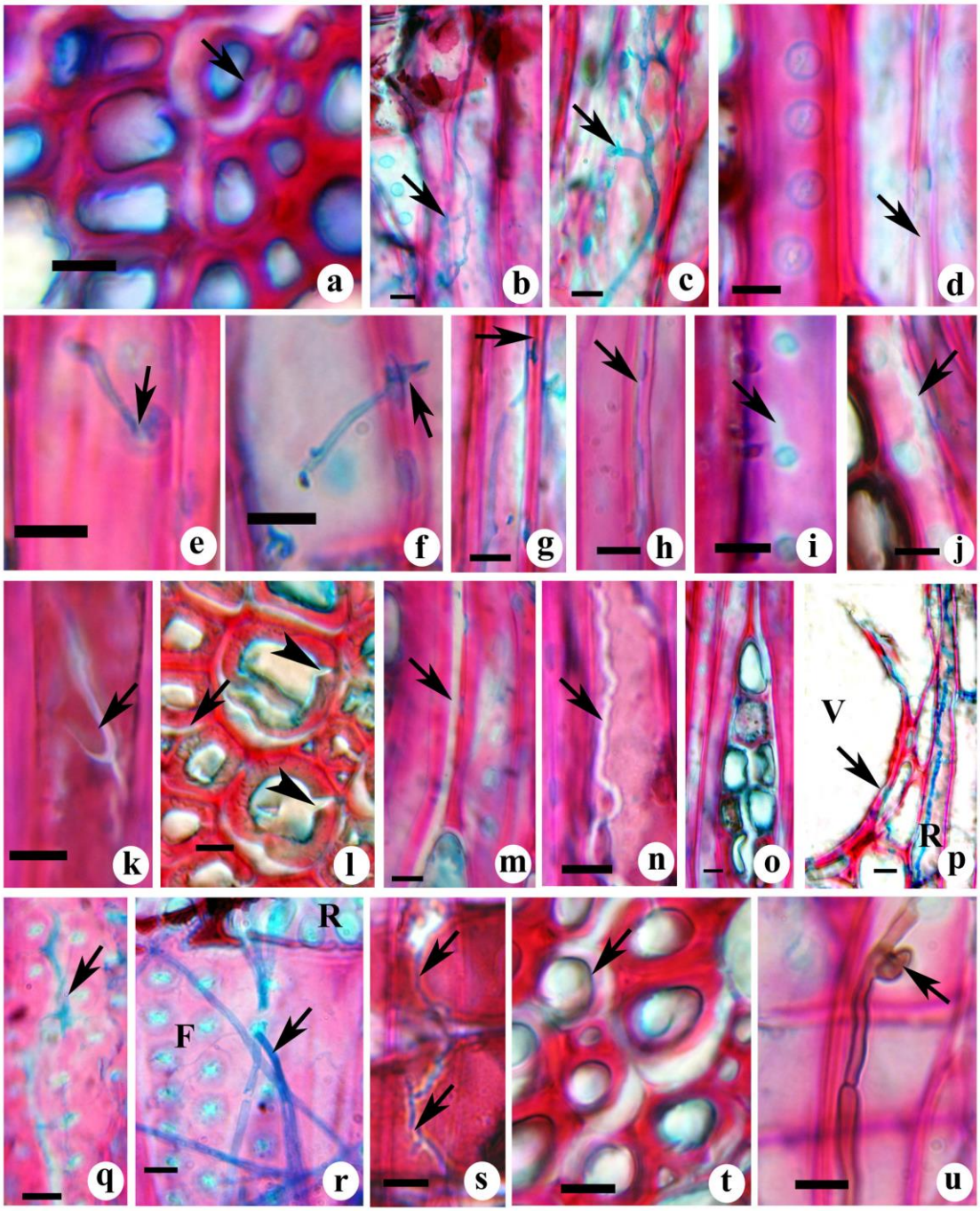

Figure 49

Figure 50 (a-h): Confocal images of transverse sections from the wood of *Eucalyptus globulus* infected with *Trametes hirsuta* (a-d) and *Trametes versicolor* (e-h).

a. Lignin degradation in the inner secondary wall layer of vessel (V) wall (arrow).
b. The advanced stage of delignification of vessel (V) wall showing disappearance of auto-fluorescence from S_2 and S_3 layers.
c. The middle lamellae region of fibre (arrows) showing delignification indicated by absence of auto-fluorescence.
d. Lignin degradation leading to collapse of vessel and separation of its associated cells (arrow).
e. Vessel (V) wall showing delignified wall with dotted appearance of fluorescence.
f. Enlarged view of vessel (V) wall delignification (arrow). Arrowhead indicates the lignin rich secondary wall showing fluorescence.

g, h. Fibres showing absence of auto-fluorescence from compound middle lamellae and cell corners following delignification.

Scale bar: a, b, e-g=10µm; c, d and h=5µm

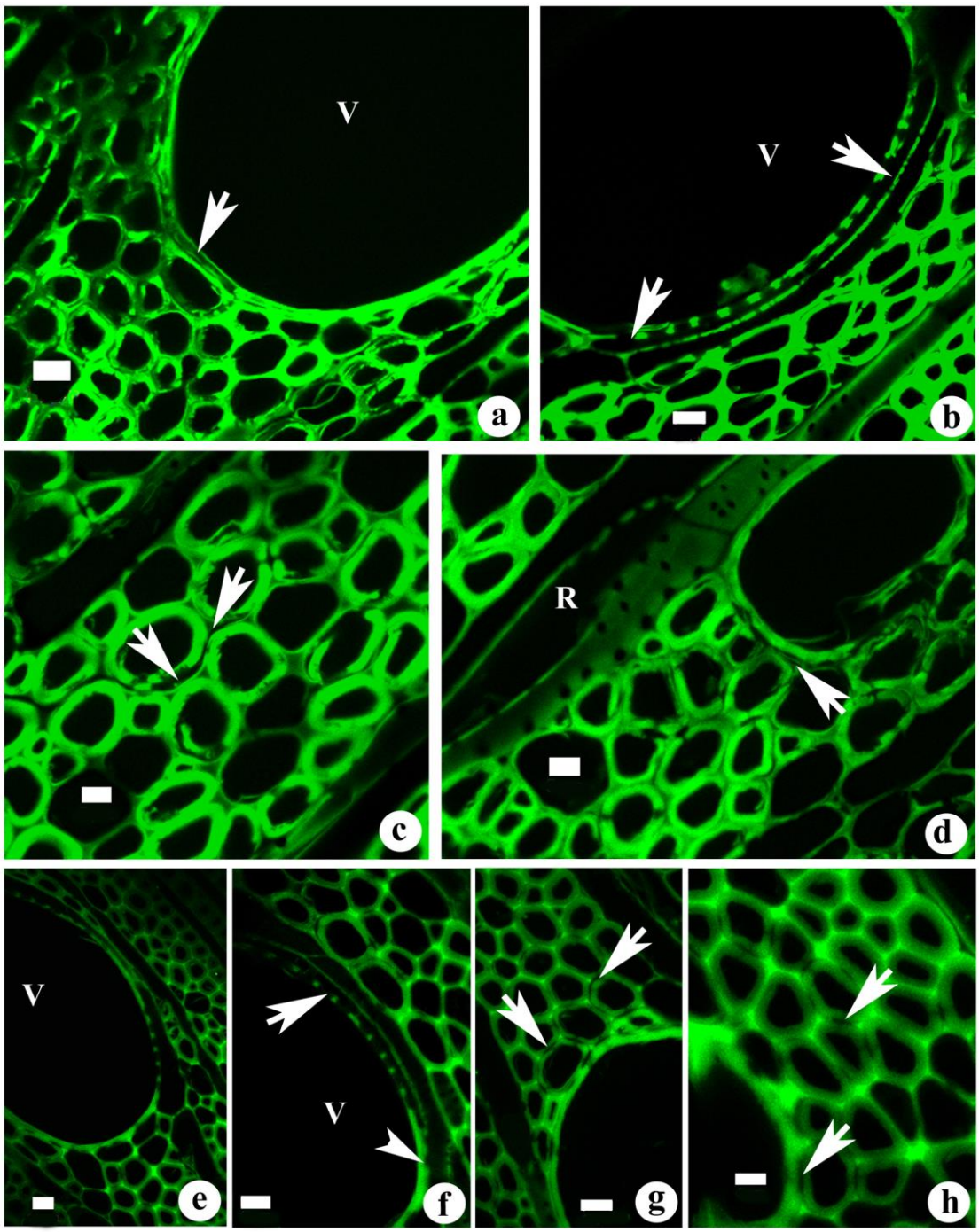

Figure 50

Figure 52 (a-h): Transverse (a, f and g) and tangential longitudinal (b-e and h) sections of *Azadirachta indica* wood blocks infected with *Trametes hirsuta* for 30 (a-h) days.

a. Defibrillation of fibres (arrows). Note fungal hyphae passing through the rays (R).
b. Mycelia passing through the simple pit (arrow) between the rays.
c. Mycelia passing between fibres through the erosion of simple pit in the radial wall (arrow).
d. The radial wall of fibre showing round to oval shaped holes of different sizes (arrows).
e. Separation of ray cell wall (arrow).
f. Axial parenchyma showing spreading of fungal hypha by breaking the cell wall (arrow). Arrowhead indicates progression of delignification from cell corners towards compound middle lamellae.
g. Breaking of cell wall between ray (R) and axial parenchyma (asterisk). Arrow and arrow head indicate the defibrillation of fibres and thinning of paratracheal parenchyma cell wall respectively. V=vessel.
h. The ray cell wall showing large gap (arrow) formed after degradation of cell wall.

Scale bar: (a-h) = 25µm

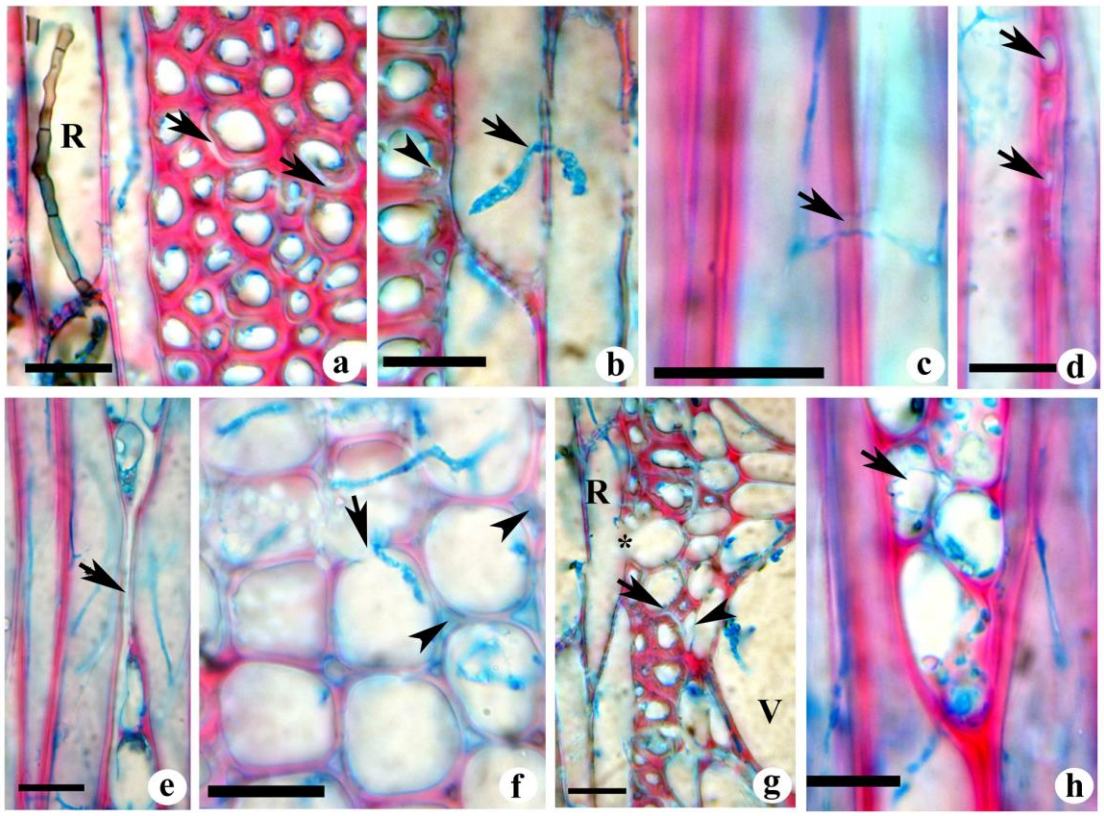

Figure 52

Figure 53 (a-j): Transverse (a, b, h and i) and tangential longitudinal (c, d, e, f, g and j) sections from the wood of *Azadirachta indica* infected with *Trametes hirsuta* for 60 (a-e), 90 (f and g) and 120 (h-j) days.

a. Extensive damage to fibre wall through defibrillation and cell separation (arrows). Note the enlarged view of completely degraded region (arrow head) of secondary wall of fibre given in the box on upside right corner.
b. Fungal hyphae passing through the compound middle lamellae between ray cell (R) and adjacent fibre (arrow). Arrowhead indicates the separated region of secondary wall between fibre and ray cell (R).
c. Boreholes on the radial (arrows) and tangential (arrowhead) wall of fibre. Note the hole on the radial wall formed through erosion of pit and extending tangentially by simultaneous degradation of secondary wall.
d. Round to oval shaped boreholes of different sizes on the fibre secondary wall (arrows). Arrowhead indicates the boreholes showing fungal mycelia.
e. The fibre showing extensive degradation of secondary wall region (arrow).
f. Fungal mycelia passing through the eroded region of secondary wall of fibre (arrow). The large borehole (arrow head) formed through degradation of middle lamellae and secondary wall is given in the box on upside right corner.
g. Delignification of compound middle lamellae region of ray cells (arrow).
h. The isolated secondary wall regions of fibres after degradation of compound middle lamellae region (arrows).
i. Spreading of degradation from compound middle lamellae to secondary wall of axial parenchyma cell (arrow).
j. The separated radial wall of fibre (arrow). Note the ray (R) with large hollow space after complete degradation of cells.

Scale bar: a-e, g, h and i= 25µm; f (box) & j= 10 µm

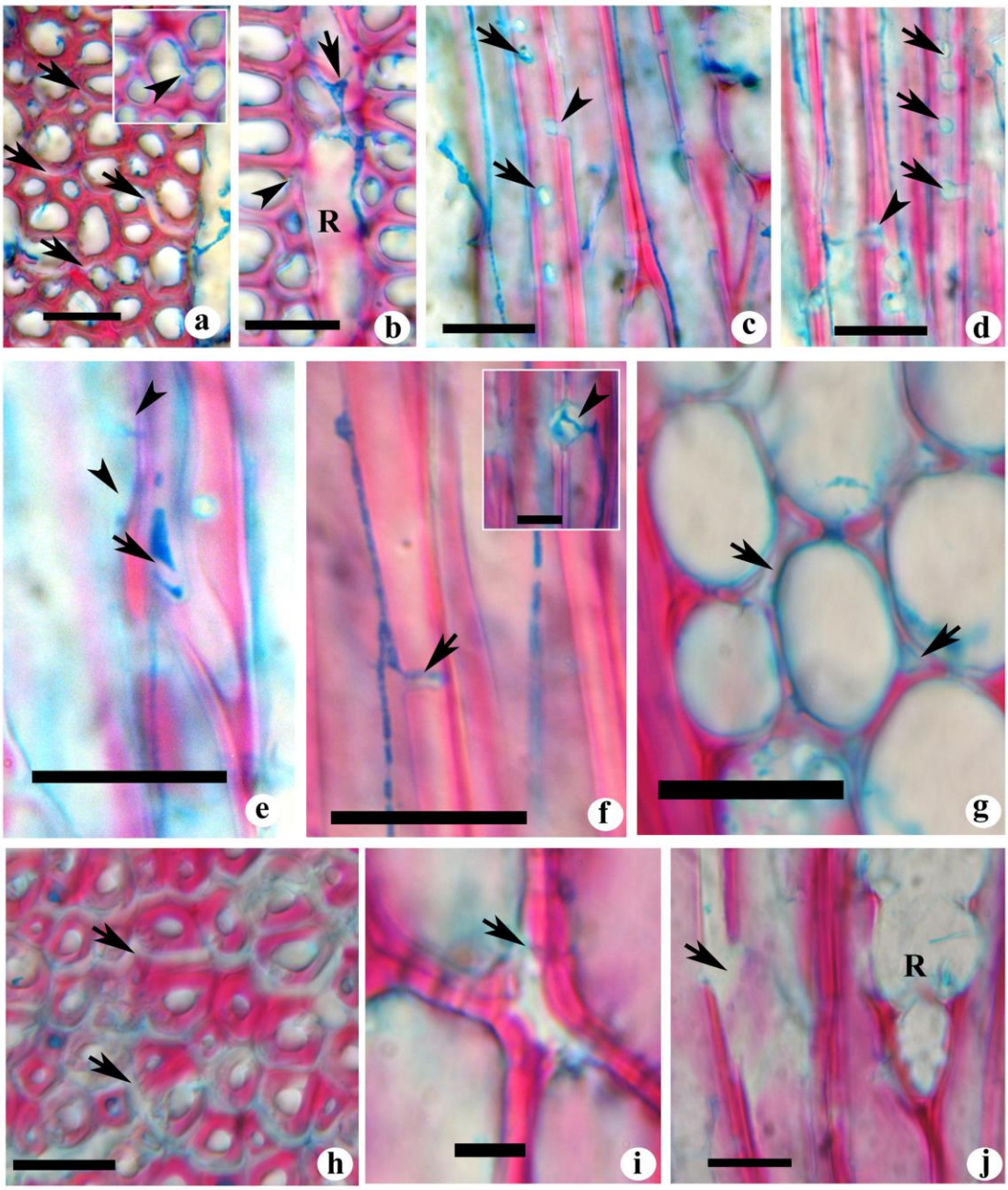

Figure 53

Figure 54 (a-l): Transverse (a, b, d-g and k) and tangential longitudinal (c and h-j) and radial longitudinal (l) sections from the wood of *A. indica* infected with *Trametes versicolor* for 30 (a-d), 60 (e-i), 90 (j) and 120 (k and l) days.

a. Fungal hypha (arrows) passing through between ray (R) and axial parenchyma (P) through simple pits.
b. Defibrillation of fibre wall (arrows).
c. Dissolution of compound middle lamellae of fibre (arrow).
d. Delignified regions (arrows) of secondary wall of parenchyma cells and vessel (V). Arrowhead indicates the cell corner regions showing lignin content during late stage of delignification.
e. Degradation of middle lamellae resulting in separation of inter vessel (V) wall
f. The gap formed after simultaneous decay of middle lamellae and secondary wall between fibres (arrows).
g. The separated region of fibre (arrow) showing lignin rich cell corner region. Arrow head indicates the cell corner region retains after separation and thinning of adjacent cells.
h. Simultaneous degradation of secondary wall of fibres. Note the small thread of compound middle lamellae region (arrow) within the degraded secondary wall.
i. The eroded region of fibre secondary wall at late stage of decay (arrows).
j. Degradation pattern of secondary wall of fibre along the angle of cellulose microfibrils (arrows).
k. The separated and eroded secondary wall regions of fibre and vessel (V) at late stage of decay.
l. The hypha within the axial parenchyma showing chlamydospore (arrow). Note the thinning of mycelia (arrowhead) while passing through the simple pit.

Scale bar: a, b, d, e, h, j, k = 25µm; c, f, g, j, l = 10 µm

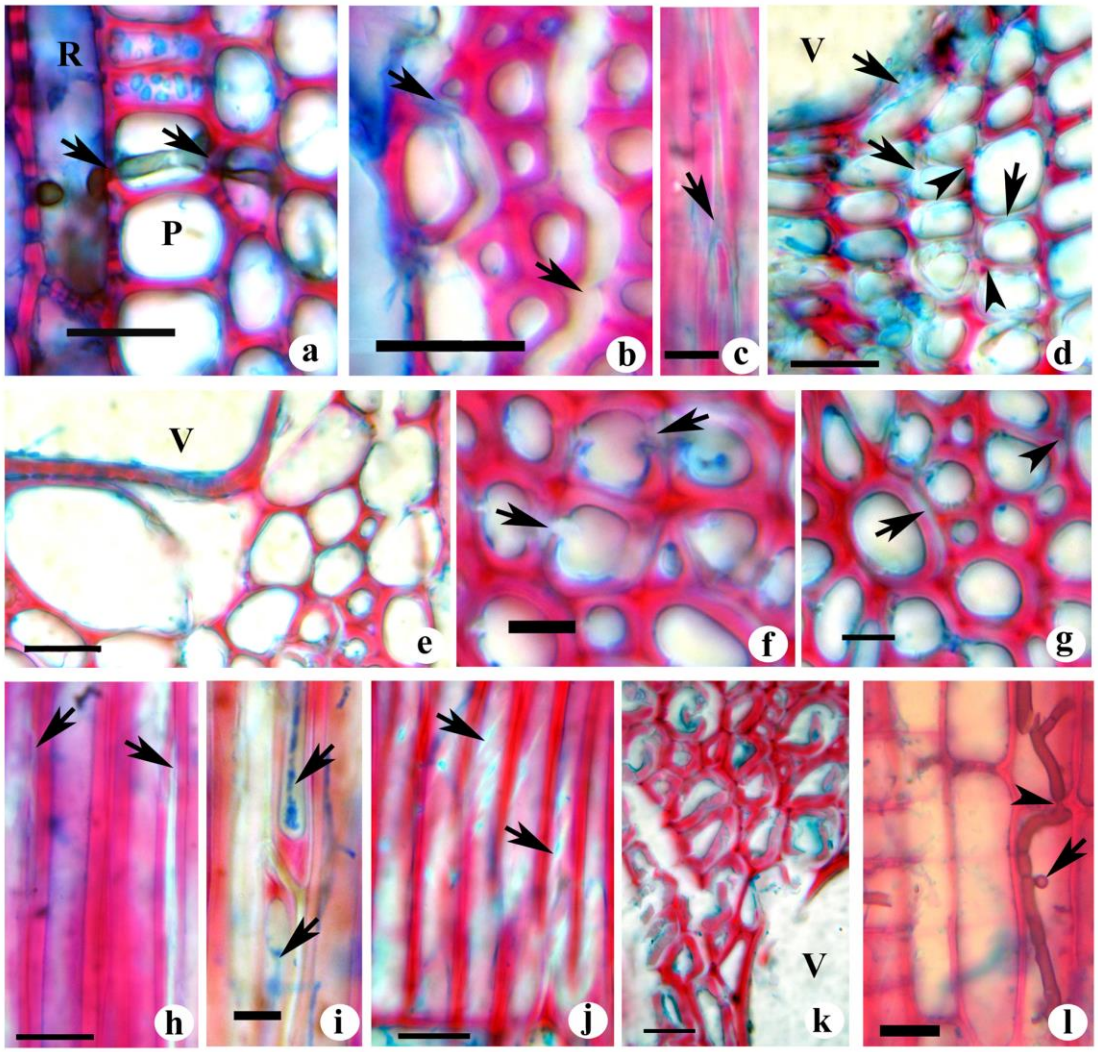

Figure 54

Figure 55 (a-j): Confocal laser scanning images from the transverse sections of *Azadirachta indica* wood blocks infected with *T. hirsuta*(a-f) and *T. versicolor* (g-j).

a. The infected wood showing lack of auto fluorescence from the wall of collapsed vessels (V) and ray cell (R). Arrow indicates the erosion channel in the fibre wall.
b. The non-fluorescent regions in the radial and tangential wall of fibres following erosion of lignin (arrows).
c. Vessel wall showing delignified region (arrow).
d. Paratracheal parenchyma (P) showing extensive degradation of lignin from the wall undergoing simultaneous rot. Arrows indicate the erosion channels in the fibre wall.
e. The non-fluorescent area representing the eroded region in the tangential wall of ray cell (arrow).
f. Degradation of lignin from the wall through which the fungal mycelia passing between adjacent cells (arrows). An overlaid image of bright field and fluorescence signals showing fungal mycelia (arrow) is given in the bottom.
g. Vessel wall showing non-fluorescent delignified regions (arrow) in the secondary wall of vessel (V) as well as in the compound middle lamella and erosion channel in the paratracheal parenchyma (P) cells (arrowheads).
h. Delignified wall through which fungal mycelia passing between ray (R) and axial parenchyma cells (arrow). An overlaid image of bright field and fluorescence signals showing fungal mycelia (arrow) is given in the bottom.
i. Paratracheal parenchyma cells showing lack of auto-fluorescence from the delignified region in the secondary wall (arrow) and cell corners region (arrowhead) inhabited by the fungal hypha.
j. Overlaid image of bright field and fluorescence signals image ‘i’. Arrow and arrowhead indicate the delignified wall regions of cells inhabited by the fungus.

Scale bar: a= 20µm; b-j= 10µm

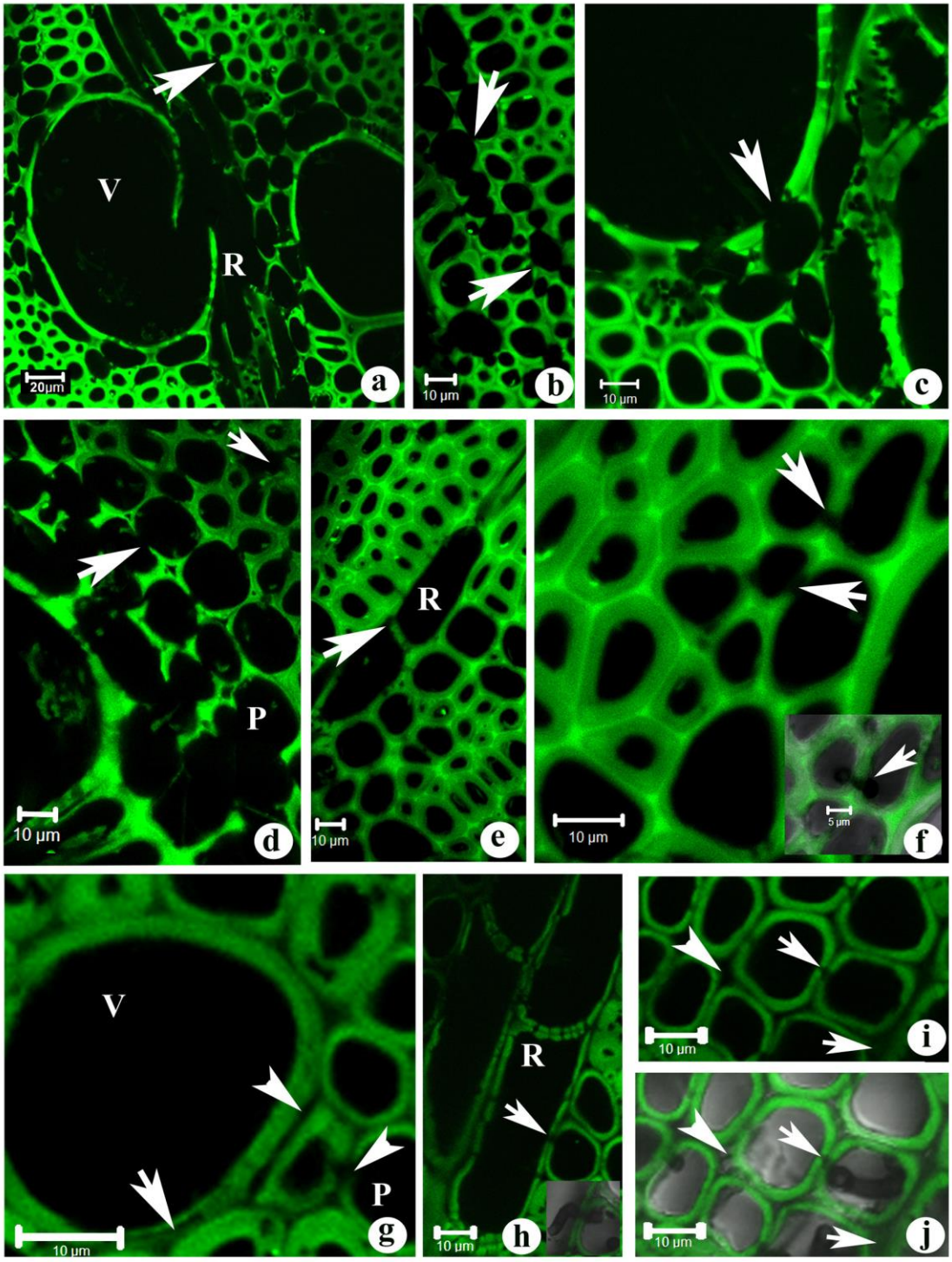
V
R
20µm
a
10 µm
b
10 µm
c
P
10 µm
d
R
10 µm
e
10 µm
5 µm
f
V
P
10 µm
g
R
10 µm
h
10 µm
i
10 µm
j

Figure 55

Figure 57 (a-q): Transverse (a, b, k, m and o) tangential (c-j, l and n) and radial longitudinal (p and q) sections of *Tectona grandis* wood blocks infected with *Trametes hirsuta* for 30 (a), 60 (b-e), 90 (f-m) and 120 (n-q) days.

v. Formation of erosion troughs and separation of secondary wall near the compound middle lamellae (arrow). Note the compound middle lamellae remain intact indicating cell wall separation may occur from S_1.
w. Separation of cell through dissolution of middle lamellae in the transverse section indicating a typical selective white rot decay pattern (arrow).
x. Separation of ray cell in the longitudinal section (arrow).
y. Fungal hyphe passing through the ray cells. Fungal mycelia entering into pit (arrow).
z. Formation of large hollow pockets within the rays (R) and formation of erosion channels on the walls of fibres (arrow).
aa. Enlargement of boreholes in the fibre wall (arrow).
bb. Boreholes become more apparent (arrow).
cc. Formation of large erosion channels due to merging of boreholes.
i, j. Formation erosion channel along the angle of cellulose microfibrils.
k. Degradation of cell wall from the side facing the paratracheal parenchyma cells (arrow).
l. Formation of large eroded regions on the cell wall due to erosion and extension of bordered pits.
m. Formation of erosion channels within S_2 layer (arrow).
n. Fungal mycelia throughout the cell lumen of all the cell types.
o. Separation of fibres adjacent to vessel wall (V).
p. Heavy erosion in the secondary wall of fibres.
q. Typical 'L' bending pattern along the length of cell wall.

Scale bar: a, d, f-h, m= 10 µm; b, c, e, n=25 µm; i-l, p, q =5 µm

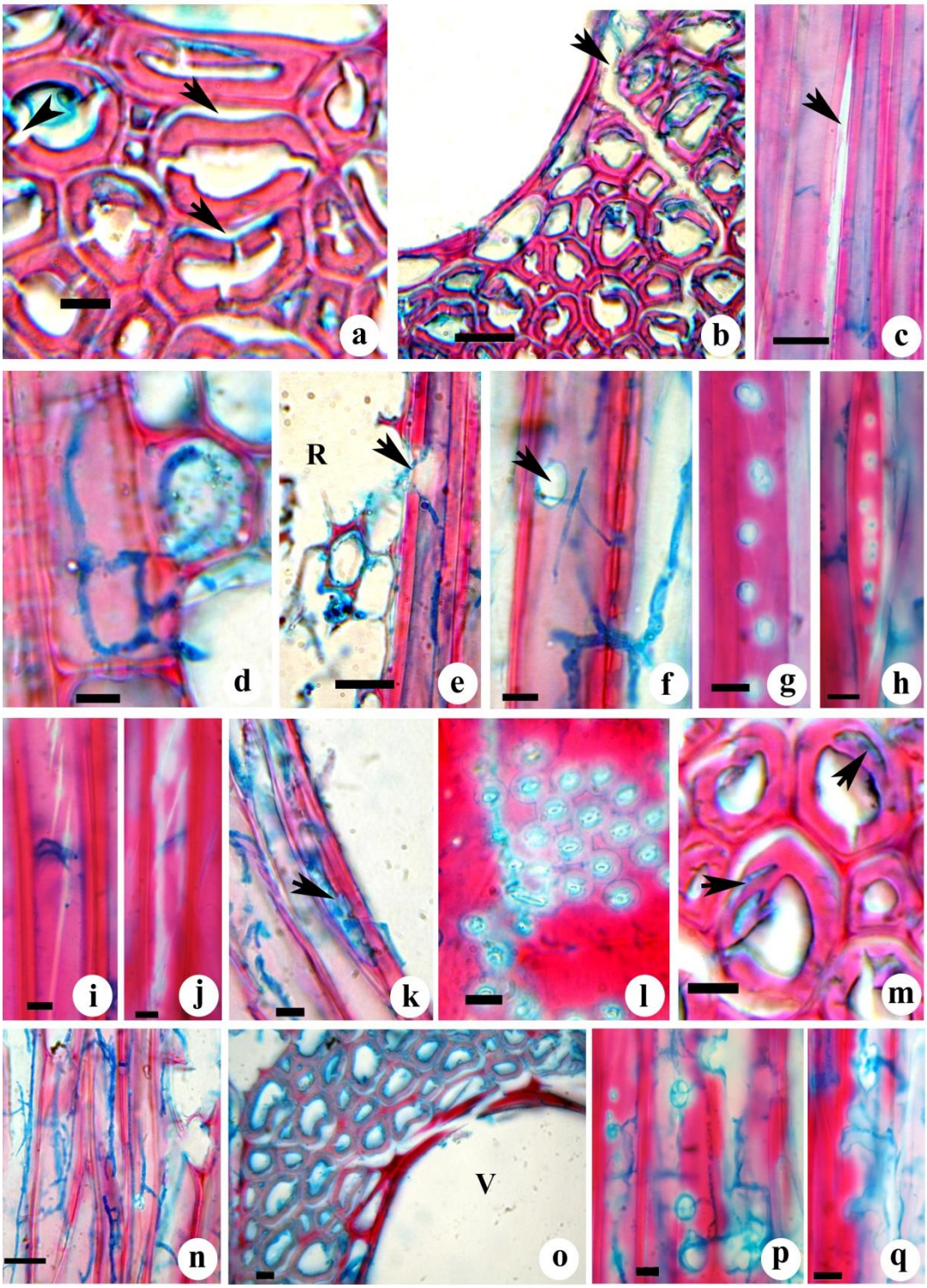

Figure 57

Figure 58 (a-g): Transverse (a, e and f) tangential (c-j, l and n) sections of *Tectona grandis* wood blocks infected with *Trametes versicolor* for 30 (a), 60 (b-d), 90 (e) and 120 (f and g) days.

dd. Cell wall separation from the outer S_1 layer (arrow).

ee. Erosion channel moving through fibre wall.

ff. Thinning of fibre wall (arrow) indicating a typical simultaneous white-rot feature.

gg. Progression of erosion channel in the wall region between the adjacent bordered pits.

hh. Formation of erosion troughs from lumen side towards middle lamellae (arrow) and separation of inter-vessel (arrow).

ii. Thinning and collapse of fibre wall.

jj. Unstained patches eroded region of wall within the lignified secondary walls of fibres.

Scale bar: a, c, f = 10 µm; b, d, e = 5 µm; g = 25 µm

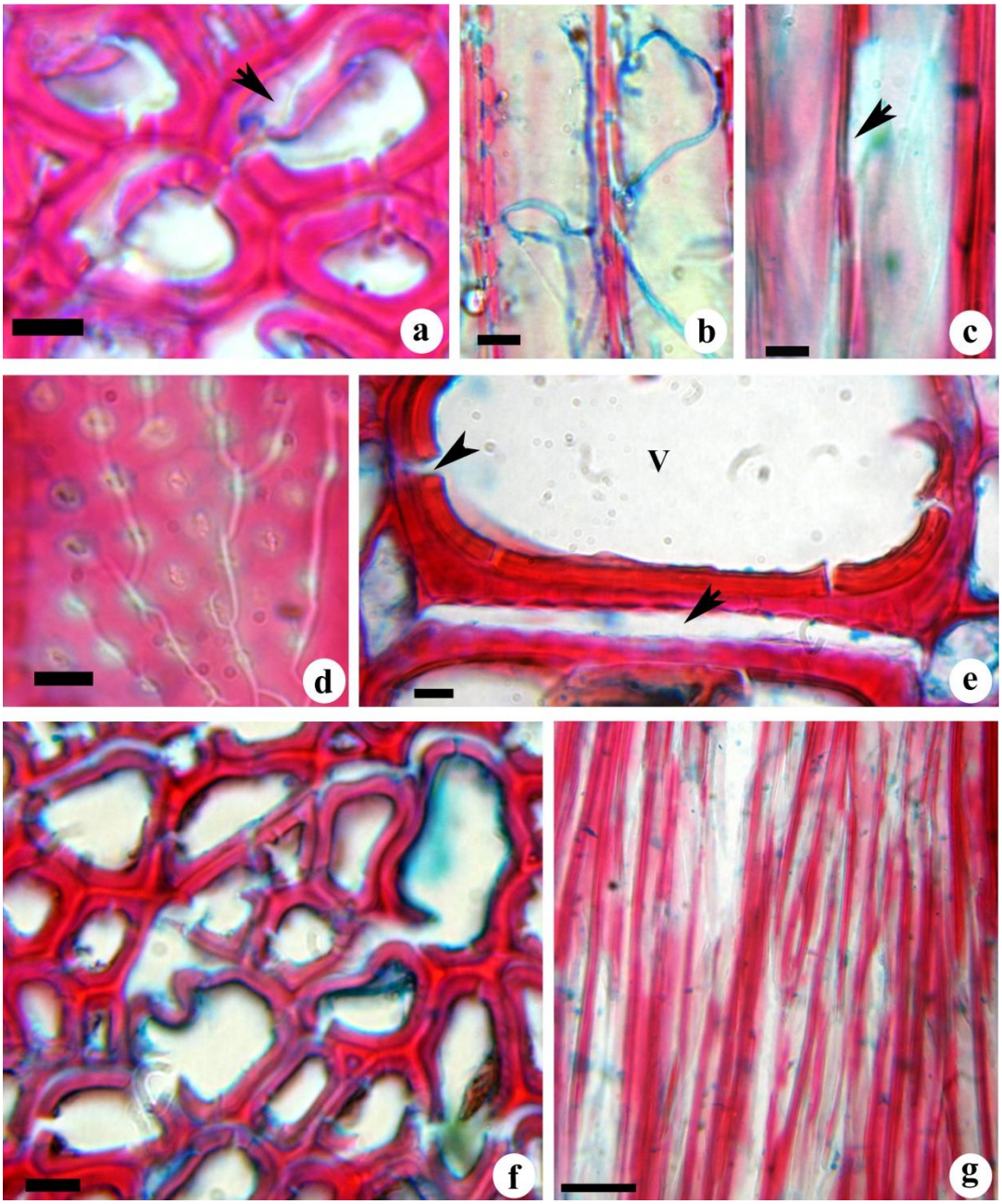

Figure 58

Figure 59 (a-m): Confocal laser scanning images from the transverse sections of *Tectona grandis* wood blocks infected with *T. hirsuta* (a-e) and *T. versicolor* (f-m).

k. Erosion of secondary wall (arrow) and expansion of pit fields appeared as larger non-fluorescent regions in the cell wall (arrowhead).
l. Separation of cell wall from outer S_1 layer of secondary wall (arrow) and existence of compound middle lamellae (arrow).
m. Absence of fluorescence from the later areas indicated the delignification of compound middle lamellae (asterisk) and collapse of cells during late stage of decay (arrow).
n. Thinning of secondary wall and formation of erosion troughs in the vessel (V) wall (arrow).
o. Formation of erosion troughs in the vessel (V) and adjacent ray (R) cells (arrow).
p. Erosion from cell lumen into compound middle lamellae (arrow) and subsequent delignification of cell corner region (arrowhead).
q. Dissolution of middle lamellae and separation of fibres (arrow).
r. Penetration of hyphae within the separated region (arrow).
i, j. Extensive thinning and erosion of fibres and ray (R) cells wall was apparent (arrow).
k, l. Complete delignification and formation of erosion in the cell wall (arrow).
m. Thinning and erosion of secondary wall of vessel (V) and associated parenchyma (P).

Scale bar: a-c, e-h, k and l= 5µm; d, i, j and m= 10µm

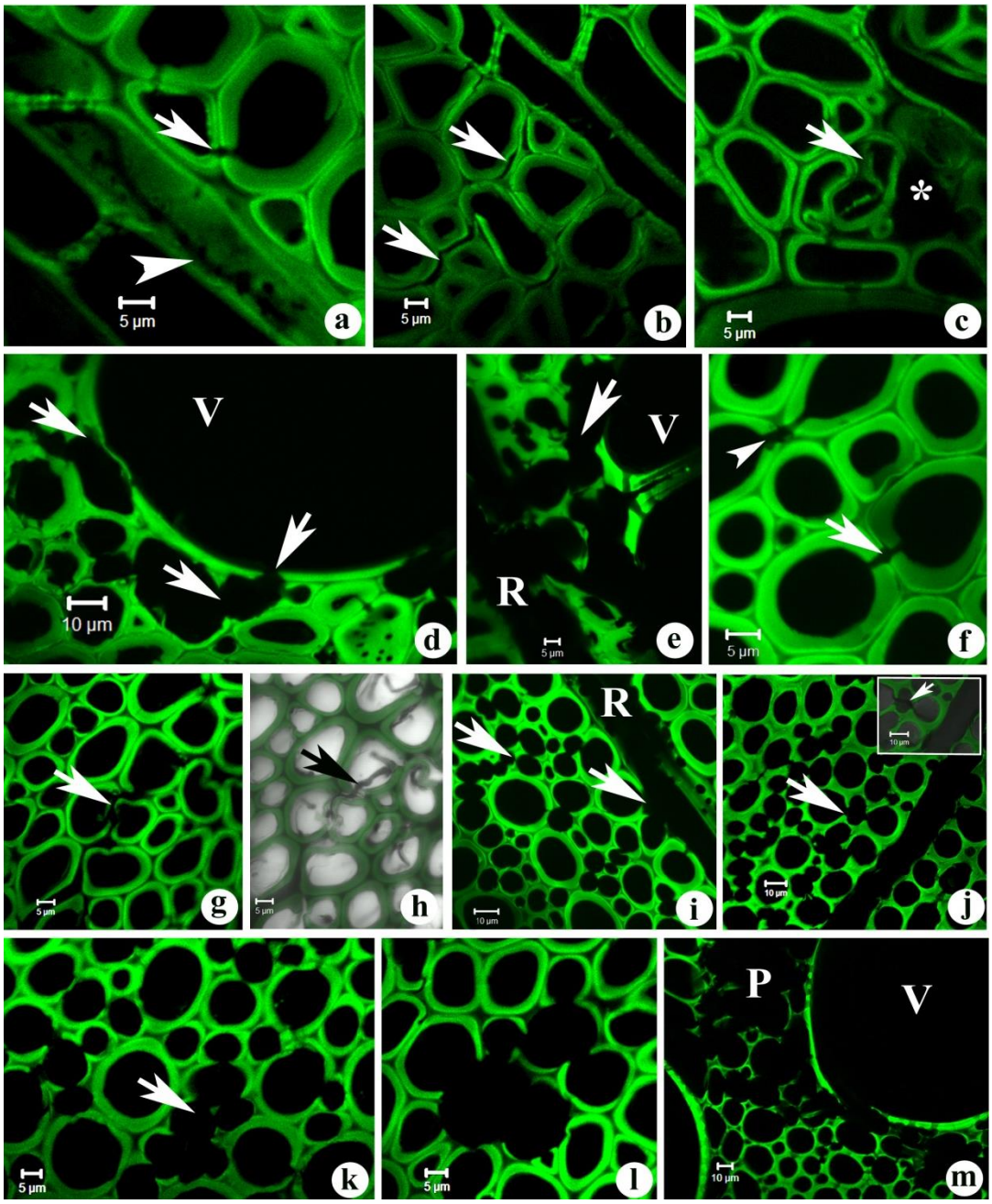
5 µm
a
5 µm
b
*
5 µm
c
V
10 µm
d
V
R
5 µm
e
5 µm
f
5 µm
g
5 µm
h
R
10 µm
i
10 µm
j
5 µm
k
5 µm
l
P
V
10 µm
m

Figure 59

Figure 61 (a-j): Transverse (f and i) and tangential longitudinal (a-e, g, h and j) sections from the wood of *Leucaena leucocephala* infected with *Trametes hirsuta* for 30 days (a and b), 60 (c-f), 90 (g and h) and 120 (i and j) days.

a. Erosion channel showing 'U'notch appearance in tangential section of a fibre cell wall.
b. Bore holes in the tangential wall of fibre.
c. Delignification of middle lamellae and separation of cell walls of fibre and rays. (arrows).
d. Ray cells showing dissolution of middle lamellae (arrow) and secondary wall
e. Separation of ray cells.
f. Progression of delignification from outer to inner secondary wall layers (arrows).
g. Extension of erosion channels through merging of bore holes.
h. Large bore holes and thin cell wall during advanced stage of decay.
i. Fibre cell wall showing erosion channels and dissolution of middle lamella.
j. The degraded regions of fibre cell wall showing feebly stained patches of thin walls (arrows). Note the hollow space formed in the middle region of ray (R) after complete degradation of cell walls.

Scale bar: a, c, d, f, g= 20 µm; b, e, h, i= 10 µm and j= 50 µm

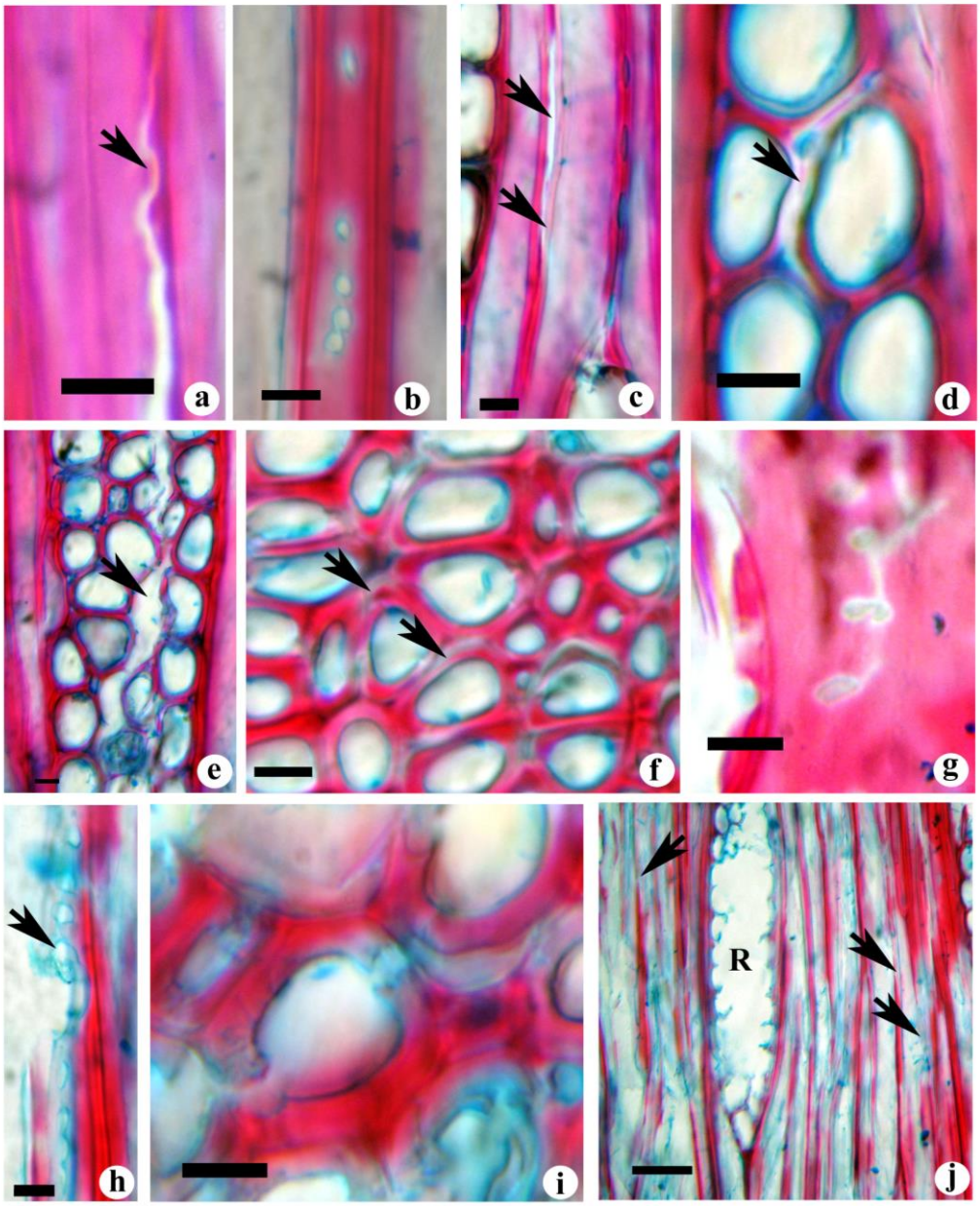

Figure 61

Figure 62 (a-l): Transverse (a and i), tangential (b-h and j) and radial longitudinal (k and l) section from the *Leucaena leucocephala* wood infected with *T. versicolor* for 30 days (a and b), 60 (c-i), 90 (j) and 120 (k and l) days.

a. The erosion of wall progressing from inner wall towards cell corner middle lamellae of fibre (arrow).
b. Thinning of fibre secondary wall (arrows).
c. Large erosion channel (arrow) and bore holes in the fibre wall.
d. Fungal mycelia forming penetration hyphae (arrow) towards the pit region.
e. Longitudinal progression of erosion channels in the tangential wall of fibre.
f. Inverted 'U' tunnelling in the fibre secondary wall (arrow).
g. Formation of 'U' notches (arrow).
h. The large eroded region of the cell wall of fibre.
i. Ray cell (R) showing wide gap formed after erosion of walls.
j. Separation of cells through dissolution of middle lamellae (arrow). Arrowhead indicates the erosion channels formed in cell wall between adjacent fibres.
k. Progression of wall erosion between adjacent pit fields in vessel.
l. Large erosion channels formed in the ray cell wall during advanced stage of decay.

Scale bar: a, e-k= 10 µm; b-d, l= 20 µm

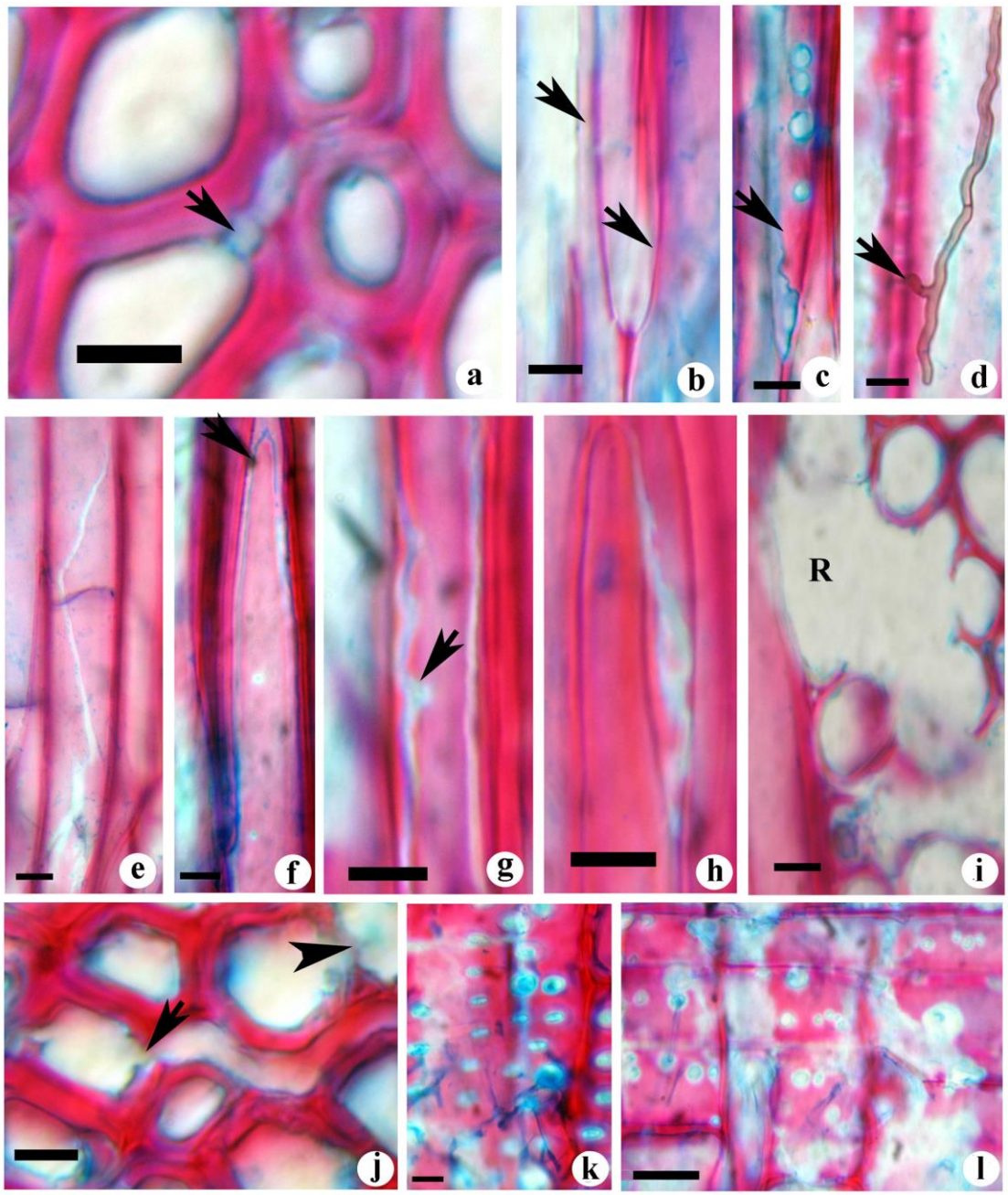

Figure 62

Figure 63 (a-k): Confocal images from transverse sections of *Leucaena leucocephala* wood infected with *T. versicolor* (a-f) and *T.hirsuta* (g-k).

a. Delignification from cell corner middle lamellae to secondary wall leading to thinning of cell wall (arrow heads). Arrowhead indicates delignified erosion trough in the radial wall of ray cell.
b. Penetration of fungal mycelia into simple pits in the ray cells. Arrowhead indicates delignified erosion trough progressing towards the cell corner of adjacent fibre.
c. Vessel (V) showing delignification begins from the wall facing the paratracheal parenchyma cell (P). Note the delignified large holes in the transverse septa (arrows) and and cell corners of parenchyma cells (arrowhead).
d. Delignification of cell corners and compound middle lamellae (arrow). Arrowhead indicates the delignified erosion trough formed in the wall between fibres.
e. Widening of pit region of fibre cell wall following the progression of pit erosion into adjacent secondary wall (arrows). Arrowhead indicates the narrow pit fields in the unaffected fibre wall.
f. Delignified regions of cell walls of vessels, paratracheal parenchyma (P) and rays (R) showing absence of fluorescence. Arrowhead indicates the delignification of cell corner middle lamellae of fibre adjacent to rays.
g. Progression of delignification from cell corners to compound middle lamellae (arrow) between axial parenchyma and fibre. Arrowhead indicates thinning of fibre cell wall.
h. Delignified erosion trough formed in the secondary wall of fibre. Arrowhead indicates the absence of fluorescence from the delignified compound middle lamellae region.
i. Erosion channel formed in both radial and tangential wall of fibres indicated by non-fluorescent regions (arrow).
j. Bright field image of ‘d’ showing the erosion channel in secondary wall of fibre.
k. Enlargement of pit fields in ray (R) cell wall through delignification. Arrow head indicates the separation of cells were pit erosion reached up to the compound middle lamellae region.

Scale bar: f=10 µm; a-e and g-k=5 µm

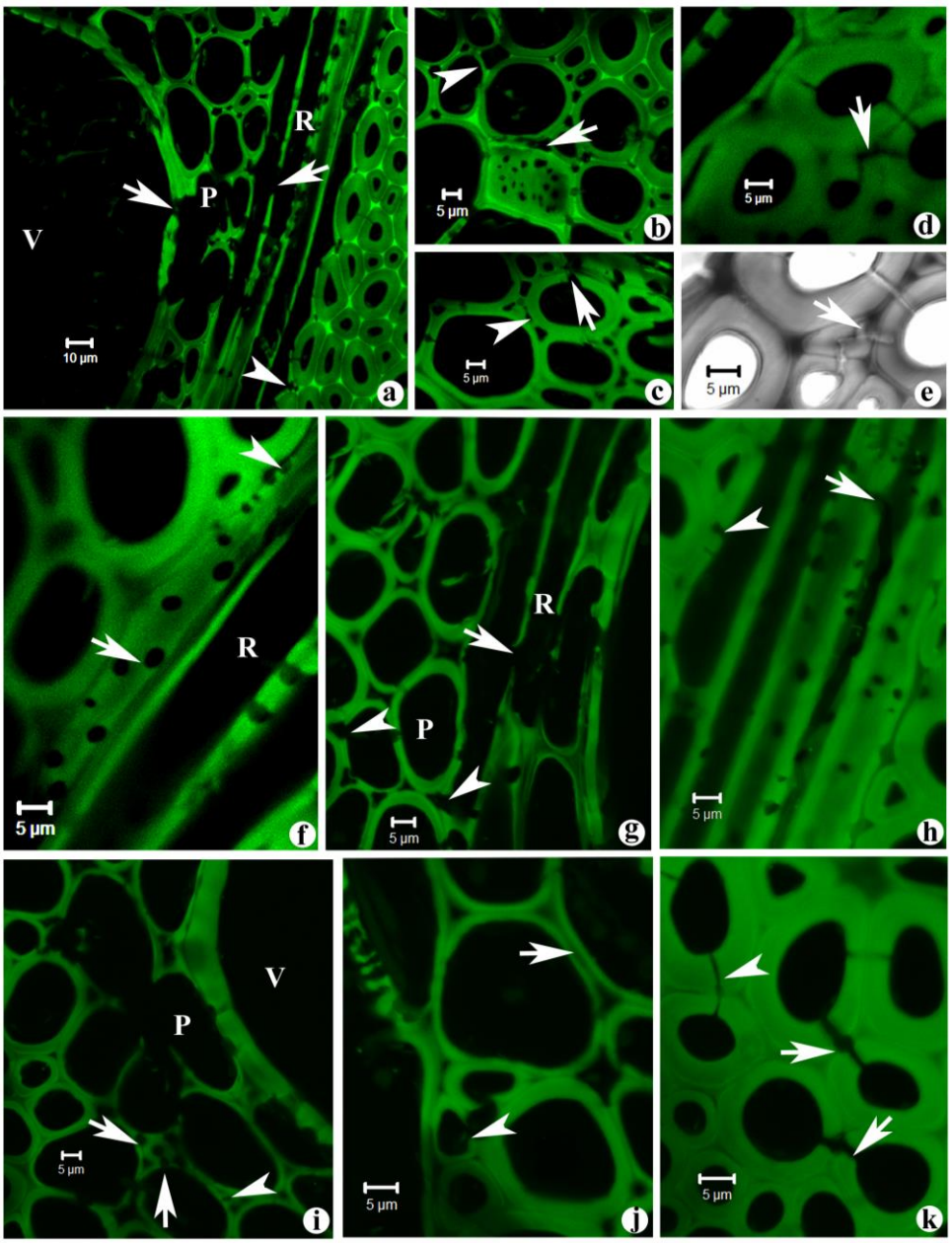
R
P
V
10 µm
a
5 µm
b
5 µm
d
5 µm
c
5 µm
e
R
5 µm
f
R
P
5 µm
g
5 µm
h
V
P
5 µm
i
5 µm
j
5 µm
k

Figure 63